UNIVERSITÀ DEGLI STUDI DELLA TUSCIA DI VITERBO

Department for Innovation in Biological, Agro-Food and Forest Systems

DIBAF

PhD in Forest Ecology, cycle XVIII

Bi-directional exchange of greenhouse gases and pollutants between a Mediterranean Holm oak forest and the atmosphere

BIO/07

Candidate

Flavia Savi

Supervisor

dr. Silvano Fares

PhD Coordinator

prof. Paolo De Angelis

- 2016 –

Contents

List of tables

List of figures

Main symbols and abbreviations

Symbols	Description	Unit or Value of Costants
Latin alphabet		
B	Stanton number	–
cp	Specific heat capacity of air	1246 J kg-1 K-1
d	Displacement height	m
D	Dispersion matrix	s
Dx	molecular diffusivity of a gas	
E	Latent heat flux	kg m−2 s−1
Fg	Ground flux (at z=0)	mmol m-2 s-2 μmol m-2 s-2 nmol m-2 s-2
FO3sto	O3 stomatal uptake	nmol m-2 s-2
Fx	Flux of a gas	mmol m-2 s-2 μmol m-2 s-2 nmol m-2 s-2
g	Gravitational acceleration	9.81 m s-2
GO3	Stomatal conductance to O3	mol m-2 s-1
Gst	Stomatal conductance to H2O	mol m-2 s-1
H	Sensible heat flux	°K m-1 s-1
H2OfluxAC	H2O fluxes above canopy	mmol m-2 s-2
H2OfluxBC	H2O fluxes at ground level	mmol m-2 s-1
hc	Canopy height	m
hv	Light	–
k	Von Karman constant	0.41
KH	Eddy diffusion coefficient	m2s-1
L	Monin-Obukhov length	m
LE	Latent heat flux	W m-2
prec	Precipitation	mm
qa	vapour pressure	kg kg−1
qs	saturation mass fraction of H2O at air temperature	kg kg−1
Ra	Aerodynamic resistance	s m-1
rad	Global solar radiation	Wm-2
Rb	Laminar boundary layer resistance	s m-1
Rc	Canopy resistance	s m-1
Rct	Cuticular resistance	s m-1

Rct(dry)0	reference value for Rct calculation in dry condition	6000 s m−1
Rct(wet)0	reference value for Rct calculation in wet condition	400 s m−1
Re	Reynolds number	–
Rg	Ground resistance	s m-1
Rg1	Constant resistence for Rg calculation	50 s m−1
Rg2	Constant resistence for Rg calculation	500 s m−1
RH	Relative humidity	%
RH soil 10	Soil relative humidity 10 cm depth	%
RH soil 100	Soil relative humidity 100 cm depth	%
RH soil 50	Soil relative humidity 50 cm depth	%
Rs	Stomatal resistance to H2O	s m-1
S	Suorce or sink strength	µmol m-2 s-2 nmol m-2 s-2
Sc	Schmidt number	–
swc	Soil water content	%
swc10	Soil water content measured at 10 cm depth	%
swcfc	Soil water content measured at field capacity	28%
T	air temperature	°K
T air	Air temperature	°C
T soil 10	Soil temperature 10 cm depth	°C
T soil 100	Soil temperature 100 cm depth	°C
T soil 50	Soil temperature 50 cm depth	°C
TL	Lagrangian time scale	s
u	Horizontal wind velocity	m s-1
*u**	Friction velocity	m s-1
UV	Ultraviolet radiation (280-360 nm)	Wm-2
v	Lateral wind velocity	m s-1
va	kinematic viscosity of air	m2 s -1
Vd	Deposition velocity	m s-1
w	Vertical wind velocity	m s-1
wh	ANN connection weight between input and hidden neurons	–
winddir	Wind direction	°
wo	ANN connection weight between hidden and output neurons	–
z	Measurement height	m
z0	Roughness length, mean hight above d at which momentum is absorbed	m

Greek alphabet

X	Concentration of a gas	ppm ppb
X^{far}	Concentration due to far-field effect	ppm ppb
X^{near}	Concentration due to near-field effect	ppm ppb
β	Regression coefficient	–
γ	Psychrometric constant	4.08×10^{-4} K^{-1}
ε	Regression intercept	–
ζ	Stability parameter	–
λ	Vaporisation heat for H_2O	2.5×10^{6} J kg^{-1}
ρ_a	Density of dry air	1.01 g m^{-3}
σ_w	Standard deviation of vertical wind velocity	m s^{-1}
Ψ_H	Stability correction function for heat	–
Ψ_M	Stability correction function for momentum	–

Abbreviations	*Description*
ANN	Artificial Neural Network
AVOC	Anthropogenic Volatile Organic Compound
BVOC	Biogenic Volatile Organic Compound
EC	Eddy Covariance technique
ES	Early Spring - Mar 20th to Apr 14th period
ILT	Inverse Lagrangian technique
KS	Kolmogorov-Smirnov test
LA	Late Autumn - Nov 11st to Dec 6th period
OVOC	Oxygenated volatile organic compound
PCA	Principal Component Analysis
PLB	Planetary Boundary Layer
PLS	Partial Least Square regression
ROS	Oxigen Reactive Species
SSA	Syngular Spectrum Analysis
VOC	Volatile Organic Compound

Abstract

Forests play a major role in regulating air quality and climate. However, plant exposure to atmospheric pollution may cause detrimental effects on vegetation. Among others, tropospheric O_3 is probably the most damaging to forest ecosystems: entering the leaves thought stomata, it causes oxidative stress and damages photosynthetic apparatus, reducing carbon assimilation. This PhD work aimed to quantify fluxes of greenhouse gases (CO_2, CH_4, O_3) in a Mediterranean holm oak forest located near Rome (Italy) exposed to high levels of tropospheric O_3 concentration. A primary goal was also to evaluate the O_3 damage on the forest carbon assimilation capacity.

Four years of eddy covariance measurements demonstrated that the ecosystem is an active CO_2 sink all year long (485 – 690 g C m^{-2} y^{-1}). For the first time, long term monitoring of CH_4 exchange above a Mediterranean forest showed that the ecosystem is a net CH_4 sink during the cold season and a net source during the dry season, thus making the annual net CH_4 exchange close to the neutrality.

Precipitation events during Summer season have been found to be one of the most important factors controlling carbon exchanges at the forest, thus influencing the CO_2 uptake and the magnitude of the CH_4 emission. The dry condition in Summer period depressed CH_4-oxidizing bacteria, so that the ecosystem acted as a net source of CH_4 in this period, thanks to translocation of CH_4 from the soil to above canopy through xylematic pathways. Furthermore, the Summer high UV radiation has been found to promote CH_4 production from photochemical reactions on leaves waxes, thus contributing to the overall strength of the Summer CH_4 emissions.

Besides being a sink for carbon, the holm oak forest represents a net sink of O_3. The annual budget has been estimated around 80 mmol m^{-2} y^{-1}. The major sink were stomata, being O_3 uptake strongly connected to the physiological plant activity and subject to water availability.

The influence of O_3 over NEE was tested using a novel approach, which combines non parametric time series decomposition and the explanatory capacity of Artificial Neural Networks. Results suggested that O_3 has a detrimental effect over NEE during Spring and Summer seasons, although the magnitude of this reduction is low (rate of reduction of NEE for unit change of O_3 stomatal uptake = 0.015).

The results of this PhD work demonstrated that this Mediterranean forest is an active carbon sink and contributes to ameliorate air quality removing O_3 from the atmosphere. However, O_3 uptake through stomata reduces carbon assimilation, although it does not represent the main limiting factor to forest productivity as compared to drought. The latter showed to be the major limiting factor at the forest leading to strong reduction of CO_2 assimilation, enhancement of CH_4 emission and limitation to O_3 uptake. These results help to foresee possible future effects of climate change and pollution on Mediterranean forest ecosystems.

List of scientific publications produced during the PhD course

Published papers:

Fares S., **Savi F.**, Muller J., Paoletti E., Matteucci G., 2014. Simultaneous measurements of above and below canopy ozone fluxes help partitioning ozone deposition between its various sinks in a Mediterranean Oak Forest. Agricultural and Forest Meteorology, 198-199:181-191. DOI: 10.1016/j.agrformet.2014.08.014

Savi F., Fares S., 2014. Ozone dynamics in a Mediterranean Holm oak forest: comparison among transition periods characterized by different amounts of precipitation. Annals of Silvicultural Research, 38(1):1-6. DOI: 10.12899/asr-801

Aromolo R., **Savi F.**, Salvati L., Ilardi F., Moretti V., Fares S., 2015. Particulate matter and meteorological conditions in Castelporziano forest: a brief commentary. Rend. Fis. Acc. Lincei 26 (3): 269-273. DOI: 10.1007/s12210-015-0414-5

Accepted paper:

Savi F., Di Bene C., Canfora L., Mondini C., Fares S., Environmental and biological controls on CH_4 exchange over an evergreen Mediterranean forest. Agricultural and Forest Meteorology.

Submitted papers:

Canfora L., Di Bene C., **Savi F.**, Migliore M., Farina R., Fares S. Evaluating factors influencing soil microbial communities and CO_2 exchanges in a Mediterranean Holm oak forest. Submitted to Environmental Monitoring and Assessment.

Fares S., **Savi F.**, Fusaro L., Conte A., Salvatori E., Aromolo R., Manes F. Particle deposition in a peri-urban Mediterranean forest. Submitted to Environmental Pollution.

1 Introduction

Forests play a major role in regulate air quality and climate. Beside fixing carbon dioxide trough photosynthesis, vegetation controls other greenhouse gases and pollutants transport across the forest-atmosphere boundary. This control is expressed primary by three principal mechanisms: dry or wet surface deposition, stomatal uptake and gaseous phase reactions. Leaves and branches provide a surface much bigger than the corresponding soil surface, air spaces inside the stomata increase the available surface where gases deposit or dissolve. Many physiological processes involve gases for chemical reactions within or outside the leaves, such as antioxidant systems in the cell walls or the emission of volatile organic compounds.

However, plant exposure to atmospheric pollution may cause detrimental effects that weaken vegetation carbon sink potential. Although pollution does not represent the main limiting factor to forest productivity as compared to other environmental factors such drought or lack of nutrients, its effect on Mediterranean vegetation is of particular concern. Indeed, the strong anthropic pressure on densely inhabited Mediterranean coasts, together with the occurrence of climatic conditions that promote pollutants formation through photochemical reactions, represents a great stress factor for vegetation.

1.1 Greenhouse gases and atmospheric pollutants

1.1.1 Carbon Dioxide

Atmospheric carbon dioxide (CO_2) is the second most abundant greenhouse gas in the atmosphere after water vapour (H_2O), with a radiative forcing of 1.69 Wm^{-2} (Shindell et al., 2009). Its concentration has substantially increased since the industrial revolution began in the 19th century, mainly due to anthropogenic activity. Three quarter of anthropogenic CO_2

emissions is attributed to fossil fuel combustion, followed by deforestation and land-use change (Brugnoli and Calfapietra, 2010).

Forests represent the major land biosphere sink of CO_2 (Melillo et al., 1993), which depends on the balance between photosynthetic fixation and CO_2 release by autotrophic respiration and biomass decomposition. This equilibrium presents a strong temporal variability at different scales (diurnal, seasonal, annual) and it is controlled by climate and by length of the growing season (Valentini et al., 2000).

Forest ecosystems net absorption of CO_2 is called Net Ecosystem Exchange (NEE) and is generally measured on annual scale. NEE represents the amount of carbon subtracted from the atmosphere and stored in live biomass, litter and soils. Although NEE is commonly positive, that is ecosystems subtract carbon from the atmosphere, in some cases is observed a net release of CO_2 from forests, imputable to many factors that enhance respiration, between them, climate variations end disturbance regimes (Rice et al., 2004; Williams et al., 2014).

Mediterranean evergreen forests ensure CO_2 sequestration and storage all year long, although the CO_2 absorption rate changes among seasons depending on temperature and water availability, which represent the main environmental stress in this region. High temperature and drought re-occur cyclically every year in Summer and natural selection processes made Mediterranean vegetation adapted to these environmental conditions. Although, when natural stress factors are coupled with anthropogenic pollution, forest carbon sequestration potential can decrease.

1.1.2 Methane

Methane (CH_4) is the most abundant hydrocarbon and the third greenhouse gas in the atmosphere after H_2O and CO_2. Its global warming potential (over 100 years) is 28-36 times higher compared to CO_2 (IPCC, 2013) and its indirect effect on aerosols and other chemical compounds by altering the atmosphere oxidative capacity (Shindell et al., 2009) make this gas of particular concern.

CH_4 concentration increased by 2.5 times since pre-industrial time (Etheridge et al., 1992). Both natural sources, i.e. wetlands, and anthropogenic activities, i.e. biomass burning, fossil fuel production, livestock and rice paddies, contribute to CH_4 global source (Denman et al., 2007), estimated at 600 T CH_4 y^{-1} (Lelieveld et al., 1998).

In forest ecosystems, soil is the primary compartment where CH_4 exchange takes place: methanotrophic and nitrifying bacteria are responsible for atmospheric CH_4 uptake, whereas emission is regulated by metanogenic archaea, strictly limited to anaerobic environments (Trotsenko and Khmelenina, 2002). Recently, studies have suggested a contribution of forest vegetation to CH_4 emission (Keppler et al., 2006), although the significance of this emission is still under debate (Bruhn et al., 2012; McLeod et al., 2008). The main mechanisms explaining CH_4 release from vegetation are: contribution via the transpirational stream through the xylem (Zeikus and Ward, 1974), anaerobic source in the trunk (Mukhin and Voronin, 2011), induction by UV radiation and heat from plant tissues (McLeod et al., 2008; Vigano et al., 2008), wounding (Wang et al., 2009), or reactive oxygen species induction (Sharpatyi, 2007; Vigano et al., 2008).

Few studies were conducted over forests ecosystems contribution to the CH_4 biosphere – atmosphere exchange (Nicolini et al., 2013) and none of them was conducted over a Mediterranean forest. Literature highlights that CH_4 flux magnitude over different forest types is widely variable, depending on forest and soil types, and even the direction of fluxes can change, reacting to different meteorological variables. This variability is mainly due to microbial responses to environmental factors influencing microbial activity such as meteorological conditions, soils texture, N availability and salinity (Stams and Plugge, 2010). Due to their role in controlling CH_4 behaviour, the understanding of soil microorganisms involved in the CH_4 cycle represents a cognitive platform for any CH4 study aimed to explore the connection between ecosystems and CH_4 fluxes.

1.1.3 Tropospheric Ozone

Tropospheric ozone (O_3) is a secondary pollutants, mainly produced through photochemical reactions of methane (CH_4), carbon monoxide (CO), and volatile organic compounds (VOC)

in the presence of nitrogen oxides (NO_x). A minor O_3 source is the downward transport from the stratosphere (Junge, 1963). Is the third greenhouse gas in the atmosphere, and contributes to the climate change with a radiative forcing of 0.35-0.37 W m^{-2} (Shindell et al., 2009). High O_3 concentrations are associated with negative effects on human health (respiratory diseases), natural ecosystems and crops (The Royal Society, 2008).

Chemistry that controls O_3 production and destruction in the troposphere is summarized by the following reactions (Monks et al., 2015):

$$NO_2 + h\nu \rightarrow NO + O \quad (1)$$

$$O + O_2 \rightarrow O_3 \quad (2)$$

$$HO_2 + NO \rightarrow NO_2 + OH \quad (3)$$

$$O_3 + NO \rightarrow NO_2 + O_2 \quad (4)$$

The above reactions do not represent a mechanism of net O_3 production since the rapid interconversion between NO and NO_2 leads to both O_3 production and destruction. This equilibrium is altered in presence of volatile organic compounds (VOCs):

$$VOC + OH + O_2 \rightarrow CO_2 + HO_2 \quad (5)$$

VOCs oxidation produces of hydroperoxyl (HO_2) , which reacts with NO, changing the [NO]/[NO_2] ration, leading to O_3 formation. From the above formulas arises that O_3 formation depends on the balance of its precursors, which have both natural and anthropogenic origin. In rural areas, O_3 formation rate is not limited by VOCs availability and increases with NO_x concentration increase (NO_x limited). In urban environment, O_3 formation rate increases with increasing VOCs concentration and it is inhibited by increasing NO_x concentration. These chemical regimes make O_3 concentration highest in rural areas located downwind of polluted cities.

Background O_3 concentrations at present days is 30-40 ppb (Parrish et al., 2012), however large regional differences are recorded due to the strong influence of weather, which promotes O_3 formation in warm, dry and sunny conditions.

O_3 lifetime in the lower troposphere is around 5 days (Fusco and Logan, 2003). O_3 photolysis is the major source of OH radicals, the primary oxidant in the troposphere:

$$O_3 + hv \rightarrow O + O_2 \quad (6)$$

$$O + H_2O \rightarrow OH + OH \quad (7)$$

Another O_3 sink in addition to the chemical destruction is the removal at the surface by dry deposition that occurs in forest ecosystems through stomatal uptake, non-stomatal uptake and in-canopy chemistry.

Stomatal uptake by vegetation allows O_3 enters the leaves, thus removing this pollutant from the atmosphere. By contact with cell walls, membranes and metabolites, O_3 generates free radicals within the apoplast, damaging cell metabolism (Hindawi, 1979). The main detrimental effect is carbon assimilation reduction, caused by photosynthetic apparatus damage. The O_3 portion entering the stomata depends on stomatal aperture, which in turn is regulated by many environmental and physiological factors, among them: light, temperature, CO_2 concentration, vapour pressure deficit, water availability, phenology (Grünhage et al., 2012).

Non-stomatal uptake includes all the reactions of O_3 with the external surface of vegetation and soil. Temperature and canopy wetness can increase reaction rates of O_3 with organic compounds on leaves (Rondón, 1993; Coyle et al., 2009). In-canopy chemistry depleted O_3 concentration through oxidation of NO emitted by soil and through oxidation of VOCs emitted by vegetation.

1.1.4 Volatile Organic Compounds

Volatile organic compounds (VOCs) are trace organic gases other than CO_2 and CH_4. Their origin can be both biogenic (BVOCs) and anthropogenic (AVOCs). Biogenic emissions are estimate around 800 Tg C y^{-1} and exceed anthropogenic of one order of magnitude (Lathiere and Hauglustaine, 2006). VOCs release in plants has multiple roles, linked to growth,

reproduction, defence against stresses, protection and communication (Peñuelas and Staudt, 2010).

They are involved in many reactions that affects atmospheric chemistry and carbon cycle. Almost 10 % of the carbon fixed by photosynthesis is released as VOCs by vascular plants (Llusia and Peñuelas, 2000). Once in the atmosphere, VOCs react and their products impact on O_3 production or destruction (as outlined in the 1.1.2 section), aerosol production and cloud formation (Holzinger et al., 2005), airborne N deposition and acidification.

A large number of chemical groups are included within VOCs. Many of them are toxic to human and ecosystems, such as aromatic hydrocarbons, aldehydes and ketones (Burn et al., 1993; Kampa and Castanas, 2008).

Isoprenoids (isoprene, monoterpenes and sesquiterpenes) are the predominant group, followed by alcohols and carbonyls. Isoprenoids are quite reactive and their lifetime vary between minutes to hours (Kesselmeier and Staudt, 1999), they are poorly water-soluble and characterized by a strong scent. Isoprene (C_5H_8) represent the 50% of BVOC emissions (Guenther et al., 2000), and is produce especially by poplars, aspen, oaks and eucalyptus trees. Monoterpens ($C_{10}H_{16}$), mainly in the form of α-pinene and β-pinene, contribute to the 10-15% of emissions (Fowler et al., 2009). The outstanding part is represent by oxygenated VOC, which are less reactive than isoprenoids and ubiquitously produces by all plant species.

Depending on the species, BVOC emission can be regulate by compounds synthesis rate or by evaporation and diffusion from storage pools. Plants can also act as sink for BVOC when their air concentration is higher than those inside plants (Noe et al., 2008).

Mediterranean costal ecosystems are almost exclusively characterized by monoterpenes emitting species (Loreto et al., 1998). One of the predominant species that characterize this environment is *Quercus ilex* L. This evergreen oak does not store monoterpenes, so that their emissions is directly correlated with temperature and light intensity (Loreto et al., 2004), which make monoterpenes emission rates varying according to daily and seasonal cycles. This emission pattern, associated with high reaction rate with OH radicals in the atmosphere, in turn affects O_3 chemistry during photochemically active periods of the year.

1.1.5 Nitrogen Oxides

Nitrogen oxides (NO_x) are treated as a chemical family that include NO and NO_2. The main NO_x sources are fossil fuel combustion, biomass burning, soils and lightening (Seinfeld and Pandis, 2016). Almost 95% NO_x emission from combustion are NO, which rapidly converts to NO_2 in the atmosphere (as outlined in the 1.1.2 section). Atmospheric concentration of these compounds is highly variable, ranging between <1 ppb in remote location to 10-1000 ppb in urban areas, where the main sources are located (Von Schneidermesser et al., 2015).

NO_x radiative forcing is 0.29 W m^{-2} (Shindell et al., 2009), and is the result of a variety of opposite interactions of NO_x with other greenhouse gases, i.e. SO_4, CH_4, NO_3, and O_3. NO_x relation with O_3 affects NO_x lifetime, which ranges from hour to days (Berntsen et al., 2005).

NO_x are harmful pollutants that negatively affect human health, inducing respiratory and heart diseases (Godish et al., 2014). Negative effects of NO_x on ecosystem can be direct, as acid deposition that compromises soil and water quality, or indirect, as formation of secondary pollutants such O_3 and particles (Van Grinsven et al., 2013).

1.2 Atmospheric pollution effects on forest ecosystems

Vegetation role as important sink for air bone pollutants and greenhouse gases is widely recognized. On the other hand, plants are damaged by filtering air pollutants, and effects on forest ecosystems can be severe. Reduction of forest productivity represents an early detection of the forest decline, before the occurrence of visible injuries.

Manipulative experiments have been widely used to test pollution sensitivity, however such experiments have several limitations, since plants are often exposed unrealistic concentrations, young seedling, and the experimental facilities, e.g. open top chambers, impact the microclimate of the trees. For these reasons, understanding how pollution affects the CO_2 uptake by open forests is of primary importance.

Among air pollutants, O_3 is probably the most damaging to forest ecosystems (Ollinger et al., 1997). O_3 phytotoxicity derives from the oxidative damages it produces inside the cell. Once O_3 penetrate the leaf through stomata, it reacts with a number of molecules in the apoplast, generating ROS, which lead to oxidation of components of the cytoplasm (Heath, 1980). The oxidative stress activates various transduction pathways that include stomatal closure, antioxidants production as ascorbate and isoprenoids (Loreto et al., 2004) and programmed cell death, which produces evident effects on leaf surface, as chlorotic spots. At ambient concentration, chronic O_3 exposure does not always produces visible injuries, and the most common effects are reduction of photosynthesis rate, plant biomass and early senescence (Ainsworth et al., 2012). O_3 detrimental effects occurs at different levels, from cellular to community scale (fig. 1.1).

Traditional method such as plant chambers has been widely used to assess the impact of O_3 over vegetation (Karlsson et al., 2000; Manning, 2005) and results were used to calculate metrics for O_3 risk assessment, such as the Accumulated Ozone over Threshold of 40 ppb (AOT40 ppb h^{-1}, Karlsson et al., 2004), and the Phytotoxic Ozone Dose with a hourly threshold Y (POD_Y), that related O_3 damage to the effective absorbed O_3 dose (nmol m^{-2} h^{-1}) through stomata (Musselman et al., 2006). Although this metrics are useful to develop legislative standards, the up-scaling of these metrics to the ecosystem level is challenging (Fares et al., 2013).

The O_3 effect on forest vegetation have been poorly investigated in situ. Some studies conducted over forests confirm that a detrimental effect of O_3 over the forest capacity to absorb CO_2 occurs at ambient O_3 concentrations, e.g. Zapletal et al. (2011) found that stomatal O_3 uptake reduce NEE under elevate solar radiation in a Norway spruce forest in Czech Republic, Fares et al. (2013) observed a reduction in gross primary production (GPP) up to 19 % caused by O_3 in a Ponderosa pine forest in California. Others did not find any effect, e.g. Zona et al. (2014), who tested the O_3 effects over the NEE of a poplar plantation in Belgium. These studies highlight that the O_3 effect on vegetation is site-specific and varies among forest types.

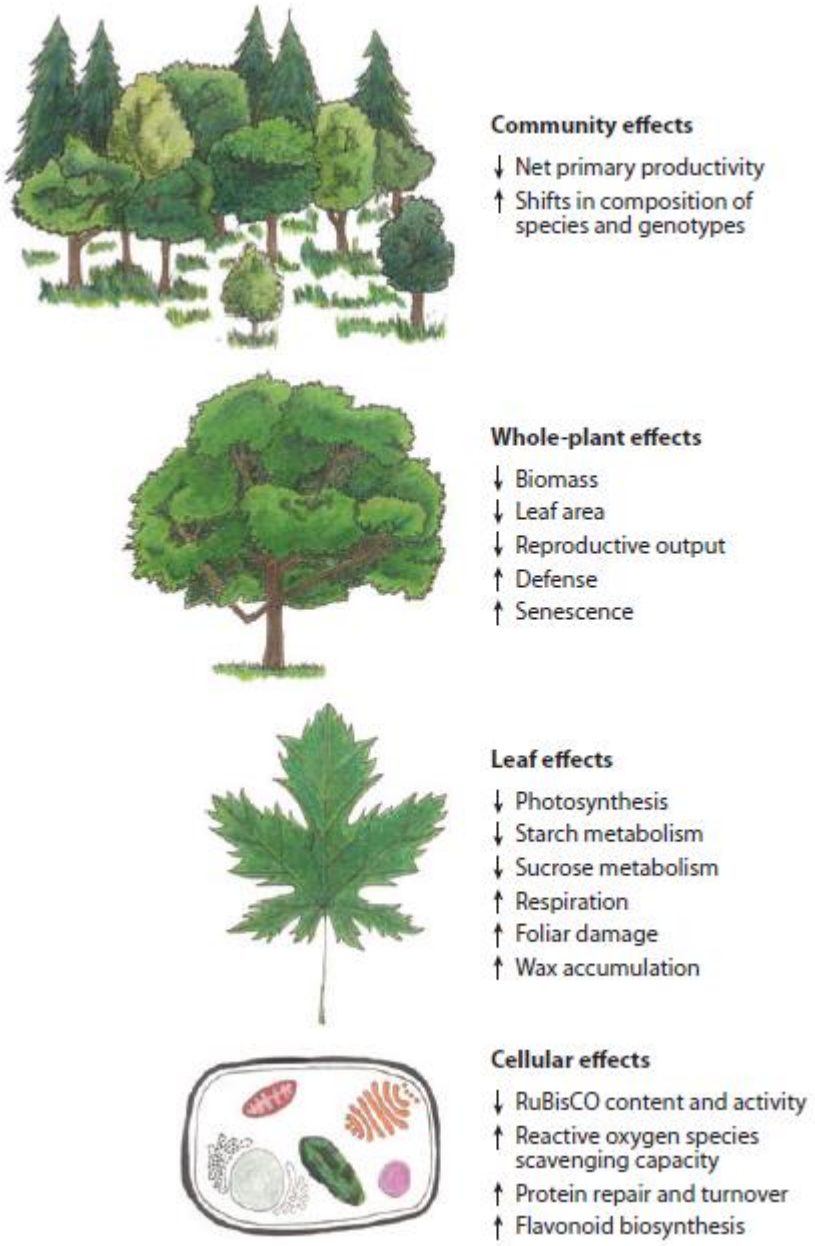

Figure 1.1: Effects of O_3 on plant processes at the cellular, leaf, whole-plant, and community scales. Arrows indicate directional changes of processes affected by elevated [O_3] (from Ainsworth et al., 2012).

VOCs species include hundreds of different substances, which can have different impacts. Laboratory studies demonstrated vegetation has a wide range of tolerance to VOCs and it is unlikely that current ambient VOCs concentration represent direct threat to plant health

(Cape, 2003). VOCs negative effect on plants is mostly indirect, recognised in their contribution to the formation of O_3.

NO_x phytotoxicity is less than other air pollutants such as O_3 and is very rare to observe visible injuries due to NO_x in the field. NO_2 is more toxic than NO, because plants absorbs NO_2 three times faster than NO, which is almost insoluble in water (Law and Mansfield, 1982). After entering the leaves, NO_2 is convert to NO_2^- in the apoplast. When it is not convert, NO_2 can interact with membrane compounds with the consequent denaturation of membranes (Pryor and Lightsey, 1981) and production of radicals, which, in turn, inactivate or destroy biomolecules (Srivastava, 1992).

1.3 Thesis overview and structure

The main objectives of the PhD work were to (1) determinate the carbon balance at the holm oak forest (2) analyse factors controlling C exchanges between the forest and the atmosphere (3) evaluate tropospheric O_3 temporal dynamics over the forest (4) quantify O_3 removal by the forest ecosystem and (5) assess O_3 interference with NEE.

To meet these objectives, CO_2, H_2O, CH_4, O_3 exchanges were measured through the eddy covariance technique over a Mediterranean forest on the Tyrrhenian coast of central Italy, between 2012 and 2015. NO_x concentrations were measured along a 5-level vertical gradient from soil to above canopy from July 2013 to February 2014. Two field campaigns, which were carried out in January 2014 and in August 2015, were designed to measure VOCs concentrations distribution within the canopy and VOCs exchanges above the canopy.

Measured data were combined with models in order to (1) infer the source/sink contribution of canopy layers to VOCs and NO_x exchanges and to (2) quantify the individual contribution of O_3 exchange pathways. The two respective models used were: (1) the Inverse Lagrangian modelling of the vertical gas source/sink distribution and (2) the Resistance modelling of O_3 fluxes.

The following diagram (fig 1.2) shows the thesis work and outlines how measurements and modelling aided to meet the objectives.

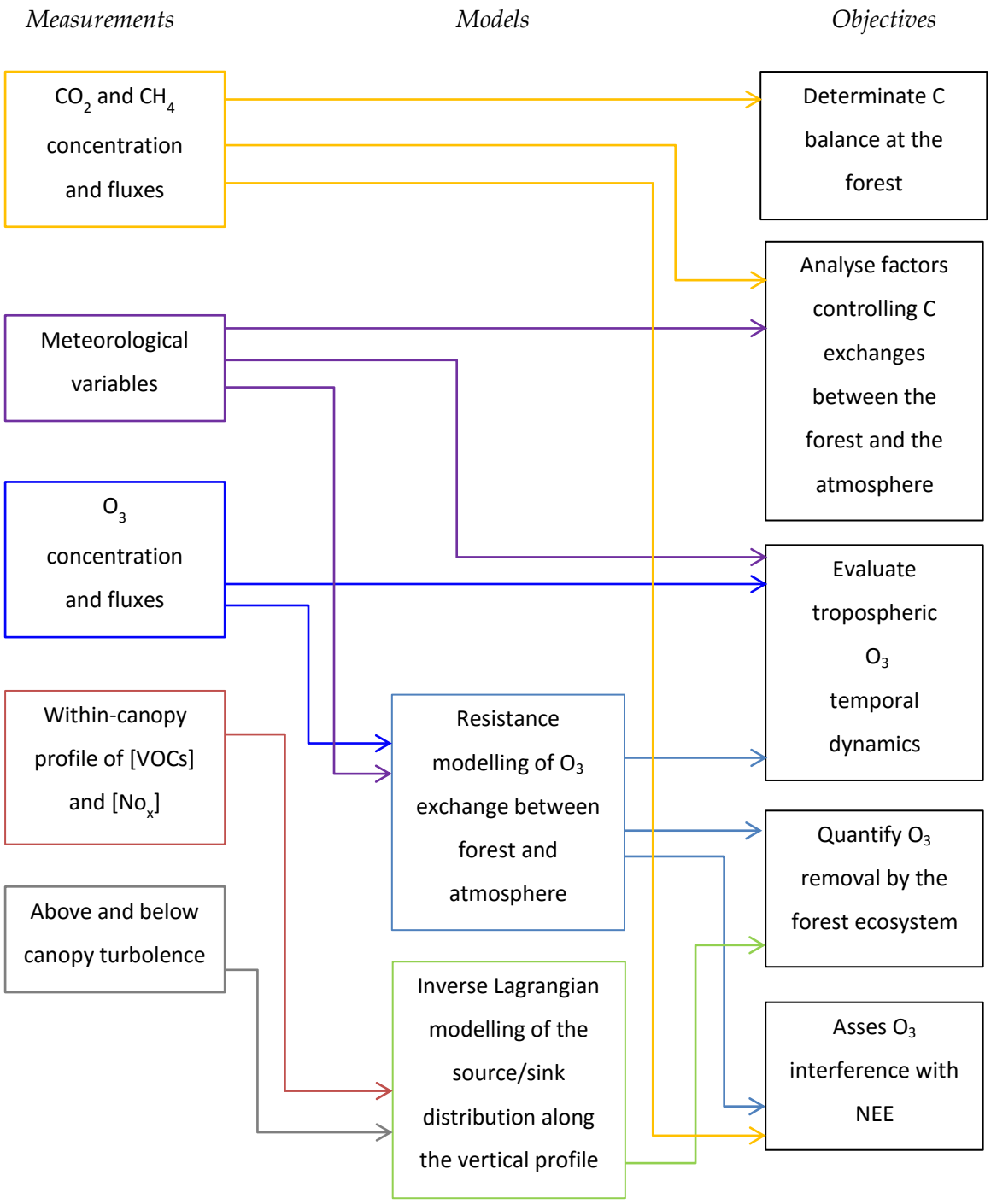

Figure 1.2: Diagram of the PhD work activities (measurements and modelling), and their relations with the thesis objectives.

2 Methods

Understanding of forest-atmosphere interactions has grown in the last decades, mainly due to the improvement of gas sensing technology and micrometeorological techniques.

In this chapter, measurements and data analysis methods are explained in details.

2.1 The study site

The presidential estate of Castelporziano is an hotspot for biodiversity in the Mediterranean, which hosted more than 1000 plants species (Davison et al., 2009). It is a protected area of about 4800 ha, of which 85% are forests. It is located on the coast of the Tyrrhenian sea, 25 km from Rome downtown. Castelporziano is included in the Long Term Ecosystem Research network (LTER – Italy).

Figure 2.1 Study site location, the red line surrounds the Castelporziano estate, the red dot indicates where the study forest is located.

The PhD research was carried out in a wild coastal rear dune ecosystem within the estate, 1.5 km from the seashore (41°70'42''N, 12°35'72''E - fig. 2.1), covered almost prevalently by an even-aged evergreen holm oak forest (*Quercus ilex* L.). Canopy mean height is 14 m and its structure is homogeneous with a leaf area index of 3.69 m^2 leaf m^{-2} ground. The understory vegetation is poorly developed and formed prevalently by small shrubs of mock privet (*Phillyrea latifolia* L.).

Soil has a flat topography, with a sandy texture, and low water-holding capacity. The main soil physic-chemical properties are as follows: 33 g kg^{-1} clay, 116 g kg^{-1} silt and, 851 g kg^{-1} sand; pH in H_2O is 6.85; total organic C, 8.73 g kg^{-1}, total N, 0.56 g kg-1; C/N ratio 13.74 (Pinzari et al., 1999; Biondi et al., 2001).

Climate is typically Mediterranean: seasonality is pronounced, Summer periods are hot and dry, winters are moderately cold. Precipitation occurs prevalently during Spring and Autumn. Mean annual precipitation, averaged over 1999-2010, were 789.3 ± 230.6 mm y^{-1} and mean monthly temperatures, averaged over the same period, range between 7.3 °C and 23.3 °C. Average, standard deviation and range of different environmental parameters measured during the study period are summarized in table 1.

Variables	*unit*	*mean*	*std*	*range*
Global radiation	Wm^{-2}	266	271	959
UV radiation	Wm^{-2}	0.09	0.11	0.46
RH	%	76	12	68
VPD	kPa	0.51	0.36	2.87
Soil Temperature	°C	15	4	17
Soil RH	%	11	5	23
Air Temperature	°C	17	5	31
G sto	ms^{-1}	0.002	0.002	0.016
LE flux	Wm^{-2}	63	78	597
u*		0.57	0.23	1.23

Table 1: Mean, standard deviation, range of environmental variables during the study period.

Wind circulation followed a sea-land breeze regime, the dominant wind direction is S-SW during the morning and N-NE during the afternoon.

Due to its location, the forest is exposed to pollutants linked to both urban and rural activities, making the forest an ideal site for testing the pollution-vegetation interactions.

2.2 Micrometeorological methods

Micrometeorology is a branch of meteorology that studies small-scale atmospheric phenomena, which occur within the planetary boundary layer (PLB). PLB is the part of the troposphere that is directly influenced by the interaction with the biosphere. There, turbulence is influenced by shear stress and temperature profile.

Shear stress can be express in velocity unit by the friction velocity (u*):

$$u^* = \left(\left(\overline{u'w'}\right)^2 + \left(\overline{v'w'}\right)^2\right)^{0.25} \quad (8)$$

where $\overline{u'w'}$ and $\overline{u'w'}$ are the longitudinal and lateral momentum.

The thermic turbulence generated by temperature profile can be quantify by the Monin-Obukhov length (m):

$$L = -\frac{u^{*3}}{k(g/T)(H/\rho_a c_p)} \quad (9)$$

where k is the Von Karman constant (0.41), g is the gravitational acceleration (9.81 m s^{-2}), T is temperature in °K, H is the sensible heat flux (°K m^{-1} s^{-1}), ρ_a is the density of dry air (1.01 g m^{-3}) and c_p is the specific heat capacity of air (1246 J kg^{-1} K^{-1}).

A dimensionless stability parameter (ζ) can be defined from L:

$$\zeta = \frac{z-d}{L} \quad (10)$$

PLB above a rough surface, such a forest canopy, can be divided into the roughness sub-layer, which is a transition zone between the within canopy and the above canopy, the

inertial sub-layer, where is possible to infer fluxes through micrometeorological technique, and the Ekman sub-layer, which is the upper part of the PBL (Garratt, 1994).

Further, the micrometeorological methods used in this work to measure and model gas exchanges above, within and below the forest canopy are listed.

2.2.1 Eddy covariance technique for flux measurements

Eddy covariance (EC) technique allows to directly measure an average vertical flux at a single height. EC technique integrates fluxes over a large area and is representative of the whole ecosystem.

Following this technique, any measured scalar (x) or wind component (u, v *or* w) is discomposed into its time-average component ($\bar{x}$) and its instantaneous deviation from the mean (x'). The vertical flux is calculated as the covariance of x' and vertical wind velocity:

$$F_x = \overline{x'w} \tag{11}$$

assuming that the w time-average is equal to 0. Positive fluxes indicate gas release to the atmosphere while negative fluxes indicate uptake from the atmosphere.

The time-averaging is often set to 30 min, which is an adequate interval to include fluctuation contributing to the flux avoiding the occurrence of change in atmospheric conditions. Sensors measuring x and w must be sufficiently fast to include the higher frequency contributing to the flux, which depends on the eddy size, function of the roughness length (z_0) and measurements height (z). Data acquisition rate can vary between few Hz and 30 Hz.

In order to obtain reliable measurements, quality assurances are required. In this work, the following procedure was applied:

Before calculation of the covariance, raw high frequency concentrations were filtered to remove spikes, identified as values exceeding 6 times the standard deviation calculated on a 1-minute window. Webb-Pearman-Leuning correction was applied to correct for air density fluctuation (WPL correction, Webb et al., 1980).

A double coordinate rotation procedure was performed to align the horizontal component of the wind (u) so that the means of lateral (v) and vertical (w) components were zero on each block of half-hour data, angle of attack was corrected following the procedure proposed by Nakai and Shimoyama (2012). Sonic temperature was corrected for the wind velocity fluctuations (Schotanus, 1983). After that, sonic anemometer and gas concentration signals were synchronized shifting the time series to maximize the covariance between them.

Half-hourly fluxes were discarded when steady state condition were not fulfilled, following the test proposed by Foken and Wichura (1996).

u* was used as a criterion to ensure well developed turbulence. u* thresholds were calculated for each year of measurement using u* and NEE nighttime data as described by Aubinet et al. (2012). Selected thresholds were 0.13 for 2012, 0.15 for 2013 and 2014, 0.16 for 2015. Data recorded during weak mixing condition (u* < u* threshold) were excluded from the analysis.

The contribution of the forest area around the tower to the EC measurements (fetch area) was evaluated according to Hsieh et al. (2000). Peak distance from measuring point to the maximum contributing source area outreached 80 m and 2 km up-wind from the tower during unstable and stable conditions, respectively. Data recorded when fetch area included cover types other than forest (peak distance from the measuring point to the maximum contributing source area > 400 m) were discarded.

Instrument detection limit was estimate for each half-hour as the root mean squared error of the covariance from zero in a range of ±30 - ±90 seconds away from the real lag, where it can be assumed that the w and x are no longer correlated (Langford et al., 2015). Half-hour fluxes below corresponding detection limit were considered not significantly different from zero.

A detailed explanation of the EC technique and quality assurance methods can be found in Foken (2008) and Aubinet et al.(2012).

2.2.2 *Inverse Lagrangian technique to evaluate source / sink distribution within the forest canopy*

The inverse Lagrangian technique (ILT) allows to derive the vertical source / sink distribution of a gas within the canopy from the turbulence structure inside the canopy and the concentration of the gas measured along a vertical profile.

It is based on the "localized near field theory" (Raupach, 1989). The model assumes a relation between the source (or sink) magnitude associated to a layer (S) and the gas concentration measured in the same layer (X). This relation is made explicit by a dispersion matrix (D) that accounts for the concentration contribution due to the gas diffusion within the canopy, determinates by turbulent transport of the order of the canopy height (h_c) or larger (*far-field effect*), and the gas persistence inside the canopy (*near-field effect*), which in turn depends on eddies smaller that h_c. The *near field effect* dominates if the travel time of a gas is small than the Lagrangian time scale (T_L), where

$$T_L = 0.3\, h_c\, u^* \qquad (12)$$

The relation can be express as:

$$X - \tilde{X} = DS \qquad (13)$$

where $\tilde{X}$ represents a concentration offset that is independent from S, and

$$X = X^{near} + X^{far} \qquad (14)$$

Given the above, the *far-field* contribution can be expressed as:

$$X_i^{far} = X(z_{ref}) + \int_{z^x}^{z_{ref}} \frac{F_x(z)}{K_H(z)} dz \qquad (15)$$

where $F_x(z)$ is the gas vertical flux at height z:

$$F_x(z) = F_g + \int_0^z S(z)\, dz \qquad (16)$$

where F_g is the ground flux (at z=0)

K_H is the diffusion coefficient:

$$k_H = \sigma_w^2 T_L \quad (17)$$

where σ_w is the standard deviation of the vertical wind component.

The *far field effect* dominates if the travel time of a gas is larger than T_L, so that:

$$X_i^{far} = \int_0^{\infty} \frac{S(z)}{\sigma_w(z)} \left[k_n \left(\frac{z_i^X - z}{\sigma_w(z) T_L(z)} \right) + k_n \left(\frac{z_i^X + z}{\sigma_w(z) T_L(z)} \right) \right] dz \quad (18)$$

How presented integrals may be turned into finite sums can be found in Nemitz et al. (2000).

2.2.3 *Resistance modelling of O_3 deposition*

A common model to represent O_3 uptake processes is the resistance analogy, where the individual strength of a sink is quantified using a resistance scheme (fig 2.2). First proposed by Hicks et al. (1987), the model consider a sink flux proportional to the difference in gas concentration between two locations, divided by the transfer resistance.

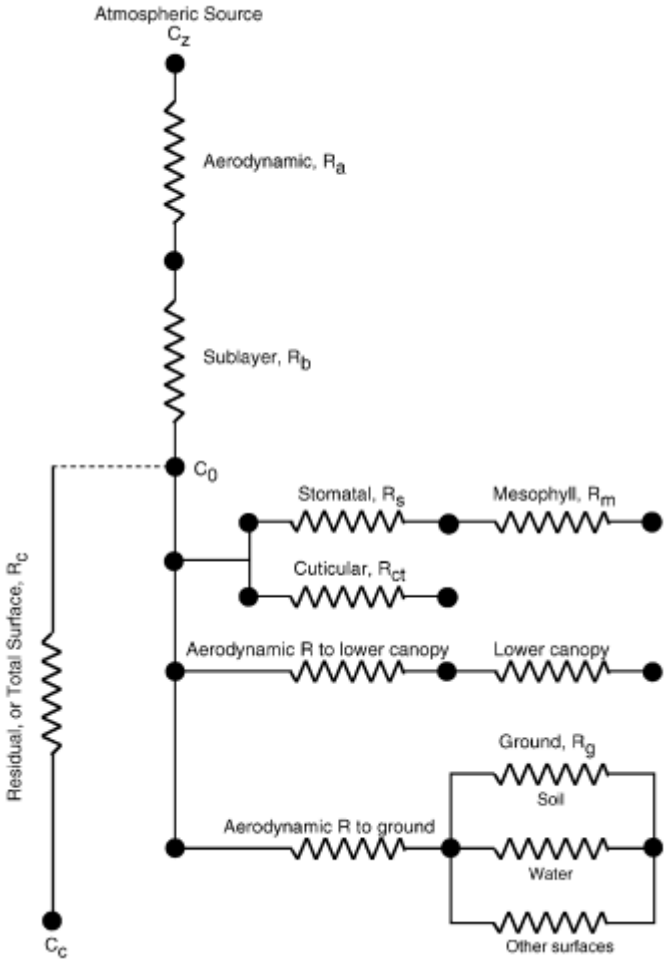

Figure 2.2 Resistance deposition model for O_3, from Wesely and Hicks (2000). C_z is the concentration at height z; C_0 is the concentration at z_0, C_c is the canopy concentration, R_a is the aerodynamic resistance at height z, R_b is the canopy boundary layer resistance, R_s is the stomatal resistance, R_{ct} is the cuticular resistance, R_m is the mesophill resistance, R_g is the ground resistance, R_c is the total canopy resistance, which would replace the right side of the scheme.

Gas deposition velocity (V_d) is computed in analogy to Ohm's law in electrical circuits:

$$V_d = R_a + R_b + R_c \tag{19}$$

Below, a brief description of the different resistances and their calculation.

Aerodynamic resistance

The aerodynamic resistance (R_a) describes the turbulent transport between z and z_0. R_a can be estimated as (Garland, 1977):

$$R_a(z-d) = \frac{u(z-d)}{u^{*2}} - \frac{\Psi_H(\zeta)-\Psi_M(\zeta)}{ku^*} \tag{20}$$

where Ψ_H and Ψ_M are stability correction for heat and momentum respectively, they are function of ζ and can be calculated as follow (Paulson, 1970):

for stable conditions ($\zeta > 0$):

$$\Psi_M(\zeta) = \Psi_H(\zeta) = -5/2\,\zeta \quad (21)$$

for unstable conditions ($\zeta < 0$):

$$\Psi_M(\zeta) = 2ln\left(\frac{1+x}{2}\right) + ln\left(\frac{1+x^2}{2}\right) - 2tan^{-1}(x) + \frac{\pi}{2} \quad (22)$$

$$\Psi_H(\zeta) = 2ln\left(\frac{1+x^2}{2}\right) \quad (23)$$

$$\text{where } x = (1 - 16\zeta)^{1/4} \quad (24)$$

Canopy Boundary layer resistance

The canopy boundary layer resistance (R_b) describes the transport trough the quasi-laminar sub-layer (Owen and Thomson, 1963) and depends on the molecular diffusivity of the gas (D_x).

$$R_b = (Bu^*)^{-1} \quad (25)$$

where B is the Stanton number that can be calculated after Garland (1977):

$$B^{-1} = 1.45Re^{0.24}Sc^{0.8} \quad (26)$$

where Re is the Reynold number (z_0u^*/v_a), where v_a is the kinematic viscosity of air, Sc is the Schmidt number (v_a/D_x).

Canopy resistance

Considering the gas uptake process happen at a unique height (z_0), the canopy resistance (R_c) is calculated as the difference between Ra+Rb and the total resistance:

$$R_c = -\frac{X(z-d)}{F_x} - R_a - R_b \quad (27)$$

where X is the gas concentration and F_x is the measured flux. Thus, R_c is inferred by measurements. R_c includes all the resistances for deposition on all canopy elements (stomata, cuticles and soil).

Stomatal resistance

If transpiration is the only source of water-vapour from the canopy surface, stomatal resistance to water vapour (R_s) can be estimated by EC measured evapotranspiration using the evaporative/resistance method (Thom, 1975):

$$R_s = \frac{cp\,\rho\,(q_a - q_s(z_0))}{\gamma\,\lambda\,E} \quad (28)$$

where q_a is vapour pressure at z-d (kg kg^{-1}), q_s is the saturation mass fraction of H_2O at air temperature (kg kg^{-1}), γ is the psychrometric constant (4.08 ×10^{-4} K^{-1}), λ is the vaporisation heat for H_2O (2.5 × 10^6 J kg^{-1}), E is the measured latent heat flux (kg m^{-2} s^{-1}).

This algorithm is based on the assumption that the gas diffusion inside the stomata is completely drive by Fick's law, i.e. molecular diffusion. The small dimension of stomata prevent gas turbulent motion, justifying this assumption (Gerosa et al., 2007).

In this work, R_s was used to calculate stomatal conductance to O_3 (G_{O3}), calculated as the inverse of R_s, multiplied for 0.61, which is the difference in diffusivity between O_3 and H_2O (Massman, 1998). G_{O3} was multiplied to O_3 concentration at the canopy level to calculate the O_3 stomatal flux. O_3 concentration at the canopy level was calculated as:

$$O_3\ canopy = \frac{[O_3]R_c}{R_a + R_{bO3} + R_c} \quad (29)$$

where R_{bO3} is the boundary layer resistance to O_3.

Soil resistance

Soil resistance includes in-canopy aerodynamic resistance (R_{ac}) and ground resistance (R_g). R_{ac} depends on *hc* and *LAI*, its formulation after Erisman et al. (1994) is:

$$R_{ac} = \frac{14\ LAI\ h_c}{u^*} \quad (30)$$

R_g depends on soil water content (swc, %) and is calculated following Zhang et al. (2002) as:

$$R_g = R_{g1} + R_{g2}\frac{swc_{10}}{swc_{fc}} \quad (31)$$

where R_{g1} and R_{g2} are constant resistances (200 and 300 s m^{-1}, respectively), swc_{10} is the swc measured at 10 cm depth, swc_{fc} is the swc at field capacity (28 %), calculated as the maximum value of swc_{10} after precipitation events (Fares et al., 2014).

R_g was used to calculate the soil O_3 deposition fraction, multiplying the inverse of R_g for the O_3 concentration measured at the soil level.

Cuticular resistance

Cuticular resistance (R_{ct}) depends on the leaf wetness and is calculates following Zhang et al. (2002), assuming that the gas concentration just above the cuticles is negligible.

$$R_{ct\ (dry)} = \frac{R_{ct\ (dry)0}}{e^{0.03RH} LAI^{1/4} u^*} \quad (32)$$

$$R_{ct(wet)} = \frac{R_{ct(wet)0}}{LAI^{1/2} u^*} \quad (33)$$

where $R_{ct(dry)0}$ and $R_{ct(wet)0}$ are constant values (6000 and 400 s m^{-1}, respectively) suggested by Zhang et al. (2002) and RH is the relative humidity of air (%). Wet condition are assumed when RH > 60%(Fares et al., 2014). R_{ct} was used to calculate the cuticles O_3 deposition fraction, multiplying the inverse of R_{ct} for the O_3 concentration at the canopy level.

2.2.4 Measurements and instrument set-up

Meteorological variables were measured at 1-minute resolution in proximity of the canopy level (15 m), onto a 20 m high tower. The instrumentation included a Davis vantage pro meteorological station (Davis Instruments Corp. CA, USA) used to monitoring relative humidity (*RH*, %), air temperature (*T air*, °C), global solar radiation (*rad*, Wm^{-2}), UV radiation (280-360 nm, *UV*, Wm^{-2}) and precipitation (*prec*, mm). Instantaneous three-dimensional wind velocity (*u*, *v*, *w*, ms^{-1}) and direction (*winddir*, °) were measured with a sonic anemometer (Windmaster 3d Anemometer, Gill Instruments Limited, UK). Photosynthetic photon flux density was measured with a LI-190 Quantum sensor (LI- COR, Licoln, NE, USA), soil humidity (RH_{soil}, %) and temperature (*T soil*, °C) were measured by a Vaisala 102 HUMICAP

180 capacitive relative humidity sensor (HMP45C, Campbell Scientific) at a single point (10, 50, 100 cm depth) inside of the flux footprint. Data collection was performed by a datalogger (CR3000, Campbell Scientific, Shepshed, UK).

O_3 concentrations were measured using a UV photometric O_3 analyser (49i, Thermo Scientific), with a precision of 0.5 ppb.

NO and NO_2 concentrations were measured by a chemiluminsescent analyser (42i, Thermo Scientific), with a precision of 0.4 ppb.

VOCs were measured with a proton-transfer-reaction mass-spectrometer (PTR-MS, Ionicon Analytik GmbH) which was located in an air-conditioned cabinet next to the tower. During measurements, gas standards were measured every 24 hour to calibrate the instrument.. 23 compounds were measured, between them: isoprene, monoterpenes, and their oxidation products (BVOCs), methanol, acetaldehyde, acetone (OVOCs) acetonitrile, benzene, hexenal, toluene and xylenes origin (AVOCs).

O3, NO_x and VOC were sampled through a 5-level vertical profile. Measurement heights were 19.7 m (above canopy), 14.9 m (canopy level), 12 m , 7 m (within the canopy) and 2.4 m (below canopy). Air was sampled using separate sampling lines (20-m long Teflon tubes, with 4-mm inner diameter) through which air flowed continuously to avoid any memory or surface effects. To avoid contamination and flow problems, Teflon filters (PFA holder, PTFE membrane, 2 μm pore size) were installed at the sampling inlets and replaced every two weeks. A custom- made valve system sampled ozone sequentially for 6 min at each measuring height. Data collection and sampling system control were performed using a data logger (CR3000, Campbell Scientific, Shepshed, UK).

Concentrations measurements for fluxes calculation were performed at 10 Hz. Air was sampled continuously at 19.7 m height near the sonic anemometer.

CO_2 and H_2O concentrations were measured by a closed path infrared analyser (LI-7200, Li-Cor, Inc., Nebraska, USA), CH_4 concentration was measured by an open path gas analyser (LI-7700, Li-Cor, Inc., Nebraska, USA).

O_3 measurements were made by chemiluminescence using coumarin dye with a custom-made instrument developed by the National Oceanic and Atmospheric Administration (NOAA, Silver Spring, MD, Bauer and Hultman, 2000). The chemiluminescence signal was calibrated against 30-min average O_3 concentrations from the UV O_3 monitor.

10 Hz data were stored in a datalogger (LI- 7550, Li-Cor, Inc., Nebraska, USA), divided into half-hour files.

An additional EC tower, 2.4 m height, were placed below the canopy. There, O_3 measurements were performed using a dry chemiluminescence Rapid Ozone Flux Instrument (ROFI Mk2; Muller et al., 2009), H_2O and CO_2 were measured by a close path infrared gas analyser (LI-7000, Li-Cor, Inc., Nebraska, USA) and wind velocity were measured using a sonic anemometer (RM Young 81000, RM Young Company, Michigan, USA). Measurements were logged at 10 Hz into a datalogger (CR 3000, Campbell Scientific, Shepshed, UK).

2.3 Statistics

Kolmogorov-Smirnov test (KS test) was used to test normality for all considered variables. According to the test results, parametric or non-parametric statistics were chosen. One-way ANOVA (parametric) or Kruskal-Wallis (non-parametric) tests were used to compare means. When differences were found, a post-hoc test was performed in order to evaluate which group differs from others.

2.3.1 Multiple Linear Regression

The attempt of multiple liner regression (Pearson and Lee, 1908) is to infer the relationship between several independent continuous variables (predictors) and a dependent variable. This relationship is represented as a linear equation:

$$y_i = \beta_1 \cdot x_{1i} + \cdots + \beta_n \cdot x_{ni} + \varepsilon \qquad (34)$$

where y is the dependent variable, $x_{1...n}$ are the predictors, $\beta_{1...n}$ are the coefficients associated to each predictor and ε is the intercept. β is the expected change of y for unit change of x, ε is the prediction of the model if all x values were set to zero.

In this work, multiple regression was used to develop two empirical models to gap-fill forest soil level H_2O and O_3 fluxes. Dataset was split into two subset. Randomly selected 70% of the dataset was used to build the models and then cross-validated with the remaining 30% of the data (chapter 4).

Different predictor values were tested trough step-wise regression, which was used to extract the best subset of predictor variables for use in the forecasting models. This technique successively adds or removes variables based on the t-statistics of their estimated coefficients. This coefficients where estimated using the least square approach, i.e., setting coefficients and intercept equal to the values that minimize the sum of squared errors within the sample of data to which the model is fitted.

Predictor variables tested by step-wise regression were: soil humidity and soil temperature measured at 10, 50, 100 cm depth, friction velocity above canopy and at soil level, air temperature above canopy and at soil level, above canopy H_2O fluxes (just for soil level H_2O flux modelling) above canopy O_3 fluxes (just for soil level O_3 flux modelling)

Multiple linear regression technique is subjects to a series of assumptions: predictor variables are assumed to be error-free, that is, not contaminated with measurement errors (*weak exogeneity*), the relation between the dependent variable and predictor should be linear (*linearity*), predictors must have the same variance in their errors, regardless of the values of the predictor variables (*homoscedasticity*), errors must be randomly distributed (*independence of errors*) and predictor must not be highly correlated each other (*lack of multicollinearity*). The latter assumption was not fulfilled, this can make some variables statistically insignificant when they should be significant, so that the model was not use to infer functional relationships between predictors and dependent variables, but just to fill data gaps, when present.

2.3.2 *Partial Least Squared Regression*

Partial Least Square (PLS) regression is a multivariate technique that combines features from principal component analysis (PCA) and multiple linear regression, and is useful when predictors are highly correlated or even collinear. PLS generates linear combinations of the original predictors (components), which best explain the variance among parameters and maximize covariance between predictors and the dependent variable. These new components, generate from both predictors and dependent variables, are no longer correlated and became the new predictors variables.

The contribution of the original variables to each components can be inferred by the associated weight. The weights interpretation is easy since the sum of the square of the weight within the component yields to 1. This property allows the partition of the variance explained by the model between the original variables.

Before performing the analysis datasets must be centered to have mean 0 and scaled to have standard deviation 1, to avoid scale influence on results. Number of components used by the model is chosen as the number of components which performed lower mean square error, calculated using k-fold cross-validation. This procedure divides dataset into k disjoint subsamples, chosen randomly but with roughly equal size, avoiding model overfitting.

In this work, PLS regression was used to infer functional relationships between environmental parameters and CH_4 flux measured above canopy (chapter 3) and to explore the interactions between stomatal O_3 uptake with NEE (chapter 4).

2.3.3 *Singulars Spectrum Analysis*

Singular Spectrum Analysis (SSA) is a non-parametric technique that decomposes a time series into a set of additive components, which are (i) a trend, (ii) a set of periodic series and (iii) a random noise (Golyandina et al., 2001). The sum of these components is the original time series. SSA results depends on the windows length chosen for the analysis.

SSA consists of two complementary stages: decomposition and reconstruction. Both stages include two separate steps, which are the follows:

Step 1. Embedding

Let Y being a time series of length n, L the window length, an integer with $2 < L < N$. The first step transfers the one-dimensional time series Y into the multi-dimensional series X (trajectory matrix). Columns of X represent all the possible position of the window L, so that $K = n – L + 1$ is the number of columns. X is a Hankel matrix, i.e. all elements along the diagonal are equal.

Step 2. Singular values decomposition of the trajectory matrix:

The second step computes the eigenvalues and eigenvectors of the matrix X, which is decomposed in d-rank one elementary matrix where d is the number of non-zero eigenvalues in decreasing order.

Step 3. Reconstruction:

In the third step, each matrix obtained by the step 2 is transformed through averaging over the diagonals (Hankelization).

Step 4. Grouping:

The last step reconstructs a one-dimension matrix, expresses as the sum of the trajectory matrices corresponding to each partition.

A detailed description of the SSA algorithms can be found in Golyandina et al. (2001)

The principal advantage of SSA with respect to other decomposition algorithms is that is not necessary to make any statistical assumptions such as stationarity of the series or normality of the residuals.

In this work, SSA was used to extract the sinusoid series corresponding to the daily dynamic from the environmental parameters time series (chapter 5). This was done because most of the environmental parameters are completely driven by the daily course, which makes them mutually correlated.

2.3.4 Feed Forward Back-Propagation Artificial Neural Network

Artificial Neural Network (ANN) were initially developed with the intent of create an artificial system to reproduce mammalian brain (Olden et al., 2004). Can be defined as a parallel processor composed by simple processing elements (neurons) connected by communication channels, with the capacity of storing knowledge (Papale and Valentini, 2003). Each neuron have small amount of local memory and works on the input they received via communication channels.

ANNs are very powerful in analysing and modelling non-linear relationships because of their capacity of learn from examples and generalize.

A training dataset composed by input and the relative output is necessary to adjust neurons weight and connections. It is important to scale the dataset, i.e. between 0 and 1, to avoid any scale influence on results. In this work, ANNs were trained by feed forward back-propagation algorithm (Rumelhart, 1986): information flows unidirectionally trough the network and the errors ANN makes using the training set to model the output are used to adjust neurons weight and connections strength. Datasets is split randomly into three subset, training, test and validation sets. Training subset is used to compute the weights of the network's neurons, the test subset for stopping the training process checking the model generalization ability. Last subset is used to validate the model.

ANNs were organized in three layer: an input layer, an hidden layer and an output layer (fig. 2.3). The optimal number of neurons in the hidden layer was determined by comparing the performance of different cross-validated networks, with 1 – 4 hidden neurons, and choose the number that produced better network performance.

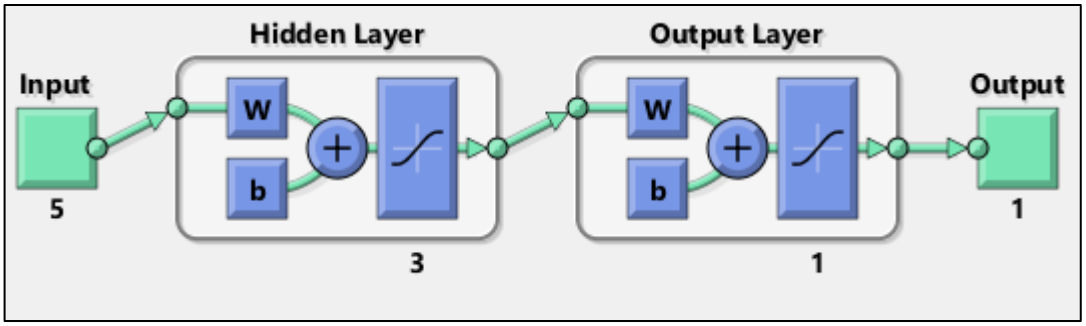

Figure 2.3 Example of an ANN structure. Input layer is composed by 5 neurons, hidden layer by 3 neurons and the output layer by 1 neuron. w is the neuron weight, b is the bias.

Once the network in trained, weights and connections are established and ANN can simulate the output when input are provided. Each input is multiplied by the respective weight assigned to its connections and arrives to the neuron in the hidden layer. There, this information is summed with the other arriving from the other input, and transformed by an activation function. Information is then transferred to the output layer, where again it is multiplied by connection weights and transformed by the activation function, to be converted into the final result (output).

ANNs are often treated as "black box" because is not possible to extrapolate equations which explain the mechanisms that occur within the network. However, some algorithms have been proposed to overcome this issue, and the relative importance of each input variable can be evaluated. Gevrey et al. (2003) and Olden et al. (2004) provide a comparison of the different methods for estimating variables importance in ANN applications, in this work, three of the existing methods were applied:

Partial derivatives method (Dimopoulos et al., 1995) :

This method produced a profile of the output variations for changes of each input variable. The link between the variation of the output and the modification of the input is the partial derivative of each activation function with respect to its input.

Given an ANN with n_i inputs, one hidden layer with n_j neurons and one output, where logistic sigmoid function is used for activation, the partial derivatives of the output with respect to one input are (Gevrey et al., 2003):

$$d_{ji} = S_j \sum_{h=1}^{n_h} w_{ho} I_{hj} \left(1 - I_{hj}\right) w_{ih} \quad (35)$$

where S_j is the derivative of the output with respect to its input, I_{hj} is the response of the h hidden neuron, w_{ho} is the weight between the output neuron and the h hidden neuron, w_{ih} is the weight between the h hidden neuron and the i input neuron.

The advantage of this technique is that a profile of each input variable can be analysed without altering its magnitude, that is without producing artefacts. The weakness of this technique is that it provides information on one input at time and does not show the interaction between inputs (Gevrey et al., 2006).

Connection weights approach (Olden and Jackson, 2002):

This method splits the connection weights (hidden layer and output layer) into components associated with each input neuron and sums the products across all the layer to establish importance ranks.

$$importance_i = \sum_{h=1}^{n} w_{ih} w_{ho} \quad (36)$$

where w_{ho} is the weight between the output neuron and the h hidden neuron, w_{ih} is the weight between the h hidden neuron and the i input neuron.

This algorithm was recognized to have the best ability to correctly identify input importance in neural networks by Olden et al. (2004), which compared the existing algorithms using Monte Carlo simulations, i.e. using data with known numeric relationships.

Perturb method (Gevrey et al., 2003)*:*

This method is a sensitivity analysis that assesses the effect of small changes in one input on the network's output. One of the input is increased in steps of 10% up to 50% of the original value, while keeping all the others input unchanged.

The major disadvantage of this technique is a single input is perturbed at time, ignoring interactions between factors. Moreover, this kind of manipulation may create combination of factors that are very unlikely to occur in the real world, e.g. high O_3 and low radiation, high radiation and low temperature, etc.

3 Carbon balance at the forest

This chapter reports research findings on the carbon exchanges at the forest. Specifically, it is focalized on CO_2 and CH_4 responses to environmental and physiological parameters, focusing on processes involved.

3.1 CO_2 exchange at the forest

CO_2 fluxes were measured over 4 years above the forest canopy, using the EC technique. An additional EC instrumentation was placed 2 m above the forest soil to evaluate the CO_2 flux soil component.

Part of this section is based on results reported in: Canfora, Di Bene, Savi et al., *Evaluating factors influencing soil microbial communities and CO_2 exchanges in a Mediterranean Holm oak forest*, submitted to Environmental Monitoring and Assessment.

3.1.1 CO_2 fluxes and their dependence from meteorology and phenology

CO_2 absorption at the holm oak forest occurred almost during all year (fig. 3.1a). CO_2 exchange trend followed phenology phases. Recurring patterns linked to meteorology were observed along the 4 years of measurements (fig. 3.1b). From January to April, forest CO_2 uptake increased in parallel with air temperature. During that period, water availability was high and daily uptake grew linearly. When Spring began, new stems and roots developed. The carbon cost of synthesize new tissues led to a rapid decrease of CO_2 assimilation and to an increase of autotrophic respiration during the second part of April. Afterwards, when new tissue started to photosynthesize, the forest CO_2 uptake grew again. Highest CO_2 uptake was recorded between May and June (up to 30 g CO_2 m^{-2} day^{-1} in May 2012). Summers marked a strong reduction of precipitation, while temperature still increase: stomatal conductance decreased to limit transpiration, leading to a decline in photosynthesis rate. CO_2

uptake reached the lowest values of the Summer season at the end of August 2013, when rain events were recorded after a dry and hot period. The decrease is probably due to soil microfauna activity. Microorganisms responded quickly to the new condition of water availability, decomposition rate increased and CO_2 was released by forest soil. At the end of September, some leaves became senescent and fell, thickening the litter carpet. Photosynthetic surface decreased as the daylight hours, while mild temperature still supporting decomposition activity. Last two weeks of November were the only period during which forest was a net source for CO_2.

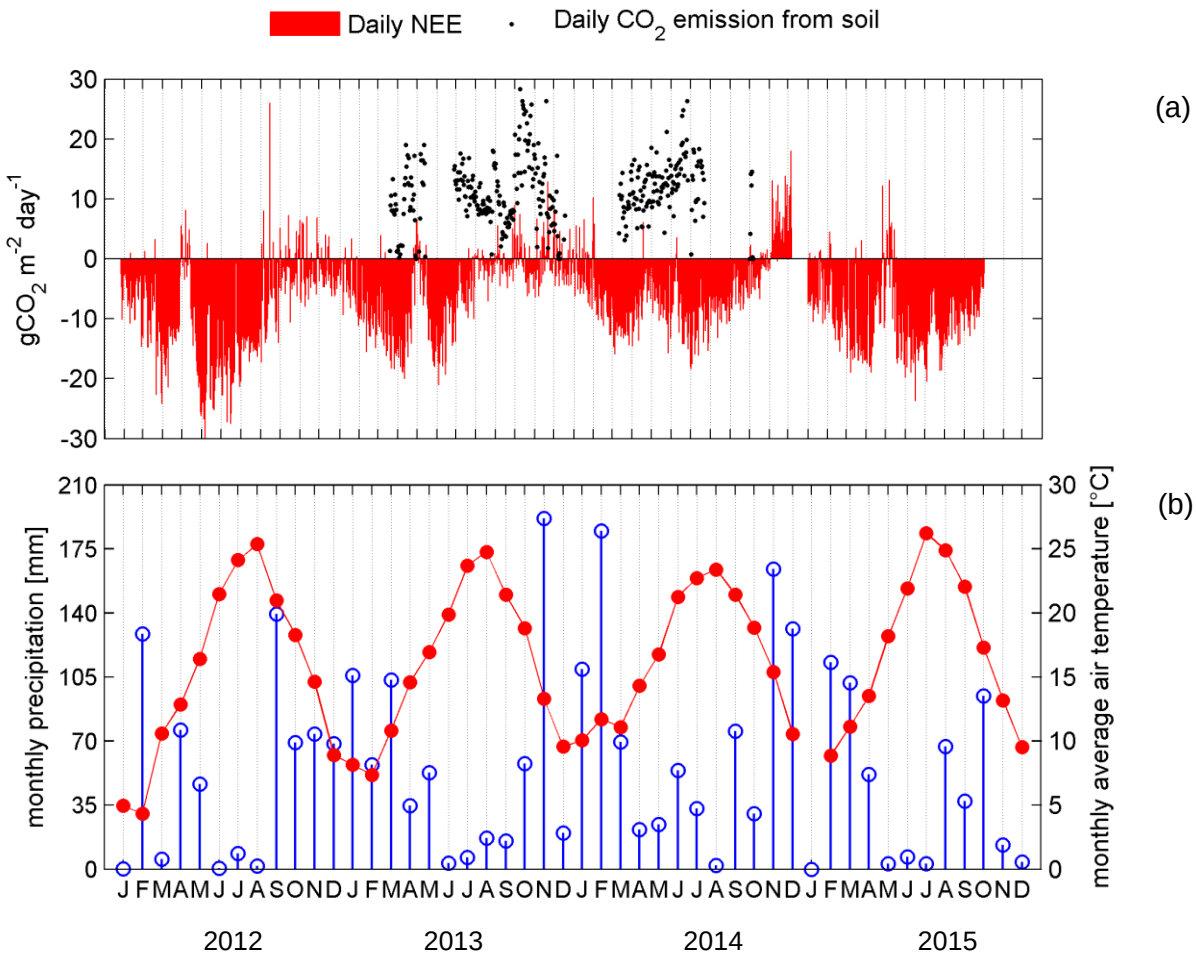

Figure 3.1 (a) daily CO_2 exchange recorded above (red bars) and below canopy (black markers, $gCO_2\,m^{-2}\,day^{-1}$); (b) monthly precipitation (blue bars, mm) and monthly mean temperature (red markers, °C), 2012 – 2015.

The Holm oak forest is a persistent CO_2 sink, although differences between the years were recorded. Figure 3.2 shows the annual NEE for 2013 and 2015. 2012 and 2014 NEE is not reported because of large gaps occurring in the dataset.

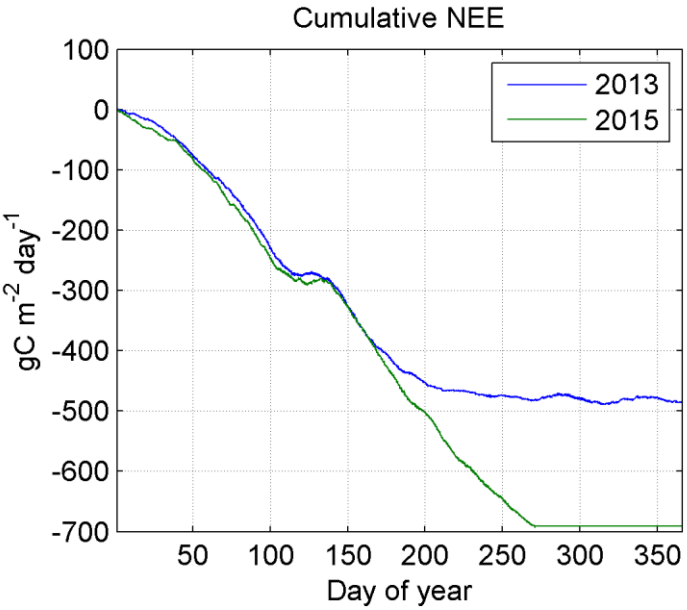

Figure 3.2 Cumulative NEE for 2013 and 2015 (g C $m^{-2}time^{-1}$).

C uptake rates were similar in the first part of the year and started to differ from the beginning of Summer (around June 15th). This divergence was due to differences in water availability during the dry seasons (27.2 and 87.4 mm recorded between June and August in 2013 and 2015 respectively).

3.2 CH_4 exchanges at the forest

Methane (CH_4) fluxes in a Mediterranean Holm oak (*Quercus ilex* L.) forest were measured over 19 months, from October 2012 to May 2014, using EC technique. EC measurements where complemented by periodic soil chambers measurements and one microbiological characterization of CH_4-cycling microorganisms along soil vertical profile (0-100 cm depth). Chambers measurements and microbiological analysis were carried out by project partners, results are discussed within this thesis.

This section is based on the paper: Savi et al., *Environmental and biological controls on CH_4 exchange over an evergreen Mediterranean forest*, accepted for publication by Agricultural and Forest Meteorology.

3.2.1 CH_4 mixing ratio above the forest

CH_4 mixing ratio measured above forest was on average 2.21± 0.27 (standard deviation) ppm during the study period, ranging from 0.23 to 7.19 ppm. CH_4 mixing ration was influenced by the proximity of the city of Rome: the mean value was about 10 % higher than the global background (around 1.8 ppm, Bian et al., 2016)and higher mixing ratio was recorded when the wind blew from N-NE, corresponding to air masses coming from the city (fig 3.3).

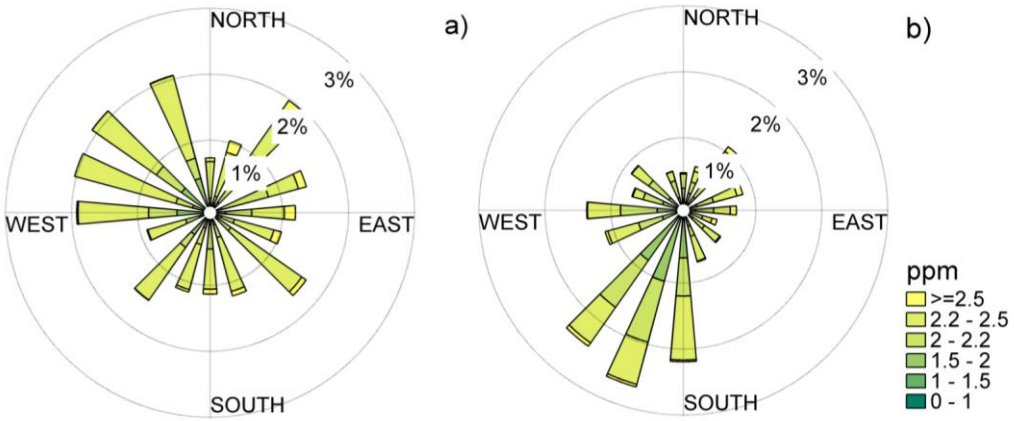

Figure 3.3 Wind roses of Autumn-Winter (a) and Spring-Summer (b) wind directions and CH_4 mixing ratio (ppm). The frequencies at which the wind blew from each direction is represented by the radial thickness of each slice, while CH_4 mixing ratio is representing by the colour of the filled area. Data recorded from October 2012 to May 2014.

CH_4 mixing ratio showed a diurnal trend (fig. 3.4), linked to the boundary layer dynamic: it accumulated in the shallow boundary layer during night and diluted after sunrise, when boundary layer height raised up (Culf et al., 1997).

Higher CH_4 mixing ratio was recorded in Winter and Autumn (Fig 3.4) as the results of different wind regimes at the site (wind blowing prevalently from the inland carrying air

masses rich in CH_4 during Winter and Autumn and blowing from the sea during Spring and Summer).

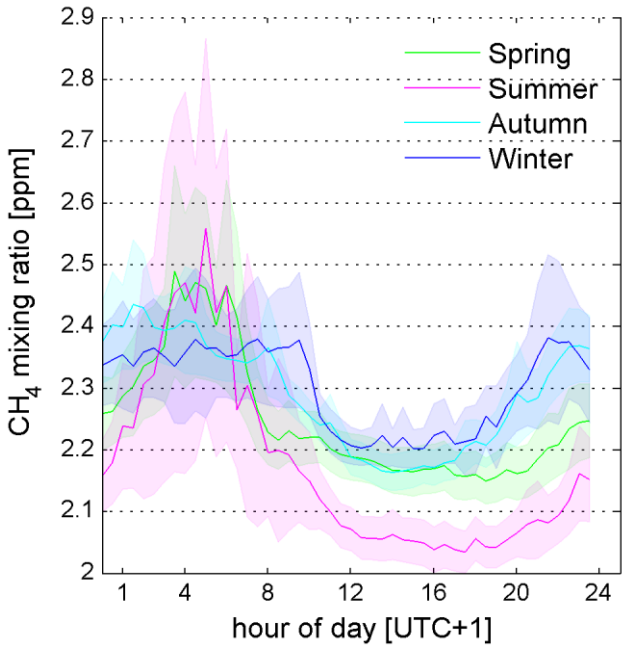

Figure 3.4 Daily course of above canopy CH_4 mixing ratio (ppm). Lines are mean values, filled area represents 95% confidence interval for the mean.

3.2.3 CH_4 fluxes above the forest

CH_4 fluxes measured during the study period were highly variables in magnitude and direction, causing the switching of the ecosystem from source to sink in a short period of time. Although averaging CH_4 fluxes over the whole study did not produce values statistically different from zero (averaged CH_4 fluxes ± standard deviation: $-6.4 \times 10^{-4} \pm 0.06$ μmol $m^{-2}s^{-1}$), a clear pattern emerged looking to the mean diurnal evolution (fig. 3.6) and through 30-day running averaging (fig. 3.5).

Considering the mean diurnal evolution presented in figure 3.6, the experimental site switched from sink to source between night and day (uptake values up to -0.019 μmol $m^{-2}s^{-1}$, release up to 0.014 μmol $m^{-2}s^{-1}$). On a seasonal scale, net uptake was observed during winters, while a net emission was observed in late Spring and Summer (fig. 3.5), so that deposition occurred during the cold wet season while emission occurred during the dry hot season.

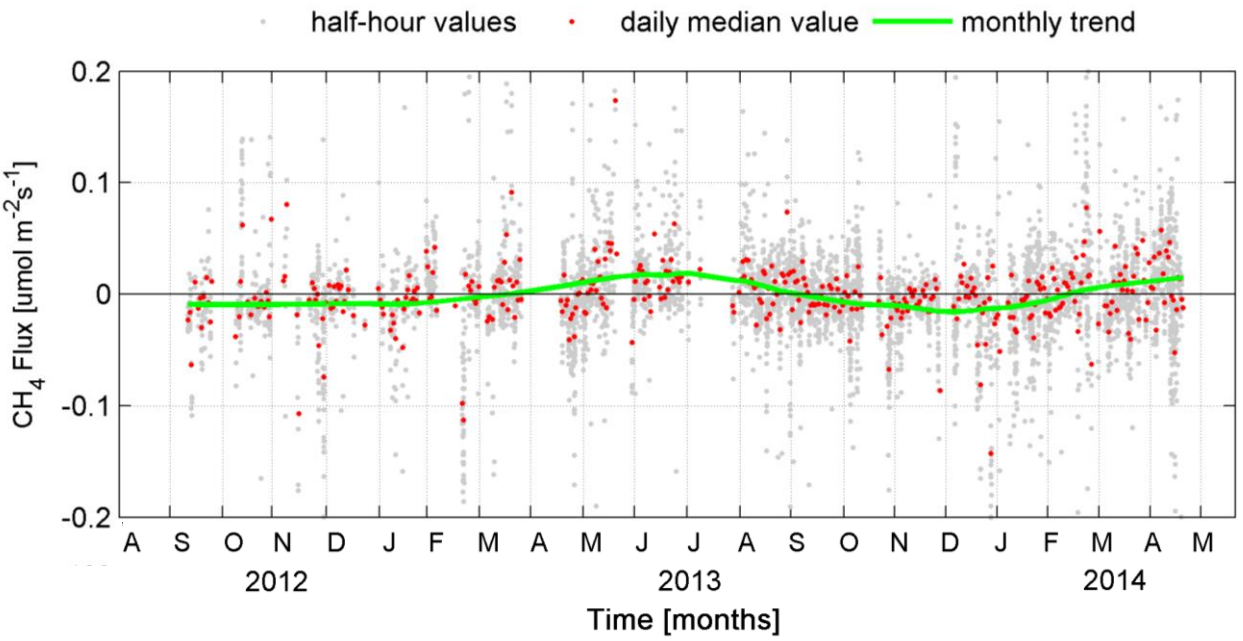

Figure 3.5 Dynamic of CH_4 fluxes above canopy (grey dots: half-hour fluxes, red dots: daily average, green line: 30-day smooth running mean)

Estimate of the effects of EC corrections and filtering procedures on measured CH_4 fluxes

Corrections and filtering procedures highly affected CH_4 fluxes. Especially, WPL correction was higher than the raw CH_4 flux itself almost all the time and completely removed the diurnal signal from the raw data (fig. 3.6). In the case of open path systems, WPL correction is expected to be large because fluxes are measured in the presence of heat and water vapour fluxes, which bias raw measurements, and can be even greater when gas concentration is large with respect to the real flux (Denmead, 2008). Despite WPL correction is great for open-path instruments, it does not represent a problem for flux calculation as proved by Peltola et al. (2013), who compared the open-path LI-7700 performance with a dried and temperature-controlled close-path instrument (TGA-100A, Campbell Scientific Inc., USA). However, Peltola et al. (2013) reported an average WPL term of 103 %, given as percentages of the uncorrected raw covariance, while average WPL term in this study was 131 %.

After WPL correction, mean diurnal evolution of CH_4 fluxes is not significantly different from zero and no diurnal pattern is visible. The filtering procedure eliminates such

uncertainty, especially during night-time, when the forest behaved as a sink for CH_4, and during the central hour of day, when the forest switch to a moderate CH_4 source.

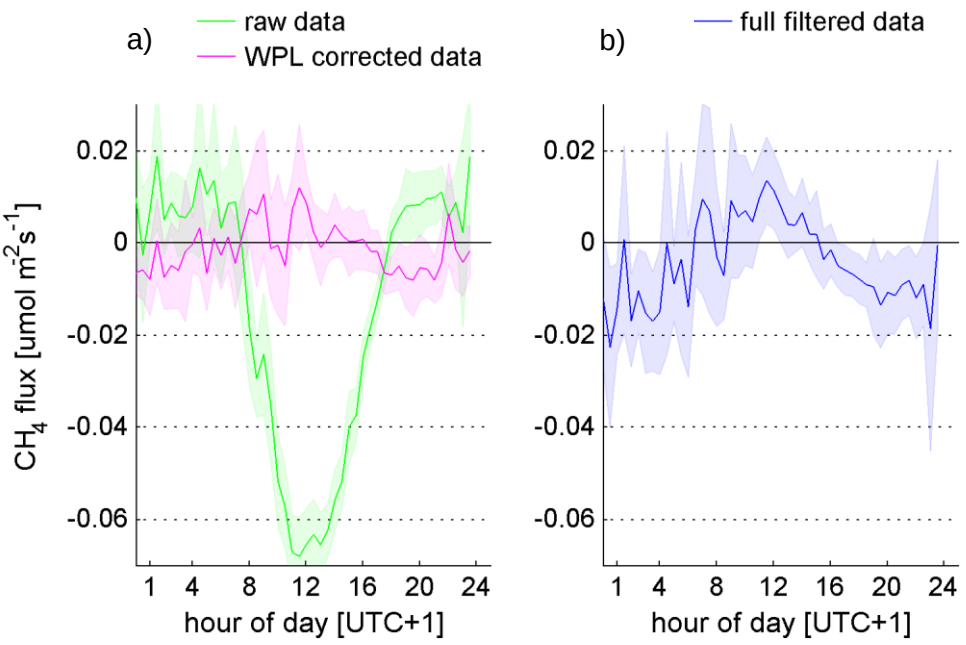

Figure 3.6 Daily distribution of raw, WPL corrected CH_4 fluxes (a) and fully filtered CH_4 fluxes (b).WPL correction includes correction for spectroscopic effects. Data were averaged over the whole study period, filled area represents 95% confidence interval of the mean.

The filtering procedure discarded 69 % of the original flux dataset. Percentages of rejected data associated to different filters and their distribution during the day are presented in figure 3.7. Turbulence was the parameter showing the most relevant impact on data exclusion (u* < u* threshold, fetch overlap non-forest area and stationarity filters). Less of 5 % of data were removed from the analysis when instrument diagnostic values, which indicates how clean are the mirrors of the instrument, were less than 20% (usually due to rain or sea salt spray deposition over instrument mirrors).

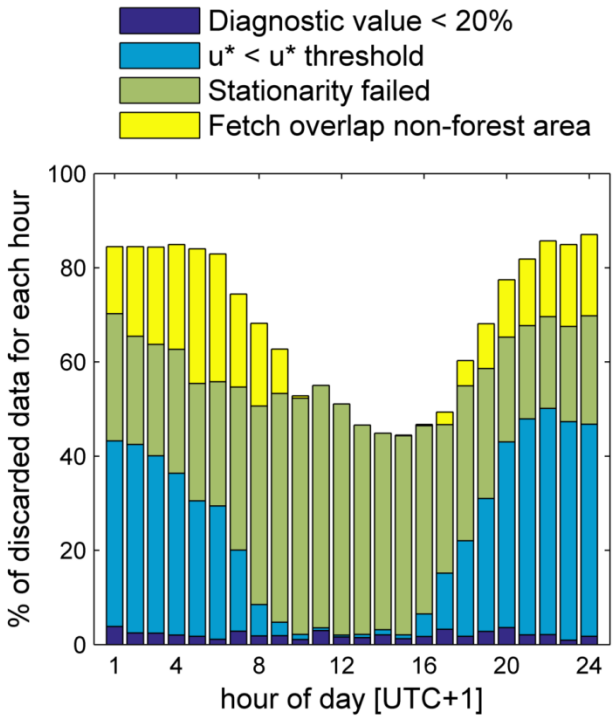

Figure 3.7 Daily distribution of above canopy CH_4 rejected data percentages associated to different filters. Filters were applied in the following order: diagnostic value < 20%, u < u* threshold, stationarity failed, fetch overlap non-forest area*

CH_4 gap-filling

2013 CH_4 flux dataset was gap-filled in order to estimate an annual budget of CH_4 exchange above the forest. Missing values were replaced using an ANN model (1-layer, 5 hidden neurons). Input variables included in the model were the day of the year, hour of day, friction velocity, latent heat flux, stomatal conductance, air temperature, air relative humidity, soil temperature, soil relative humidity, solar radiation and UV radiation.

The annual CH_4 budget resulting from the gap-filled dataset was -265.04 μmol $m^{-2}y^{-1}$, so that, annually, the ecosystem was a small sink for CH_4. The goodness of the gap-filling model, indicated as coefficient of determination (r^2), was 0.24. This value is derived by the fit between the model and observed CH_4 flux and does not account for the modelling error present at the gaps.

3.2.4 Environmental and biological controls on CH_4 exchange

PLS analysis was performed in order to test for relationships between all the environmental parameters and CH_4 fluxes at a time. Dataset was split in two (Spring / Summer and

Autumn/ Winter). This was done because the environmental variable influence over CH_4 fluxes may be considerably different between these two periods. Then, the analysis was performed over the original half-hour dataset and over the dataset averaged over daily scale. This was done in order to give the due importance also to the environmental variables that act over CH_4 fluxes with a time-lag, i.e. precipitation.

Precipitation (prec), global solar radiation (rad), UV radiation (UV), relative humidity (RH), vapour pressure deficit (vpd), soil temperature (soil T) and soil relative humidity measured at 10 cm depth (soil RH), air temperature (air T), wind direction (winddir), stomatal conductance (Gst), latent heat flux (LE) and friction velocity (u*) were included in the PLS model as potential drivers of CH_4 fluxes.

PLS results are summarized in tables 2, 3 (half-hour dataset), 4 and 5 (daily dataset), figure 3.8 shows the relative importance of each environmental predictor included in PLS models.

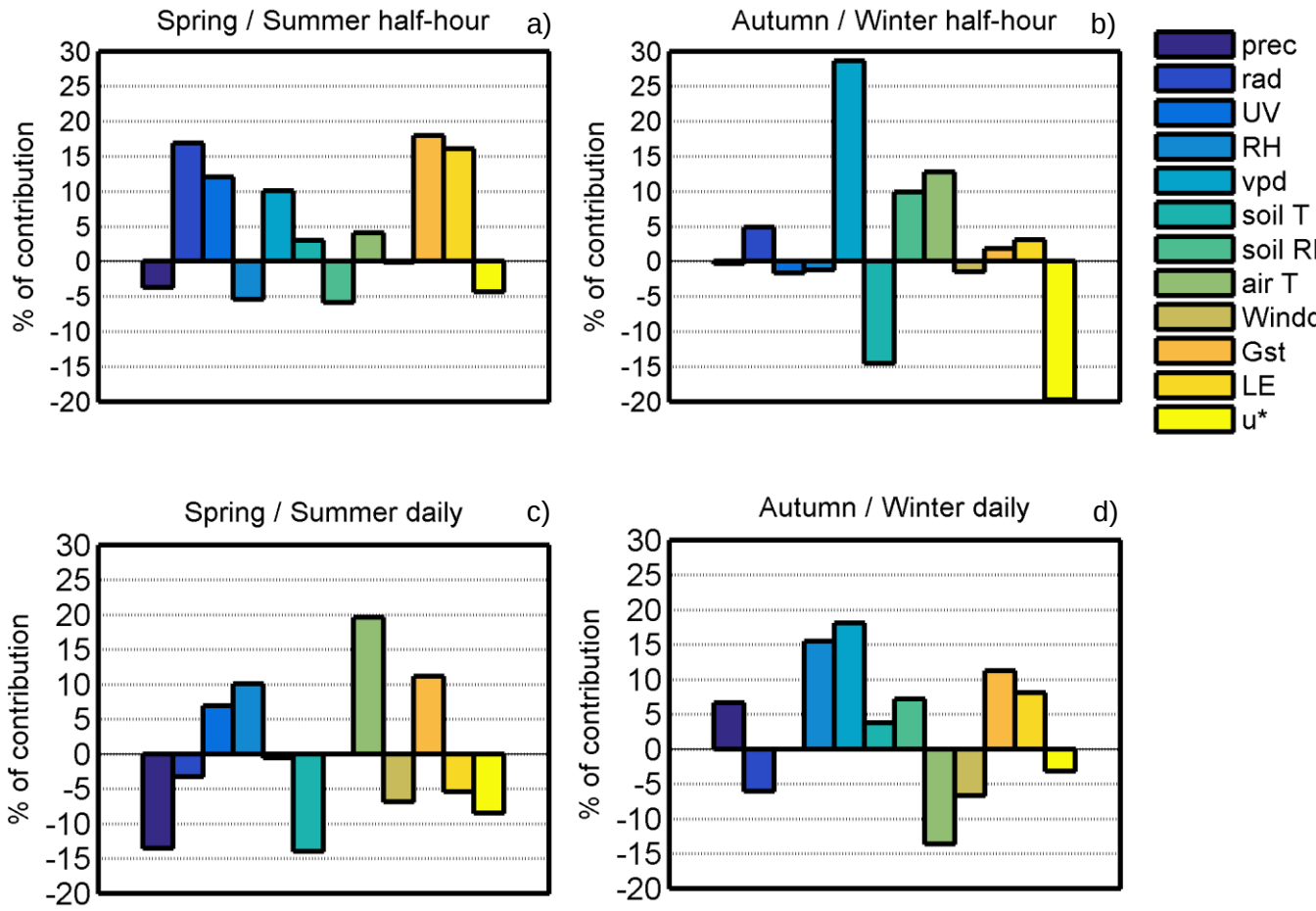

Figure 3.8 Relative importance (%) of each predictors within the PLS models. (a) PLS model performed over half-hour Spring / Summer dataset, (b) PLS model performed over half-hour Autumn / Winter dataset, (c) PLS model performed over daily Spring / Summer dataset, (c) PLS model performed over daily Autumn / Winter dataset.

Predictors	*Weights - Spring / Summer HALF-HOUR*								
	Comp1	Comp2	Comp3	Comp4	Comp5	Comp6	Comp7	Comp8	Total contribution
Precipitation	-0.02	0.01	-0.08	-0.07	0.20	**-0.66**	0.29	-0.39	-3.77 %
Global rad	**0.47**	0.07	-0.14	0.01	0.15	0.24	0.40	0.02	16.84 %
UV rad	**0.45**	0.03	-0.26	-0.25	-0.24	0.07	-0.06	-0.27	12 %
RH	-0.15	0.46	-0.06	-0.13	0.55	**0.52**	0.01	-0.22	-5.41 %
VPD	0.26	-0.30	0.41	0.37	**0.39**	-0.01	0.41	0.03	10.05 %
Soil T	0.08	-0.14	0.30	**-0.60**	-0.14	0.13	0.31	0.22	2.97 %
Soil RH	-0.12	0.09	-0.38	0.27	-0.33	0.12	0.44	-0.38	-5.90 %
Air T	0.27	-0.13	0.29	-0.33	-0.05	0.05	-0.17	**-0.51**	4.10 %
Wind dir	0.02	-0.19	0.29	0.40	-0.39	0.38	-0.06	-0.19	-0.15 %
Gsto	0.41	0.17	-0.28	0.06	-0.13	-0.06	0.08	0.48	17.99 %
LE flux	**0.48**	0.10	0.00	0.26	0.19	-0.13	**-0.48**	-0.09	16.06 %
u*	-0.06	**-0.76**	**-0.50**	-0.08	0.29	0.20	-0.12	-0.01	-4.37 %
Partial r^2	0.067	0.005	0.001	0.005	0.001	0.001	0.002	0.015	
model r^2 = 0.10									
MSE = 0.0038									

Table 2: Components weights calculated by PLS regression performed over Spring / Summer dataset, averaged over half-hour timescale. Partial r^2 represent the variance explained by each component, model r^2 is the sum of all partial r^2, MSE is the mean squared error calculated using 10-fold cross-validation. Weights whose squares are larger than 0.2 are shown in bold type.

Predictors	*Weights - Autumn / Winter HALF-HOUR*												
	Comp1	Comp2	Comp3	Comp4	Comp5	Comp6	Comp7	Comp8	Comp9	Comp10	Comp11	Comp12	Total contribution
Precipitation	0.12	0.11	-0.01	-0.08	-0.10	0.09	0.03	-0.10	0.41	**-0.80**	0.35	0.00	-0.31 %
Global rad	0.34	-0.18	0.21	-0.24	0.01	-0.25	0.39	-0.03	0.17	0.33	**0.47**	-0.43	4.83 %
UV rad	0.39	-0.13	0.26	-0.12	0.01	-0.36	0.01	-0.35	-0.57	-0.26	0	0.32	-1.72 %
RH	0.31	**0.50**	-0.15	0.15	0.29	0.06	0.18	-0.37	0.29	0.29	0.05	0.44	-1.22 %
VPD	0.05	-0.36	0.32	0.35	-0.08	0.08	0.12	**0.45**	0.12	0.06	0.25	0.58	28.65 %
Soil T	0.23	-0.29	-0.55	0.08	-0.39	**-0.45**	-0.32	-0.05	0.28	0.11	-0.03	0.11	-14.54 %
Soil RH	-0.22	0.26	0.55	-0.06	-0.05	**-0.53**	-0.14	0.04	0.41	0.01	-0.32	0.03	9.86 %
Air T	0.41	-0.12	0.06	**0.58**	0.09	0.04	0.23	0.03	0.11	-0.18	**-0.49**	-0.36	12.77 %
Wind dir	0.13	0.09	0.25	-0.07	**-0.78**	0.42	0.06	-0.27	0.03	0.17	-0.14	0.01	-1.51 %
Gsto	0.14	-0.33	-0.09	-0.62	0.18	0.19	0.23	0.12	0.27	-0.03	-0.47	0.21	1.81 %
LE flux	0.26	-0.23	0.29	-0.02	0.30	0.30	**-0.72**	-0.18	0.16	0.11	0.08	-0.11	3.03 %
u*	**-0.50**	**-0.47**	0.03	0.19	0.09	-0.01	0.21	**-0.64**	0.16	0.01	0.02	0.04	-19.74 %
Partial r^2	0.009	0.001	0.017	0.007	0.003	0.003	0.004	0.020	0.003	0.00	0.00	0.00476	
model r^2 = 0.07													
MSE = 0.0023													

Table 3: Components weights calculated by PLS regression performed over Autumn / Winter dataset, averaged over half-hour timescale. Partial r^2 represent the variance explained by each component, model r^2 is the sum of all partial r^2, MSE is the mean squared error calculated using 10-fold cross-validation. Weights whose squares are larger than 0.2 are shown in bold type.

Predictors	*Weights - Spring / Summer DAILY*									
	Comp1	Comp2	Comp3	Comp4	Comp5	Comp6	Comp7	Comp8	Comp9	Total contribution
Precipitation	-0.34	-0.09	-0.38	0.39	0.41	-0.46	-0.24	0.32	-0.09	-13.53 %
Global rad	0.38	-0.17	0.01	0.44	-0.03	0.04	-0.26	-0.50	-0.34	-3.28 %
UV rad	0.25	-0.26	-0.28	0.26	-0.23	0.06	0.00	-0.13	0.29	6.93 %
RH	0.21	**0.45**	-0.38	0.18	0.31	0.13	0.09	-0.18	0.07	10.04 %
VPD	0.05	-0.40	**0.51**	0.05	0.12	-0.13	-0.13	0.10	-0.02	-0.57 %
Soil T	0.23	-0.37	-0.40	**-0.58**	-0.02	-0.43	-0.16	-0.20	0.06	-14.05 %
Soil RH	-0.20	0.28	0.18	0.23	-0.43	-0.33	-0.44	-0.15	0.46	-0.04 %
Air T	0.36	-0.18	0.28	0.17	**0.50**	-0.04	0.06	0.10	0.44	19.60 %
Wind dir	0.21	0.02	0.08	0.21	-0.29	-0.32	0.18	0.25	**-0.54**	-6.89 %
Gsto	0.17	-0.24	-0.26	0.22	-0.38	0.15	0.24	**0.49**	0.27	11.14 %
LE flux	0.05	-0.09	-0.11	-0.10	0.01	**0.52**	**-0.71**	0.32	-0.14	-5.43 %
u*	**-0.57**	**-0.47**	-0.10	0.19	0.00	**0.25**	0.19	-0.33	-0.01	-8.51 %
Partial r^2	0.035	0.019	0.017	0.023	0.013	0.029	0.030	0.012	0.047	

model r^2 = 0.23

MSE = 7.0×10^{-4}

Table 4: Components weights calculated by PLS regression performed over Spring / Summer dataset, averaged over daily timescale. Partial r^2 *represent the variance explained by each component, model* r^2 *is the sum of all partial* r^2*, MSE is the mean squared error calculated using 10-fold cross-validation. Weights whose squares are larger than 0.2 are shown in bold type.*

Predictors	*Weights - Autumn / Winter DAILY*									
	Comp1	Comp2	Comp3	Comp4	Comp5	Comp6	Comp7	Comp8	Comp9	Total contribution
Precipitation	-0.13	0.25	0.45	0.08	-0.65	-0.10	**0.48**	-0.02	0.03	6.59 %
Global rad	0.14	0.15	-0.17	-0.35	0.12	0.22	0.38	-0.36	-0.22	-6.05 %
UV rad	0.00	0.00	0.00	0.00	0.00	0.00	0.00	0.00	0.00	0 %
RH	0.42	-0.20	0.21	0.41	-0.10	**0.47**	-0.08	-0.12	**0.49**	15.49 %
VPD	-0.24	0.40	0.44	-0.10	**0.49**	-0.15	0.09	0.11	0.40	18.02 %
Soil T	0.15	**-0.46**	0.13	**-0.59**	-0.26	-0.39	-0.10	-0.15	0.31	3.71 %
Soil RH	-0.24	0.35	-0.23	0.20	-0.21	-0.19	-0.37	**-0.69**	0.16	7.20 %
Air T	0.14	-0.13	**0.65**	-0.01	0.26	0.03	-0.22	-0.43	-0.43	-13.66 %
Wind dir	-0.13	0.04	0.16	0.06	-0.19	-0.15	**-0.55**	0.36	-0.19	-6.75 %
Gsto	-0.04	-0.14	-0.10	0.12	0.31	-0.32	0.10	-0.11	0.38	11.20 %
LE flux	-0.05	0.32	0.02	**-0.53**	-0.09	**0.51**	-0.32	0.06	0.24	8.10 %
u*	**-0.78**	**-0.49**	0.06	0.02	0.01	0.35	0.08	-0.11	0.03	-3.23 %
Partial r^2	0.004	0.033	0.010	0.009	0.002	0.004	0.008	0.004	0.105	

model r^2 = 0.18

MSE = 6.8 x 10^{-4}

Table 5: Components weights calculated by PLS regression performed over Autumn / Winter dataset, averaged over daily timescale. Partial r^2 *represent the variance explained by each component, model* r^2 *is the sum of all partial* r^2*, MSE is the mean squared error calculated using 10-fold cross-validation. Weights whose squares are larger than 0.2 are shown in bold type.*

PLS analysis returned higher r^2 in Spring / Summer period than Autumn / Winter period, indicating that PLS models better explain relationships associated with CH_4 emissions. Furthermore, the variance explained by the PLS regression increases with increasing time scale: at the half-hour timescale, the variance explained by the PLS regression was low (up to 10 % in Spring / Summer). The low fit of the PLS model at short time-scale may depend on the fact that relationship between environmental factors and half-hour CH_4 fluxes is not completely linear or because CH_4 fluxes are driven by microbial processes which production rates does not always depend on the instantaneous effect of environmental factors. Models built over the averaged dataset were more robust than the ones built over the half-hour dataset because the latter did not include the effects generated by events occurred non-simultaneously with the measured CH_4 fluxes. This is the case of precipitation, which influence fluxes on a daily time-scale but has a minimum impact to the half-hour fluxes.

Results from the PLS regression confirmed that different environmental drivers influenced CH_4 fluxes at different time-scales.

At half-hour scale, during Spring / Summer period, CH_4 fluxes were prevalently directed upwards and the main driver were the ones whose dynamics followed a daily half-sinusoid curve. The main environmental factors associated with CH_4 emissions were stomatal conductance, followed by global radiation, LE flux and UV radiation (fig. 3.6 a). This result supports the hypothesis that two mechanisms for CH_4 emission exist at the site: a biological process such as plant-mediated transport through xylematic way (Zeikus and Ward, 1974), and a chemical process such as CH_4 formation under UV radiation (McLeod et al., 2008).

The possibility of CH_4 transport via xylem is supported by the microbiological analysis: CH_4-cycling community gene abundance investigated along soil depth indicated that most of the CH_4 emitting archaea are located at 80 cm depth (fig. 3.9). The deep and broad *Q. ilex* root system (Castell et al., 1994) can act as channelling for CH_4, intercepting CH_4 close to the production sites and avoiding CH_4 oxidation in the oxygenated upper soil layers, where CH_4-oxidizing bacteria are active. In agreement with this hypothesis, soil CH_4 fluxes measured by chambers consistently showed a CH_4 uptake ($-1.64 \cdot 10^{-3}$ μmol m^{-2} s^{-1} on average).

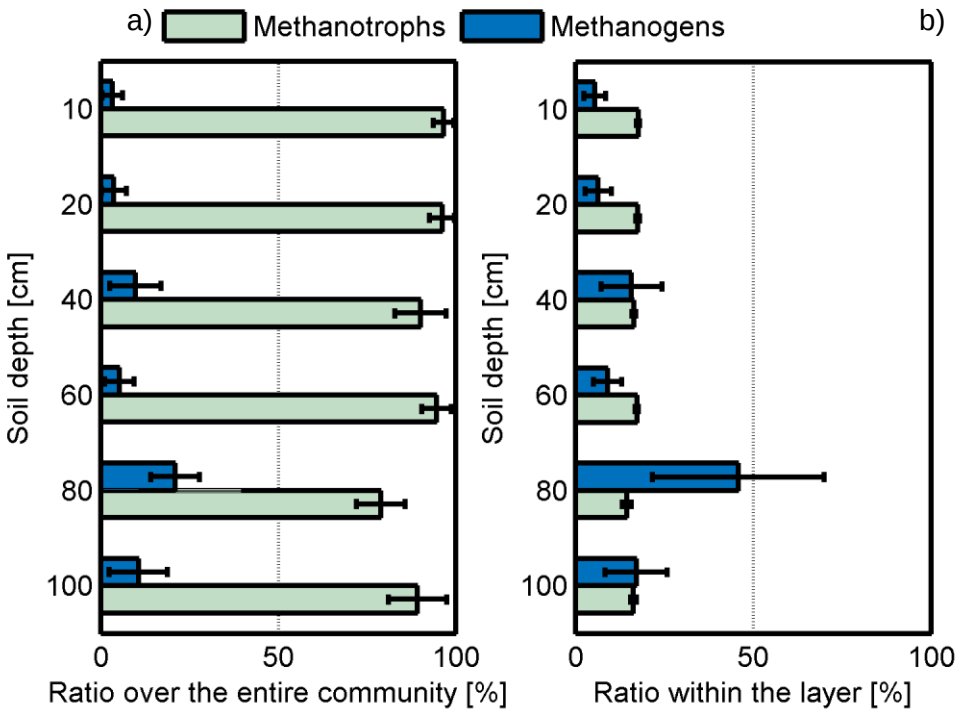

Figure 3.9 Ratio of methanogens and methanotrophs abundance over the soil CH_4-cycling communities (a) and per cent distribution within the layers of methanogens and methanotrophs relative to each population abundance (b). Blue bars: methanogens, light green bar: methanotrophs, error bars indicate standard deviations.

Concerning the relationship between UV radiation and CH_4 emission, it has been demonstrated that UV radiation induce CH_4 formation from pectin, a highly activated methyl donor (Bruhn et al., 2009; Vigano et al., 2008). However, in water-stress adapted *Q. ilex* leaves, pectin is well protected from UV radiation by thick cuticles rich in waxes (Martins et al., 1999), which can reflect or absorb UV radiation. A more reasonable UV-induced CH_4 emission at Castelporziano site can be the 2-step mechanism for CH_4 formation from leaf surface wax layer, recently proposed by (Bruhn et al., 2014). This process involves photolysis of carbonyl compounds, which origin methyl radicals through Norrish reactions type I and II.

As expected, factors affecting half-hour CH_4 during Autumn / Winter were others than the one observed during Spring / Summer (fig. 3.6 b). CH_4 fluxes in Autumn / Winter were mainly directed downwards, although diurnal pattern with a slight emission during day and

uptake during night recurred during all the measurements period. Factors that negatively correlated with them were u* and soil temperature. u* relation with CH_4 uptake was already observed by Wang et al. (2013), who found that increasing turbulence and vertical mixing enhance the transport of CH_4 from the upper canopy to the soil level. At Castelorziano site, microbiological analysis showed that methanotrophs abundance in the upper soil layer greatly exceeds methanogenic abundance, so that it is reasonable to infer that CH_4 transported to the soil can be depleted at the oxidizing surface.

PLS model performed on Autumn / Winter dataset highlights that soil temperature enhances CH_4 uptake, stimulating CH_4 oxidizing activities. In the same model, air temperature behaves the opposite way, enhancing CH_4 emission. Air temperature has a direct positive impact on VPD, which is the main factor that positively correlated with CH_4 fluxes. Air temperature range is highly affected by the daily cycle, and the difference between night and day are more pronounced than soil temperature. At daily time-scale, when the variability of air temperature is decreased by daily averaging, air temperature positively correlated with CH_4 fluxes in Spring / Summer (fig 3.6 c) while correlation is negative during Autumn / Winter period (fig 3.6 d). This finding highlights how the same parameters can act in opposite directions when their influence is tested concurrently with other environmental parameters. It is rational to hypothesize that water availability controls the sign of temperature influence on CH_4 fluxes in the daily-scale models. During hot and dry season, the methanotrophs inhabiting the upper layer were partially inhibited by the dry conditions, while methanogens residing in the deeper layers were unaffected, with concurrent high temperature and humidity, the latter assured by the high water table (around 1 and 2 m depth; Bucci, 2006), so that temperature promoted CH_4 production, leading to a net CH_4 source. During the cold season, when precipitations did not represent a limiting factor in the upper soil layer, methanotrophic communities were active and high temperature led to an increase of CH_4 oxidation.

4 Ozone deposition and uptake by vegetation

This chapter reports research findings on the O_3 exchanges at the holm oak forest.

High frequency O_3 measurements above the canopy were carried out from February 2012 until October 2015, and again from March to August 2015. High frequency O_3 measurements were performed below canopy from July to November 2013, in order to evaluate the soil contribution to the total O_3 flux.

Results reported here were published in the papers:

Fares et al. (2014) *Simultaneous measurements of above and below canopy ozone fluxes help partitioning ozone deposition between its various sinks in a Mediterranean Oak Forest*, Agricultural and Forest Meteorology 198: 181-191.

Savi and Fares (2014) *Ozone dynamics in a Mediterranean Holm oak forest : comparison among transition periods characterized by different amounts of precipitation*, Annals of Silvicultural Research 38:1-6.

4.1 O_3 mixing ratio above the forest

O_3 photochemical origin, dependent on solar radiation and temperature (Pellegrini et al., 2007), made O_3 mixing ratio rise during the hot seasons and, considering the daily dynamic, pick during the central hour of day (fig. 4.1).

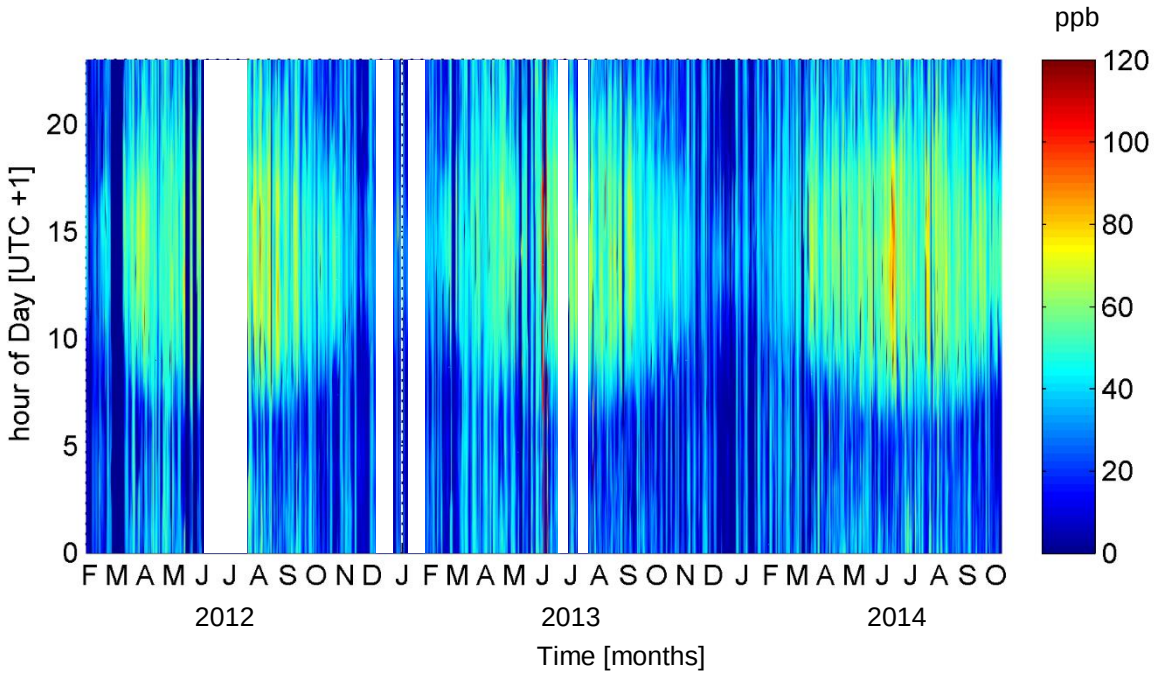

Figure 4.1 Surface-plot of O_3 mixing ratio (ppb) recorded at the site between 2012 and 2014. On the y axis: hour of day, on the x axis: months.

The sea-land breeze regime that characterizes the study site (winds blowing from sea during the day and from the inland during the evening hours and night) affected O_3 mixing ratio: Differences were indeed observed in the plumes coming from the sea and from the land during the central hours of the day (fig. 4.2), suggesting that air coming from the city was depleted in O_3 especially at night due to reactions of O_3 with NO and AVOC emitted by vehicles and industrial activities (Fares et al., 2009). Air coming from the sea showed higher concentrations of O_3 than air coming from the city, mainly due to slow O_3 deposition on water and the capacity of the air masses above the sea to form O_3 through photochemical reactions (Velchev et al., 2011). During the few times that wind circulation diverged from its typical pattern (Fig. 5 a, b), O_3 concentration at night was higher (Fig. 4.2 b), thus confirming that that air masses not directly coming from the urban areas are more rich in O_3.

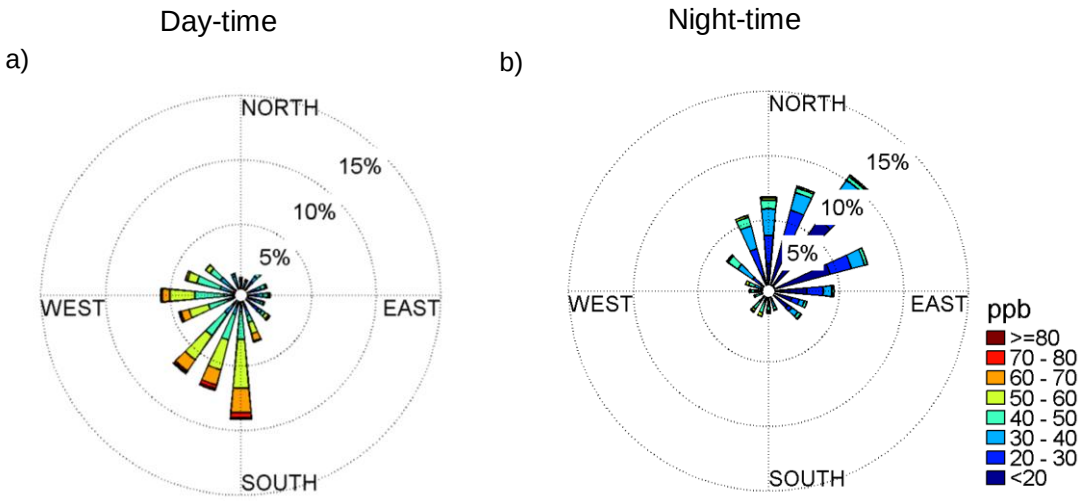

Figure 4.2 Wind roses of Day-time (a) and Night-time (b) wind directions and O_3 mixing ratio (ppb). The frequencies at which the wind blew from each direction is represented by the radial thickness of each slice, while O_3 mixing ratio is representing by the colour of the filled area. Data recorded from February 2012 to October 2014.

4.2 Above canopy O_3 fluxes

The holm oak forest was a consistent O_3 sink during all the study period (fig. 4.3), although the sink magnitude varied throughout the year, with maximum uptake values recorded in Spring (fig. 4.4 b). The primary reason of this variability is the O_3 concentration dynamic, which is higher in the hot season (fig 4.1). The second one can be found in the phenology of the forest: during the growing season, vegetation is active and stomata are wide open, supported by favourable climatic conditions (high water availability and mild temperature). Moreover, new stems and leaves are produced during Spring, extending the surfaces where O_3 is depleted.

Looking at the daily dynamic (fig. 4.4 b), total O_3 fluxes peaked during the central hours of the day, as a result of stomatal and non- stomatal sinks (Gerosa et al., 2009).

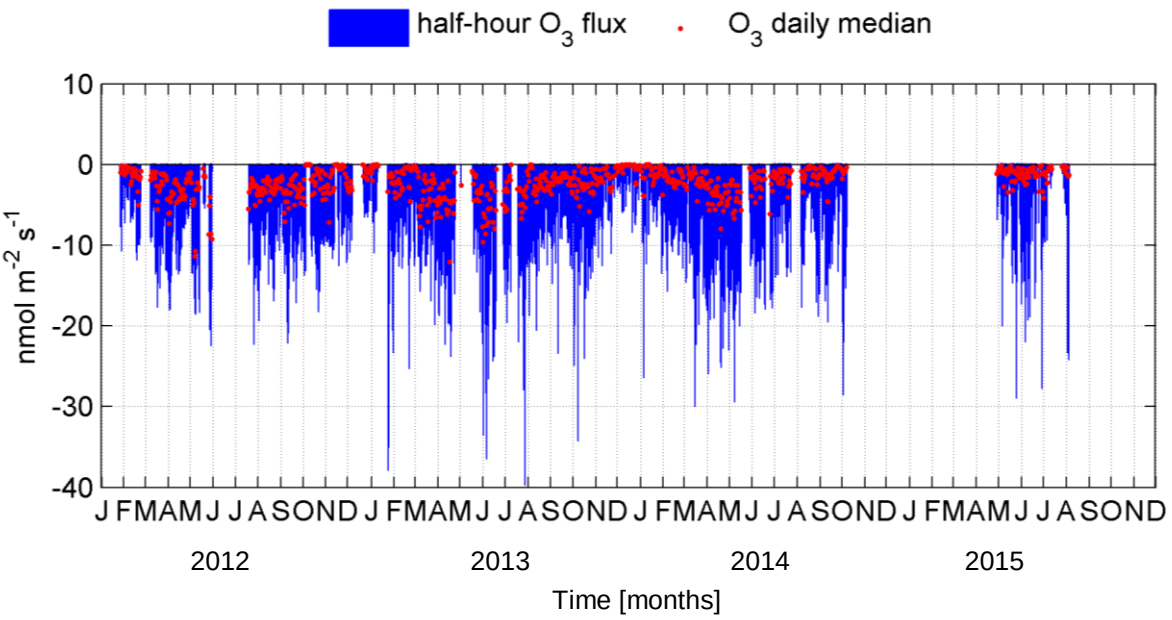

Figure 4.3 O_3 fluxes measured above the canopy. Blue bars are the half hour fluxes, red dots are the daily median values.

4.3 Partitioning of O_3 deposition between its sinks at the forest

Forests have the capacity to remove O_3 from the atmosphere through both stomatal and non-stomatal mechanisms, which include deposition on cuticles and soil and include gas-phase reactions with NO_x and reactive VOC.

In this section, the contribution of stomatal sink and deposition to cuticules and soil are evaluated. Fluxes recorded in 2013 were partitioned for the four seasons, based on the notion that sinks will change in response to meteorological variables and plant phenology during the year.

A short insight into gas phase reactions with VOC and NO_x is presented.

4.3.1 O_3 stomatal sink

Stomatal O_3 fluxes were estimated from the measured EC evapotraspiration, using the evaporative / resistance method (eq. 28). In order to minimize the errors associated with the

E component of the equation, soil evaporation was directly measured using a second EC system below the canopy (Wilson et al., 2001). The results were used to parameterize an empirical model of soil evaporation to gap-fill periods where direct measurements were not available.

The model was built using multiple linear regression based on step-wise procedure. Four case studies were tested (tab 6), each one with different combination of predictors. The first case of study only use soil meteorological variables (soil humidity and temperature measured at 10 50 and 100 cm depth), for the other cases, EC measurements and meteorological variables recorded above canopy were included (air temperature above and below canopy, u* above and below canopy, H_2O flux above canopy).

The equation selected to model H_2O fluxes at ground level ($H2O_{fluxBC}$, mmol m^{-2} s^{-1}) was:

$$H2O_{fluxBC} = b_1\, RH_{soil10} + b_2\, T_{soil10} + b_3\, u^* + b_4 H2O_{fluxAC} + \varepsilon \qquad (37)$$

where $H2O_{fluxAC}$ (mmol m^{-2} s^{-1}) is the measured EC H_2O flux above canopy.

Soil evaporation modelled using eq. (37) from case study 2 (tab 6) showed a good agreement with measured values ($r^2 = 0.45$). Case 2 model uses only predictors that does not derived by below canopy EC station, so that the equation can be used to gap fill the periods when below canopy EC measurements were not available. Nevertheless, an underestimation of 32% was observed comparing the daily course of modelled values vs measured values. Because the EC footprint is much smaller below the canopy than above the canopy, soil evaporation is measured over a much smaller area than evapotranspiration (Wilson et al., 2001). Wilson and Meyers (2001) estimated this error to be on the order of 10 %. In this study, the error may be due to the incapacity of the model to predict spikes in water evaporation from soils after precipitation events.

Predictors for H_2O flux below canopy	Case 1		Case 2		Case 3		Case 4	
	coeff	*P*	*coeff*	*P*	*coeff*	*P*	*coeff*	*P*
Soil RH 10	-0.0637	0.5149	**-0.2719**	**0.0019**	-0.0807	0.2403	**-0.2693**	**0.0047**
Soil RH 50	0.1035	0.1480	n.a.	n.a.	n.a.	n.a.	n.a.	n.a.
Soil RH100	0.0642	0.4134	n.a.	n.a.	n.a.	n.a.	n.a.	n.a.
Soil T 10	**0.0112**	**<0.0000**	**0.0026**	**0.0261**	-0.0017	0.175	**-0.0081**	**<0.0000**
Soil T 50	0	0.8267	n.a.	n.a.	n.a.	n.a.	n.a.	n.a.
Soil T 100	-0.0018	0.3075	n.a.	n.a.	n.a.	n.a.	n.a.	n.a.
*u**	**1.5651**	**<0.0000**	**0.0439**	**0.0005**	n.a.	n.a.	**1.417**	**<0.0000**
u soil level*	n.a.	n.a.	n.a.	n.a.	**1.2777**	**<0.0000**	**0.0118**	**<0.0000**
H_2O flux	n.a.	n.a.	**0.0428**	**<0.0000**	n.a.	n.a.	n.a.	n.a.
T air soil level	n.a.	n.a.	n.a.	n.a.	**0.0084**	**<0.0000**	**-0.0545**	**0.0001**
T air above canopy	n.a.	n.a.	n.a.	n.a.	n.a.	n.a.	-0.0034	0.1751
Cross-validation								
r^2	0.3161		0.4504		0.1339		0.3999	
Intercept(ε)	-0.2063		0		-0.02		-0.03	
DF	2455		2085		2557		2481	

Table 6: Results from the multiple linear regression analysis for prediction of H_2O fluxes below the canopy. n.a. = not available in the case study. The significant predictors which were included in the model are in bold. r^2 from linear correlation between measured and modelled data was calculated using the 30% of the data not used to parameterize the model.

Results shows that the stomatal O_3 uptake happened all year long due to the long vegetative period of the holm oak forest (Manes et al., 2007). However, stomatal O_3 sink was highly variable through the year (fig 4.4 d) because of its dependence from environmental variables, such as light, temperature and water availability, which regulate stomatal aperture.

Stomatal O_3 flux peaked in Spring (−10 nmol m^{-2} s^{-1}), when high temperature promoted O_3 photochemical production and stomatal aperture is supported by high water availability, resulting from the abundant precipitation (2013 cumulative precipitation was 665 mm, of which 20% fell in Spring).

In Summer, maximum O_3 stomatal uptake was only −3 nmol m^{-2} s^{-1}. Stomatal uptake decreased during the central hour of day, due to the decreased physiological activity of vegetation associated with the vpd effect on leaves (Mereu et al., 2009; Fares et al., 2010),which caused stomatal closure as defence strategy against water loss by transpiration when water supply is limited.

Stomatal closure was responsible for low O_3 fluxes during fall as a result of persisting conditions of drought and high temperatures (fig 4.4 a)

Although total O_3 fluxes during winter were low, high values of stomatal O_3 uptake were recorded, resulting from a long vegetative period. Indeed, the mild temperatures in November (mean 13.1 ◦C) and at the end of the Winter season promoted suitable conditions for vegetative growth.

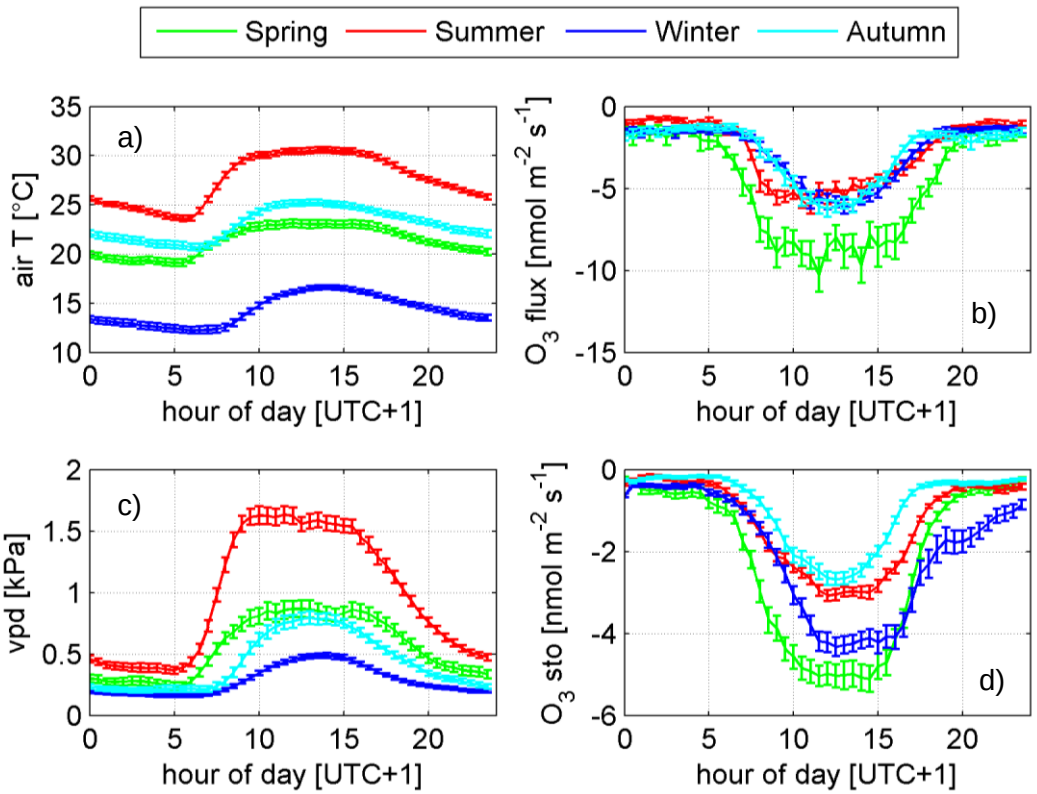

Figure 4.4 Mean daily evolution (±standard deviation) of air temperature (air T, °C, a), vapour pressure deficit (vpd, kPa, c), total and stomatal O_3 fluxes (b and d) for the each season of the year 2013.

4.3.2 O_3 deposition to soil: below-canopy EC measurements and modelling

Similar to water fluxes, below-canopy O_3 deposition was modelled by means of a polynomial regression with the intent to gap-fill O_3 flux to soil and compare it with above-canopy O_3 flux measured for the entire year. The model was run in four case studies testing different combinations of predictors: air temperature above the canopy, u* measured above the canopy and at the soil level and O_3 mixing ratio (tab. 7). All case studies seemed to predict well O_3 fluxes at soil level ($r^2 > 0.57$). For comparison with measured fluxes, the equation resulting from the first case study (eq. 38, $r^2 = 0.62$) was adopted, due to its easy application using just two predictors: O_3 mixing ratio and u* measured above the canopy.

$$O_{3fluxBC} = b_1[O_3] + b_2u^* + \varepsilon \qquad (38)$$

A good agreement between modelled and measured data was achieved (fig. 4.5), mainly because the physical process of O_3 deposition to soil is well represented by turbulence, as already shown by others (Lamaud et al., 2002). However, this simple empirical method may therefore not be applicable to other plant ecosystems.

Predictors for O_3 flux below canopy	Case 1		Case 2		Case 3		Case 4	
	coeff	*P*	*coeff*	*P*	*coeff*	*P*	*coeff*	*P*
[O_3]	**-0.0431**	**<0.0000**	**0.0485**	**<0.0000**	**-0.044**	**<0.0000**	**-0.0406**	**<0.0000**
*u**	**-1.3586**	**<0.0000**	n.a.	n.a.	n.a.	n.a.	**-1.9604**	**<0.0000**
u soil level*	n.a.		**-21.7161**	**<0.0000**	**-15.7571**	**<0.0000**	n.a.	n.a.
T air above canopy	-0.0215	0.4269	-0.0267	0.1997	0.0368	0.1825	**0.0806**	**0.0118**
O_3 flux	n.a.		n.a.	n.a.	**0.1064**	**<0.0000**	**0.1174**	**<0.0000**
Cross-validation								
r^2	0.6231		0.571		0.6551		0.6674	
Intercept(ε)	0.8423		2.0248		1.9668		-0.5236	
DF	406		408		283		282	

Table 7: Results from the multiple linear regression analysis for prediction of O_3 fluxes below the canopy. n.a. = not available in the case study. The significant predictors which were included in the model are in bold. r^2 from linear correlation between measured and modelled data was calculated using the 30% of the data not used to parameterize the model.

In order to test a more conventional resistance model with potential broad applications to other forest ecosystems, a previously adopted empirical algorithm was tested (eq. 30 and eq. 31). The constant R_{g1} and R_{g2} commonly used in literature are 200 and 300 s m^{-1} respectively (Fares et al., 2012; Mészáros et al., 2009). Using these values we obtained a 30% over-prediction of fluxes, comparing with measured below canopy O_3 fluxes, and a r^2 of 0.19. Therefore, R_{g1} and R_{g2} were iteratively calculated by comparing measured and modelled fluxes, with a best result using values of 50 and 500 s m^{-1} for R_{g1} and R_{g2}, respectively. The new parameterization helped to reach a slope between measured and modelled fluxes closer to 1 (slope = 0.85), but the statistical significance remained poor (r^2 = 0.2).

Results shown as diurnal mean evolution are reported in fig 4.5

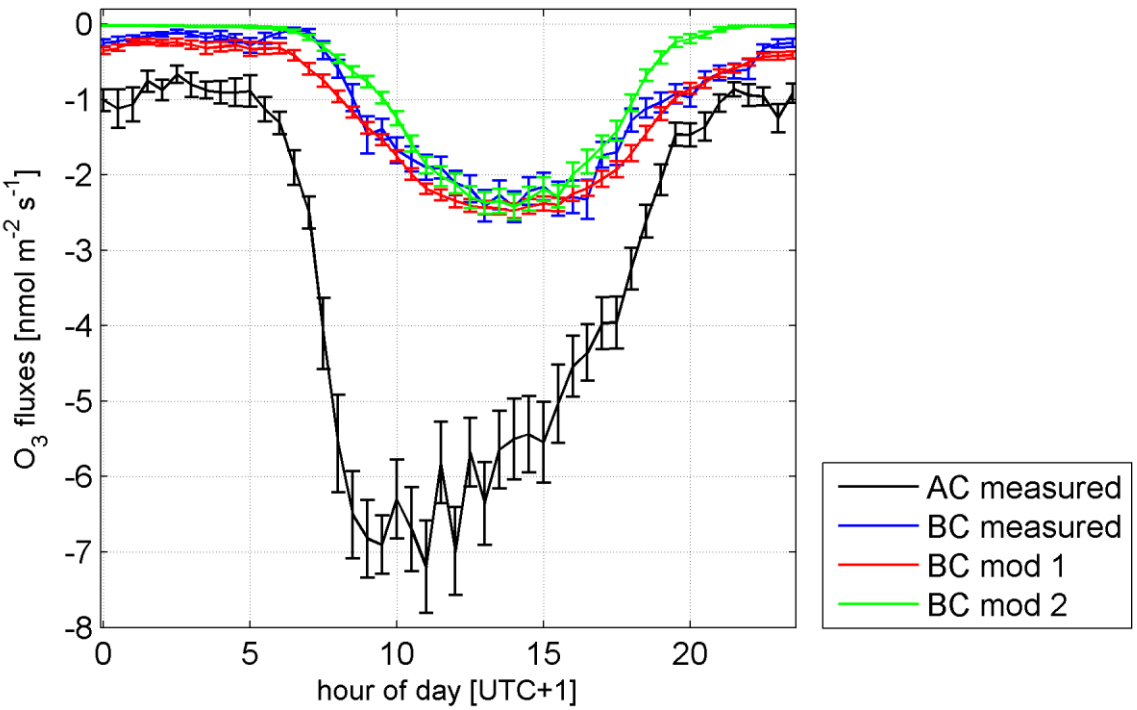

Figure 4.5 Daily mean evolution (±standard deviation) of total O_3 fluxes measured above the canopy (AC), below the canopy (BC), modelled according to the empirical model (mod 1, eq. 38) and modelled according to the resistance method (mod 2, eq. 30 and 31). The averages were performed for the period when below-canopy O_3 flux measurements were performed.

Daytime below-canopy O_3 fluxes during the period in which they were directly measured were about 2 times lower than the total above-canopy fluxes (maximum measured BC O_3 fluxes: -2.4 nmol m^{-2} s^{-1}). Soil O_3 uptake was greater during day-time, when O_3 is transported to the soil by turbulence, which is more intense when solar radiation is high.

Night-time O_3 deposition to soil was almost negligible, an indicator that when stomatal aperture is minimized, other sinks may be responsible for O_3 removal (about −1 nmol m^{-2} s^{-1}).

4.3.3 O_3 deposition to cuticles

O_3 cuticular deposition was modelled according to the resistance method by eqs. 32 and 33.

Deposition over cuticles represented up to 30 % of the total O_3, ranging from −0.5 nmol m^{-2} s^{-1} during night to maximum values during the day of −2.5 nmol m^{-2} s^{-1}. The data refer to the same temporal window used to calculate soil deposition, i.e. the time of the year when below canopy EC measurements were performed. Our measurements are in agreement with other studies, which evaluated O_3 deposition to cuticles between 10 to 57% in agricultural and forest ecosystems (Fares et al., 2012; Tuzet et al., 2011). However, whilst the O_3 soil fluxes were validated by measurements, cuticle deposition still remained uncertain due to the lack of experimental validation.

4.3.4 Gas-phase reactions

Gas phase reaction was not quantified at the holm oak forest. However, some evidences of NO_x reaction below canopy are provided.

During night, under conditions of low turbulence and shallow boundary layer, NO emitted by soil accumulated below canopy, as shown by the concentration profile in fig. 4.6a. In the morning, when the sun rose, energy input to the system increased promoting turbulence, which transported O_3 near the soil surface. There, O_3 reacted with NO (eq. 4), generating NO_2, which increased in the early morning (fig 4.6 b).

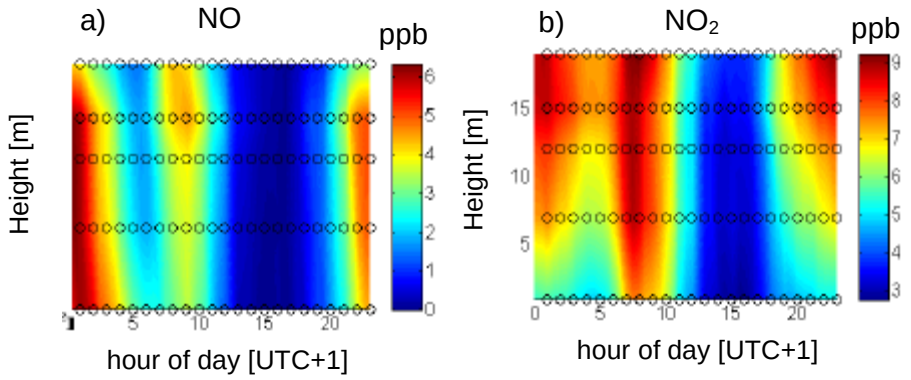

Figure 5.6 Surface plot of NO (a) and NO_2(b) mixing ratio vertical profile, averaged for the hour of day. NO_x were measured along a vertical profile within the forest during two weeks in December 2014.

The dynamic descripted above is confirmed by the ILT modelling of NO_x fluxes, derived from the concentration profiles. A net NO_2 release was recorded in the morning, concurrently with NO and O_3 uptake (fig. 4.7).

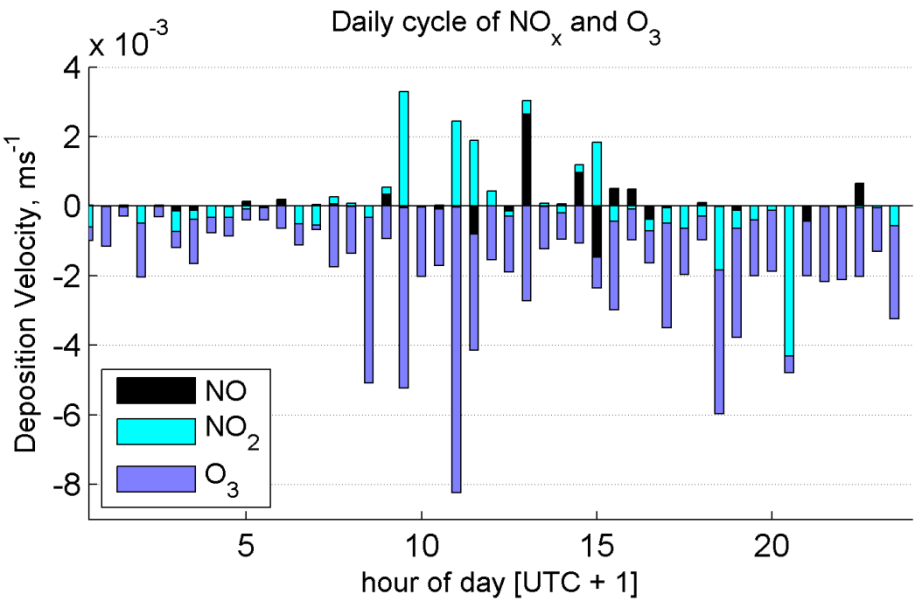

Figure 5.7 Mean daily evolution of NO (black bars), NO_2 (light blue bars) and O_3(blue bars) deposition velocity, modelled through ILT. NO_x were measured along a vertical profile within the forest during two weeks in December 2014.

BVOC have been found to explain up to 26% of total ozone fluxes in some forest ecosystems (Kurpius and Goldstein, 2003; Fares et al., 2010). However, O_3 loss due to reaction with monoterpenes may be not significant at the holm oak forest. *Q. ilex* is a monoterpenes emitter. If temperature-dependent BVOC emission consumed O_3, large O_3 fluxes would be observed in Summer (Kurpius and Goldstein, 2003). Measurements show that that total O_3 fluxes during Summer were low and comparable to Winter and Autumn, thus not supporting the hypothesis of BVOC / O_3 reaction. Anyway, is not excluded that under conditions of low turbulence, nocturnal O_3 losses by reactions with monoterpenes emitted by *Q. ilex* may contribute to O_3 removal, as previously demonstrated by Stewart et al. (2013). Fig. 4.8 shows the source / sink distribution along a soil-canopy-atmosphere profile, modelled by ILT technique using vertical profile concentration recorded in Summer 2015 at the forest site. Bars represent values averaged for night – early morning hours (2 am – 9 am). The facts that in the lower layers of the profile a small sink for monoterpenes were measured, support the hypothesis that BVOC may play a role in O_3 uptake at night.

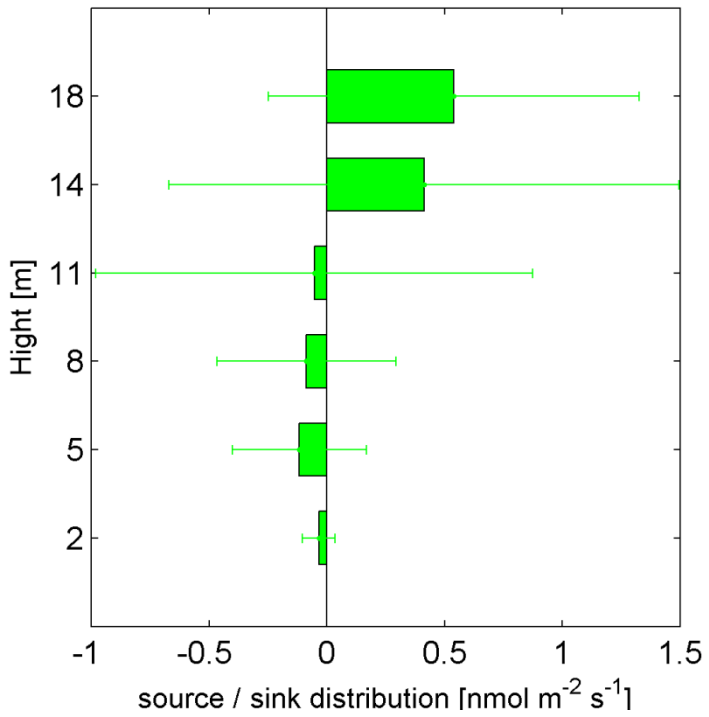

Figure 5.8 Source / sink distribution along a soil-canopy profile of mototerpenes. Source / sink contribution were modelled by ILT, using profile [monoterpenes] distribution during two weeks in August 2015

4.4 Dependence of forest O_3 uptake from water availability

In Mediterranean climate, where drought is the main limiting factor (Vargas et al., 2013), water availability play a key role in the regulation of O_3 removal from the atmosphere.

The effect of water availability on the O_3 sink capacity of the holm oak forest was investigated during two transition periods: before the beginning of the driest season, from March 20th to April 14th (early Spring, ES) and before the coldest season, from November 11st to December 6th (late Autumn, LA) of two consecutive years (2012 - 2013).

The uncommon low precipitation recorded in ES and LA periods in 2012 (fig 4.9) allowed to evaluate the influence of water availability on O_3 fluxes during seasons which are not commonly affected by drought stress: mean precipitation averaged in the year 1999-2010 were 61 ± 24 mm in April and 130 ±54 mm in November.

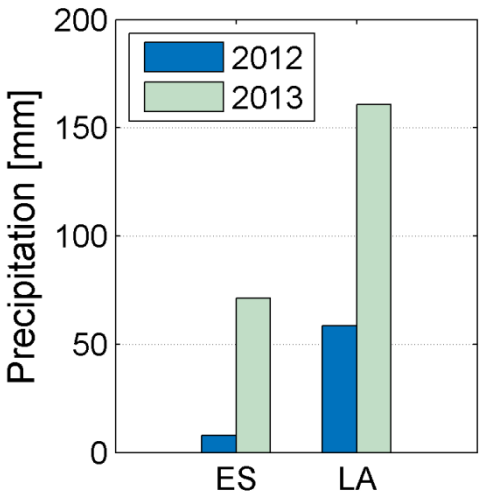

Figure 4.9 Cumulative precipitation recorded in Early Spring (ES) and Late Autumn (LA) during 2012 and 2013. For ES: 8 mm in 2012 vs 58.4 mm in 2013; For LA: 71.4 mm in 2012 vs 160.8 mm in 2013

ES mean temperature was similar across the two years (12.1 ± 4.2 °C and 12.6 ± 2.9°C for 2012 and 2013, respectively, fig 4.10 a) while LA was colder during 2013 than 2012 (13.4 ± 3.9 °C and 10.6 ± 4.2 °C for 2012 and 2013, respectively, fig 4.10 b). During the ES hottest hours LE flux intensities were 16% lower in 2012 than 2013, as expected considering the scarcity of precipitation occurred in 2012 (fig 4.10 c). Interestingly, the relation is inverse in LA (LE fluxes were 23% minor in 2013 than 2012, fig 4.10 d) suggesting that the water availability did not represent a limiting factor during this period. Vpd (fig 4.10 e), which depends

directly from temperature and LE, was higher in 2012 ES than ES 2013 values, while similar values were recorded in LA across the two years (fig 4.10 d).

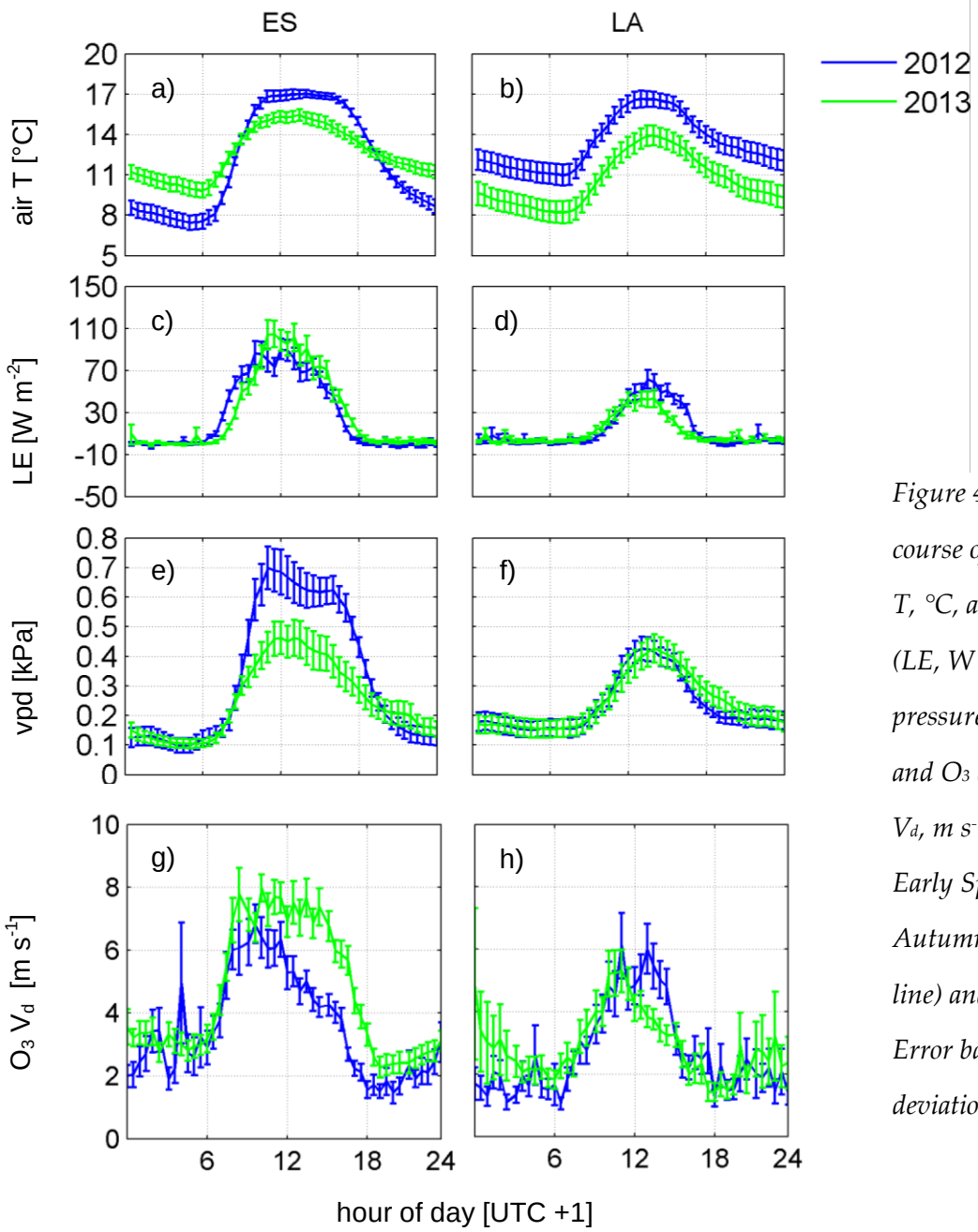

Figure 4.10 Mean daily course of ait temperature (air T, °C, a - b), latent heat flux (LE, W m^{-2}, c - d), vapour pressure deficit (vpd, kPa, e - f) and O_3 deposition velocity (O_3 V_d, m s^{-1}, g -h) recorded during Early Spring (ES) and Late Autumn (LA) in 2012 (green line) and 2013 (blue line). Error bars represent standard deviation.

O_3 deposition velocity (flux normalized by concentration) recorded in ES 2012 was 23.6 % lower than 2013, although no significant differences were observed between measured O_3 mixing ratio at the top of the canopy for the two years (41.4 ± 16.4 ppb and 41.5 ± 10.8 ppb in ES for 2012 and 2013, respectively). This behaviour can be ascribed to the reduction in the O_3 flux stomatal component, given the dependence of stomatal conductance on water

availability. On the other hand, water availability seems not influenced O_3 deposition velocity during LA, when similar values were recorded despite the difference in precipitation.

By comparison of the two years, water availability showed to be an important limiting factor during Spring, since in this season plants are more photosynthetically active and more sensitive to drought, while in Autumn, when the stomatal sink is not predominant, the effect of drought on the total O_3 flux was less appreciated.

5 Ozone effects on Net Ecosystem Exchange

In Mediterranean climate, when high radiation and temperature promote photochemistry, vegetation is often exposed to phytotoxic O_3 doses, which can compromise the forest capacity of assimilate CO_2. O_3 mixing ratio above 40 ppb were observed almost during all year (fig. 4.1), although the O_3 dose assimilated by vegetation through stomata varies across the seasons (see section 4.3.1).

This chapter reports research findings on the O_3 impact on NEE at the holm oak forest.

O_3 effect on the capacity of the forest to assimilate CO_2 has been tested in parallel with other biological and meteorological parameter in order to evaluate the real contribution of the pollutant.

5.1 Testing the ozone effect on NEE using the Artificial Neural Network approach

Relationship between ecological variables are often non-linear. ANN is a valid tool to illustrate properly these relations due to its capacity in dealing with non-linear relationships. Their modelling ability has been tested in various ecological context (Lek and Guegan, 2000) and recently some studies used ANNs predictive capacity to model gases exchanges over forests in order to fill gaps in datasets (Papale and Valentini, 2003; Zona et al., 2014). In this work, ANNs were used from their explanatory point of view: NEE was modelled using physiological and meteorological predictors, then the contributions of the independent variables in the prediction process where analysing.

5.1.1 Preparation of the dataset

The diurnal cycle of solar radiation completely determines the daily course of most of the variables used in this study, i.e. vpd, O_3 photochemical production, stomatal conductance, NEE. This strong confounding effect may mask the correlation between predictor variables

and NEE. To overcome this issue, the half-hour time series of each variable was pre-treated using Singular Spectrum Analysis (SSA) to extract the seasonal component linked to the daily cycle. SSA consists of two complementary stages: first the time series is decomposed into a set of independent time-series (set of periodic series plus an aperiodic noise), second, the series corresponding to the daily component (lag window = 48 points) is reconstructed. The reconstructed daily component was subtracted to the original series, and the residuals were used to train the ANNs, after being standardized between 0 and 1. Figure 5.1 shows the extraction of the daily component of the NEE time series (red line, a) and the residuals (green line, b) obtained from subtracting the daily component from the original time series (blue line, a). Figure 5.1 c highlight the sinusoidal dynamic of the reconstructed series (red line), so that, the residuals represent the deviation from the daily component. The daily component is not constant throughout time but varies in function of the daylight hours. The same procedures was applied to all the time series that follow the daily dynamic (solar radiation, vpd, O_3 photochemical production, stomatal conductance and NEE). This procedure highly reduced the correlation between the variables used to train ANNs and avoid solar radiation covering the effects of the other predictors.

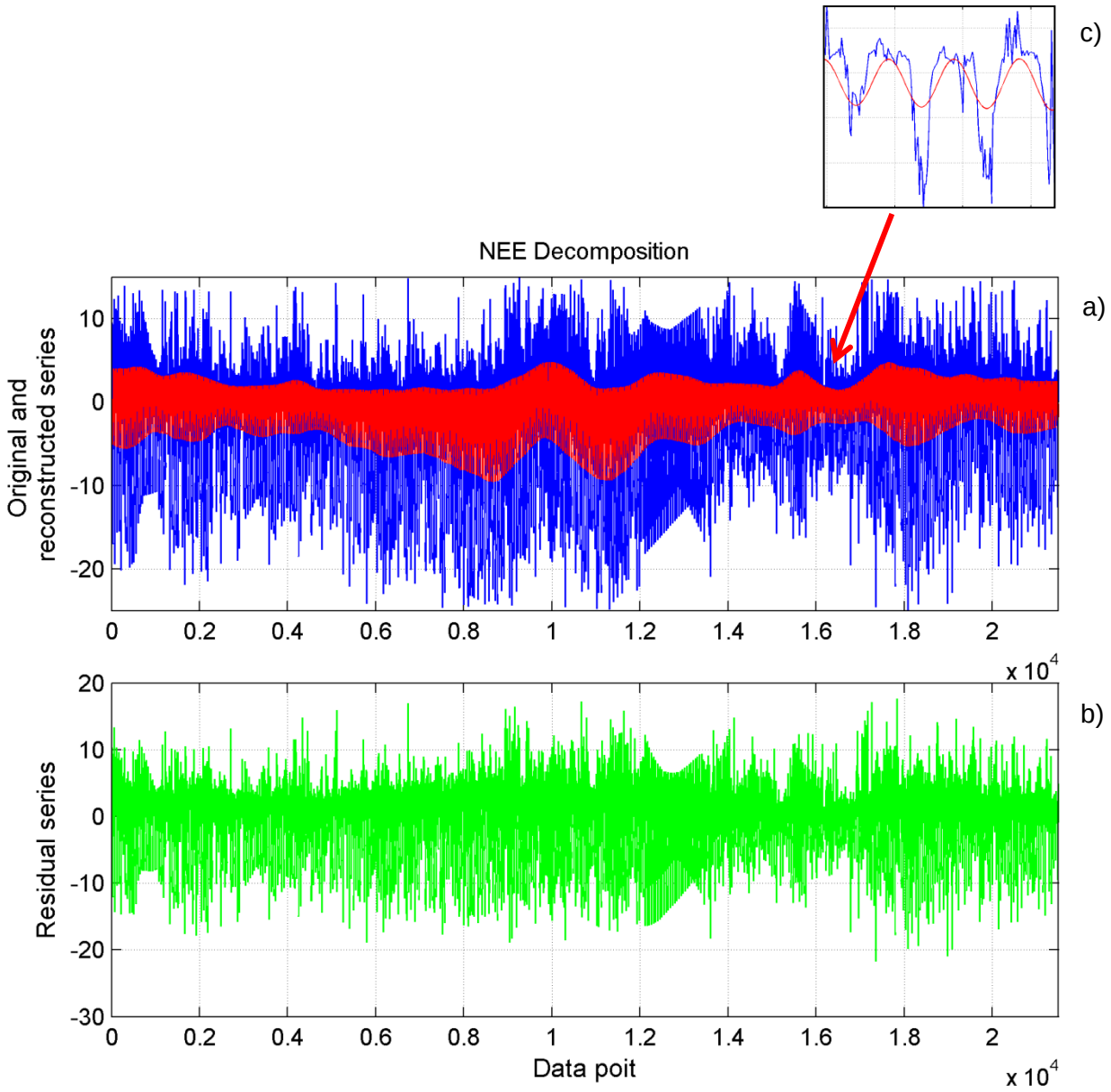

Figure 5.1 NEE decomposition through SSA. a) Original NEE time series (blue line, µmol m^{-2} s^{-1}) and reconstructed series corresponding to the daily component (red line, lag window = 48 points); b) Residuals obtained from subtracting the daily component from the original series (green line); c) zoom of the panel a.

5.1.2 *Artificial Neural Network training*

ANNs used in this work were composed by one hidden layer, 5 input neurons, 3 hidden neurons and one output neuron, sigmoid functions were used as activation functions for each neuron. ANNs were trained using the feed-forward backpropagation algorithm (Rumelhart, 1986). The ANNs structure is shown in figure 5.2:

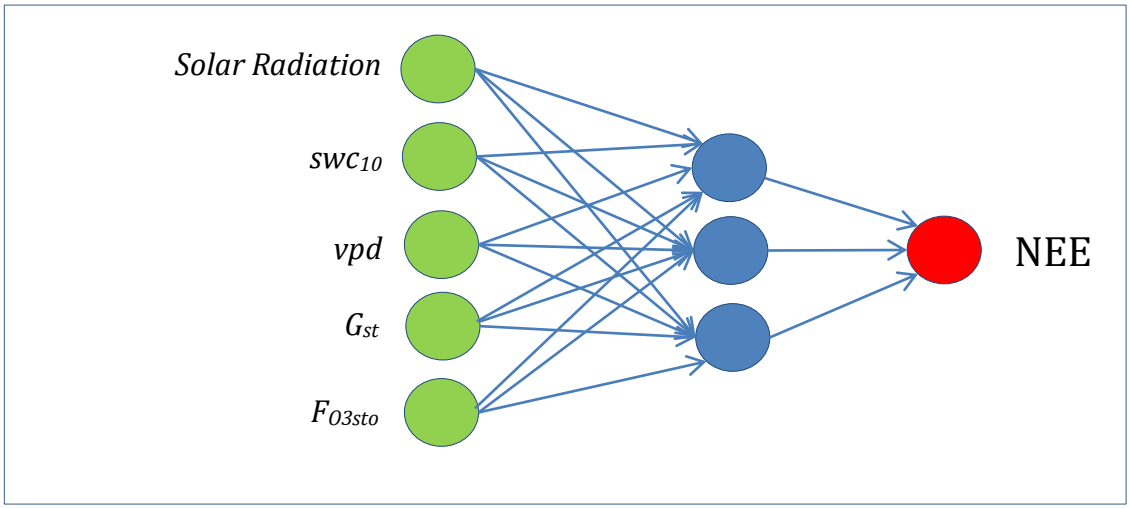

Figure 5.2 ANNs structure: green circles represent the input neurons, blue circles are the hidden neurons composing the hidden layer, red circle represents the output neurons.

The input used in this analysis were solar radiation (W m^{-2}), soil water content measured at 10 cm depth (swc_{10}, %), vapour pressure deficit (*vpd*, kPa), stomatal conductance to H_2O (G_{st}, m s^{-1}) and O_3 stomatal uptake (F_{O3sto}, nmol m^{-2} s^{-1}). The latter was included in the analysis under the assumption that, if O_3 has a detrimental effect on vegetation (and thus on NEE), it would be caused by the O_3 entering the leaves.

The ANN were trained using the residual variables obtained from the SSA procedure, as explained in the previous section, normalized between 0 and 1 to avoid scale effects. Dataset was split into three subset (training, validation and test sets), as explained in the method chapter (section 2.3.4).

100 different ANNs were built and trained with the same dataset, results showed further represent the average results of the 100 ANNs.

5.1.3 *Artificial Neural Network performance*

ANNs were able to reproduce NEE residual and no statistical differences between the measured data and ANN outputs means were observed (ANOVA F = 4.36, p value > 0.001). r^2 values for all the 100 ANN models range between 0.13 and 0.16. This result was expected, since the correlation between the variables in the model was reduced by SSA decomposition before performing ANN analysis.

The daily component of the NEE series were added to the ANN output (NEE residuals) to make a comparison of the measured NEE values and ANN model outputs (fig 5.3). Boxplots show agreement between measured and modelled values, although ANN model was not able to reproduce the extreem values of the NEE distribution. This lead to a standard deviation of the modelled data lower compared to the measured data (lowering r^2 value).

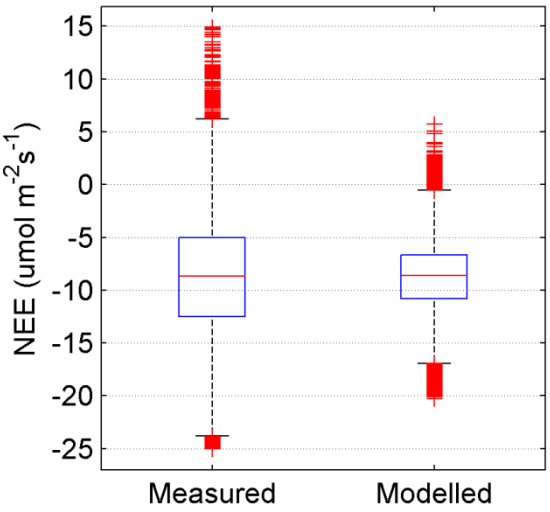

Figure 5.3 Boxplot comparing measured and modelled NEE. Red lines indicate the median values, boxes are the 1st and 3rd quartiles, whiskers indicate maximum and minimum values, red crosses are outliers.

5.1.4 *Contributions of the input variables in the ANN prediction process*

The effect of the input variables on the ANN operation was evaluated trough three different algorithms.

The first is the connection weight approach (Olden and Jackson, 2002). This method allows to derive the importance of each variable analysing the connection weight assigned to each input and hidden neurons by the training process.

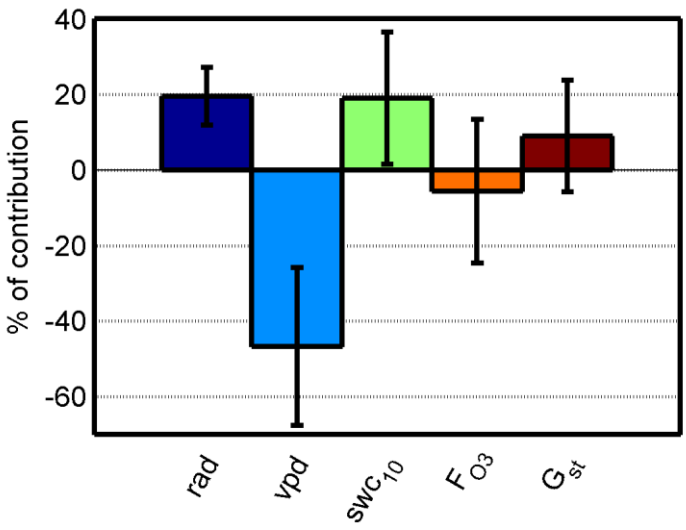

Figure 5.4 Results from the connection weight analysis. Importance of each input variable is expressed as per cent of the total variance explained by the ANN models. Bars represent the means of the ANN models, error bars indicate standard deviation.

vpd is the the major predictor controlling ANN operation (mean importance ± sd -46.7 ± 20.9), as expected for a Mediterranean forest, where vpd highly influenced the stomatal aperture (Manes et al., 2007), and thus CO_2 uptake. Due to the subtraction of the daily component to the inputs of ANNs, solar radiation was not the primary factor affecting NEE, but the second (mean importance ± sd 19.6 ± 7.7). Almost with the same importance, follows swc_{10} (mean importance ± sd 19.1 ± 17.5). The high standard deviation denotes that not always the swc_{10} influence was high, not surprising for a site where drought condition return cyclically each year. Follows G_{st} (mean importance ± sd 14.8 ± 9) and eventually F_{O3sto} (mean importance ± sd -5.6 ± 19). The least two predictors are mutually correlated, since the F_{O3sto} is derived multiplying $[O_3]$ to G_{st}. The fact that the ANN recognize the negative effect of F_{O3sto} over NEE, although the high uncertainty, provides an evidence of the detrimental effect of O_3 over NEE at the holm oak forest.

The effect of the variation of F_{O3sto} on NEE was calculate through the partial derivatives method (Dimopoulos et al., 1995). Partial derivative of NEE with respect to F_{O3} generated a profile of variation of NEE for small changes in F_{O3}. Partial derivative profile represents the rate of change of the output at each point of the time series, plotted versus each corresponding input (fig. 5.5). As figure 5.5 shows, the influence FO_{3sto} on NEE is non-linear. The rate of change of NEE with respect to F_{O3sto} variation is rather low (up to 0.015).

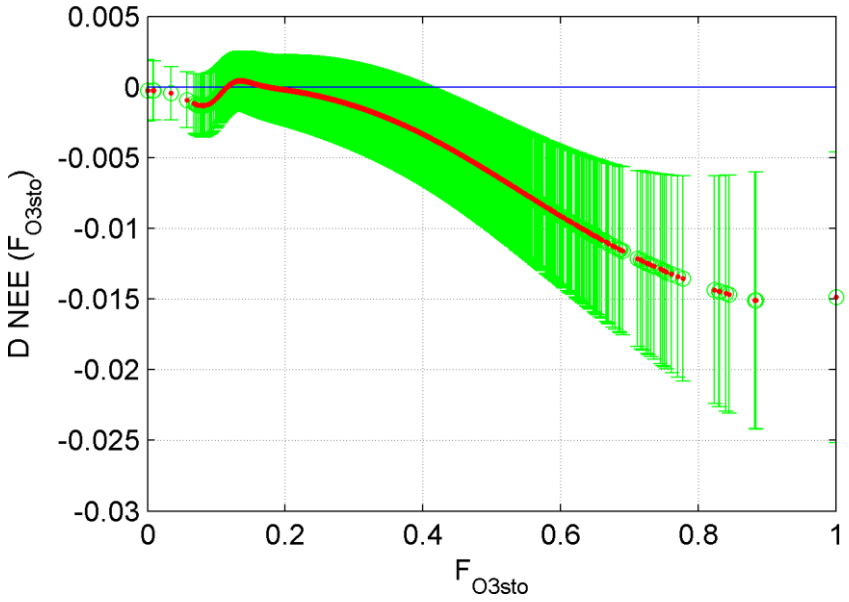

Figure 5.5 Partial derivative of NEE with respect to F_{O3sto}, plotted against F_{O3sto}. All values are scaled between 0 and 1. Red line represent the averaged partial derivative, calculated over the results of 100 ANNs, green bars represent standard deviation.

A sensitivity analysis was performed in order to quantify the effect of F_{O3sto} on NEE. [O_3] used to calculate F_{O3sto} was reduce from 10 to 30 %, and the F_{O3sto} computed with the reduced values were insert as input of the ANNs models. If the O_3 has an impact on NEE, reducing [O_3] is expected to increase NEE. [O_3] reduction significantly affects modelled NEE (ANOVA f = 104.82 p value < 0.01) and a post-hoc test confirmed that also the smallest reduction (10 %) generate an increase of modelled NEE.

Figure 5.7 shows the NEE increase for a [O_3] reduction of 30%, plotted against F_{O3sto}. ANNs perceives [O_3] as a limiting factor for NEE only during Spring and Summer seasons, so that, for a 30% reduction of [O_3], NEE increase up to 4 %.

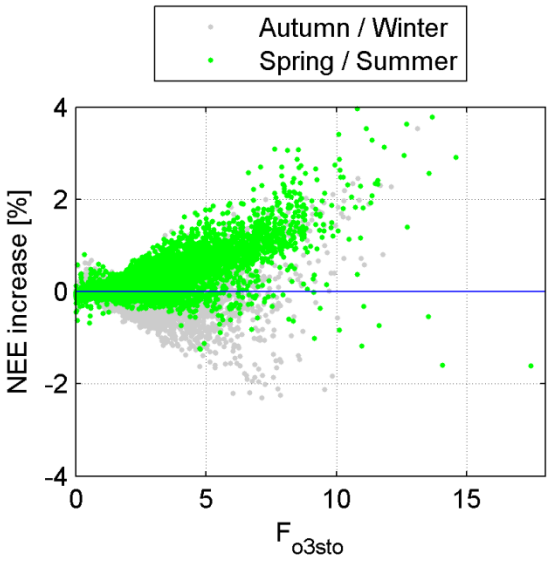

Figure 5.6 Scatterplot of NEE increase for a [O3] reduction of 30 %. Grey dots are Autumn / Winter data, green dots are Spring/Summer data.

The negative effect of O_3 over NEE averaged along the day assumes a bell-shape form (fig. 5.7). During the central hour of day, the O_3 effect is reduced, due to the partial closure of stomata to limit transpiration (mid-day depression). As shown by figure 5.8, stomatal conductance (blue line), is high in the morning, when [O_3] is still low, thus limiting the stomatal O_3 uptake (green line) and reducing the possible negative effect on NEE (red line). This behaviour was already observed in other forests ecosystems (Kurpius et al., 2002; Fares et al., 2010).

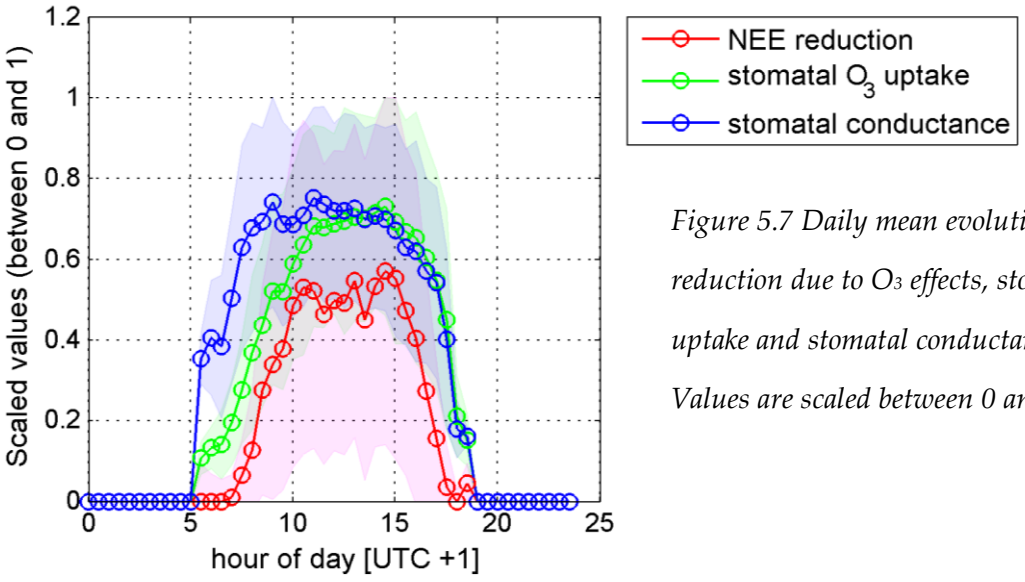

Figure 5.7 Daily mean evolution of NEE reduction due to O_3 effects, stomatal O_3 uptake and stomatal conductance. Values are scaled between 0 and 1.

5.2 Testing the ozone effect on NEE using Partial Least Square approach

In order to test a more conventional approach, based on linear relationships, the effect of O_3 over NEE was tested using PLS analysis.

The predictor variables were the same used in ANN analysis: solar radiation (W m^{-2}), soil water content measured at 10 cm depth (swc_{10}, %), vapour pressure deficit (vpd, kPa), stomatal conductance to H_2O (G_{st}, m s^{-1}) and O_3 stomatal uptake (F_{O3sto}, nmol m^{-2} s^{-1}). As for ANNs, the PLS modelling was performed using the residual variables obtained from the SSA procedure.

In order to separate two relevant periods for plant growth, dataset was split in two (Spring / Summer and Autumn/ Winter). Splitting the dataset would improve the model prediction ability, since predictors may influence NEE differently in the two periods.

Results of the PLS analysis are summarized in tab.8 and tab. 9.

Predictors	*Weights - Spring / Summer*				
	Comp1	Comp2	Comp3	Comp4	Total contribution
Global rad	**0.41**	**0.66**	0.24	**-0.56**	18.69 %
swc_{10}	**-0.73**	-0.10	-0.12	**-0.63**	-35.10 %
VPD	0.52	**-0.45**	**-0.61**	-0.38	-32.96 %
F_{O3sto}	0.11	-0.40	**0.47**	-0.38	-7.74 %
G_{st}	0.15	-0.44	**0.58**	0.02	5.50 %
Partial r^2	0.015	0.029	0.026	0.025	
model r^2 = 0.10					
MSE = 21.33					

Table 8: Components weights calculated by PLS regression performed over Spring / Summer dataset, averaged over half-hour timescale. Partial r^2 represent the variance explained by each component, model r^2 is the sum of all partial r^2, MSE is the mean squared error calculated using 10-fold cross-validation. Weights whose squares are larger than 0.2 are shown in bold type.

Predictors	*Weights - Autumn / Winter*				
	Comp1	Comp2	Comp3	Comp4	Total contribution
Global rad	**0.85**	**0.24**	0.11	-0.38	37.48 %
swc_{10}	-0.15	-0.71	-0.13	**-0.61**	-18.34 %
VPD	0.22	-0.05	**-0.94**	0.24	6.05 %
F_{O3sto}	0.29	**-0.52**	0.30	**0.65**	22.67 %
G_{st}	0.36	-0.41	0.02	-0.04	15.45 %
Partial r^2	0.098	0.007	0.016	0.026	
model r^2 = 0.15					
MSE = 19.5					

Table 9: Components weights calculated by PLS regression performed over Spring / Summer dataset, averaged over half-hour timescale. Partial r^2 represent the variance explained by each component, model r^2 is the sum of all partial r^2, MSE is the mean squared error calculated using 10-fold cross-validation. Weights whose squares are larger than 0.2 are shown in bold type.

The variability explained by PLS models was 10 % in Spring / Summer analysis and 15 % in Autumn / Winter analysis.

Figure 5.8 shows the relative importance of each predictor variables within the PLS models (fig 5.8 a: Spring / Summer; fig 5.8 b: Autumn / Winter).

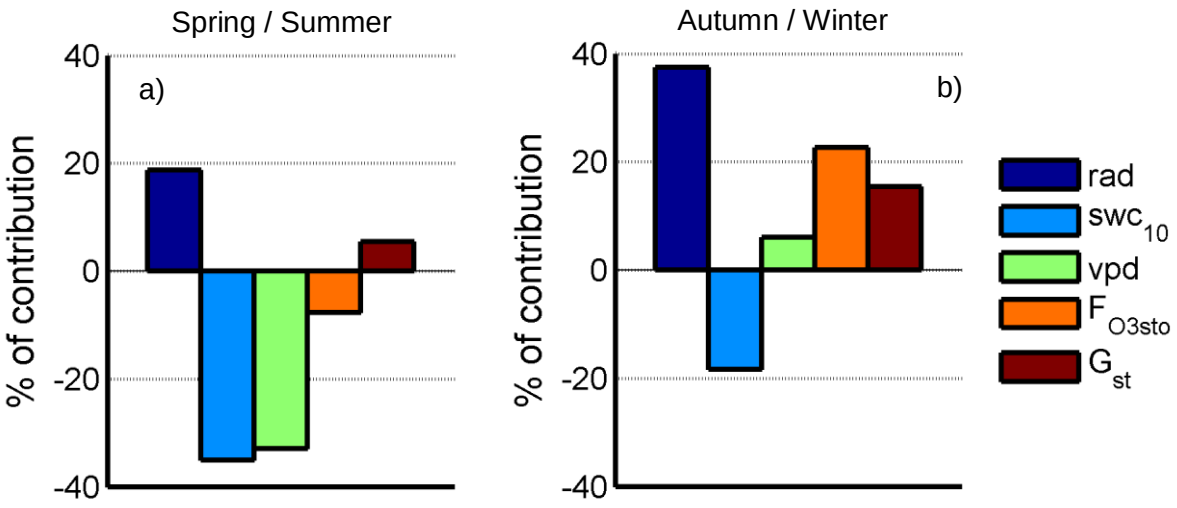

Figure 5.8 Relative importance (%) of each predictors within the PLS models. (a) PLS model performed over half-hour Spring / Summer dataset, (b) PLS model performed over half-hour Autumn / Winter dataset.

The factors that most influenced NEE during Spring /Summer period where swc_{10} (-35.10 % of the total variability explained by the model) and vpd (-32.96 %). In this model, swc_{10} is perceived as a factor that decreased NEE. This unexpected result may depend by the fact that a linear regression is not able to adequately reproduce relationship between swc_{10} and NEE. In Mediterranean climate water availability highly impact plants activity (Granier et al., 2007). However, highest swc_{10} values are often measured during rain events, when cloudy condition reduces the amount of PAR available to vegetation (fig. 5.9). This relation may be the cause of the erroneous perception of swc_{10} as a negative factor affecting NEE.

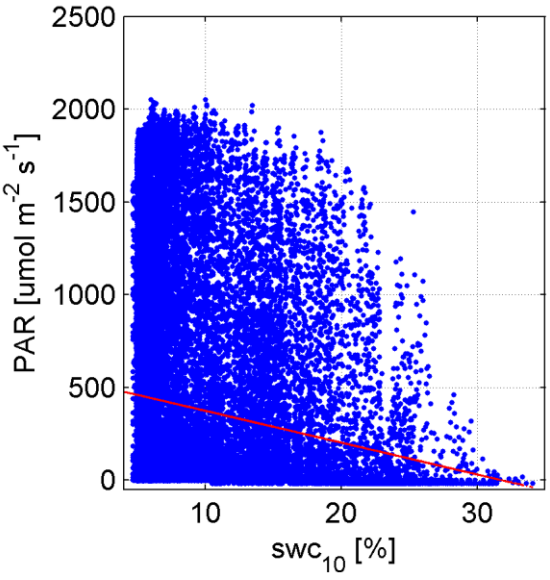

Figure 5.9 Plot of swc_{10} (%) vs PAR (photosynthetic active radiation, µmol m-2 s-1). Red line is the linear fit. Data recorded over the whole study period.

In Autumn / Winter, solar radiation in the most important factors influencing NEE (37.48%).

F_{O3sto} is perceived as negative predictor only during the Spring / Summer period, contributing with a -7.74 % in explaining the NEE variability. As previously observed in the ANN analysis, the fact that the model assigns a negative value to F_{O3sto} (calculated as G_{st} multiplied for $[O_3]$) whilst recognizing the positive effect of G_{st}, proves that the model discerns the detrimental effect of $[O_3]$ component from G_{st} component of F_{O3sto}.

In the Autumn / Winter PLS model, F_{O3sto} acted positively, enhancing NEE. This means that during the cold seasons, $[O_3]$ is not a limiting factor.

6 Synthesis and overall discussion

Four years of measurements of CO_2 fluxes over the holm oak forest, combined with 19-month CH_4 flux measurements, demonstrate that the ecosystem is an active carbon sink all year long (485 – 690 g C m^{-2} y^{-1}), despite the ecosystems behaves as a CH_4 source during part of the year. Precipitation has been found one of the most important factor controlling carbon exchanges at the forest. Especially, precipitation amount that falls during Summer season can strongly determinate the CO_2 uptake at the forest, so that the difference between a dry summer and a wet summer can account for almost 200 g C m^{-2} in the annual C budget. Moreover, the magnitude of the CH_4 emission at the forest is regulated by precipitation. The dry condition of the Summer period has been found to depress CH_4-oxidasing bacteria so that during the dry season the ecosystem acts as a net source of CH_4, transported from the soil depth to the above canopy through xylematic pathways. Furthermore, the Summer high UV radiation has been found to promote CH_4 production from the leaves wax, increasing the overall strength of the summer CH_4 source. However, the persistent soil sink smoothed the overall importance of plant-mediated transport and leaf production of CH_4, thus leading to an annual CH_4 budget close to the neutrality (-265.04 μmol m^{-2} y^{-1}).

Besides being a sink for C, the holm oak forest represents a net sink of O_3 also. The annual budget has been estimated around 80 mmol m^{-2} y^{-1}. The major O_3 deposition pathways are through stomata, soil and cuticles. The relative importance of the three sinks is reported in fig. 6.1 for each season:

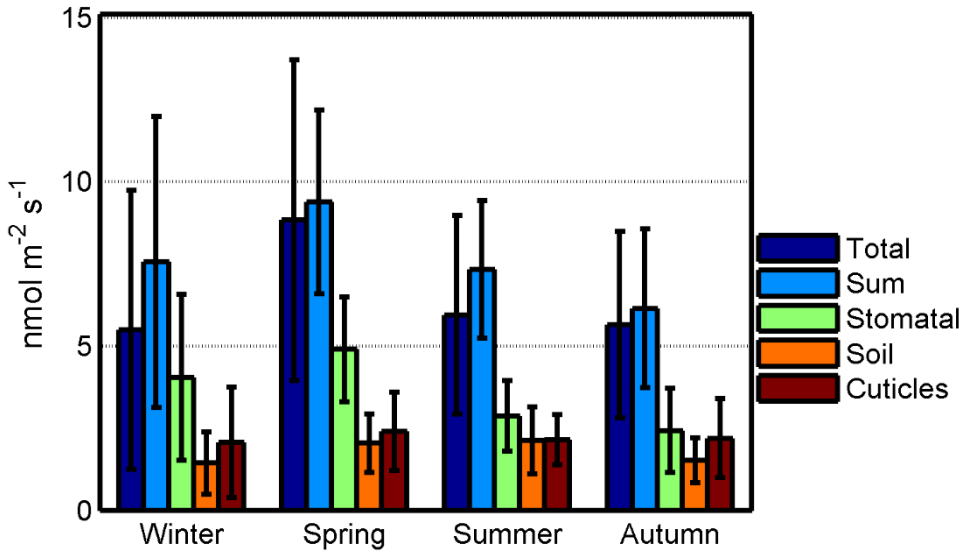

Figure 6.1 Bar chart showing total, stomatal, cuticular and ground O_3 fluxes. The sum of the three measured O_3 sinks is also shown to highlight divergence with total ozone fluxes. For each season, data were averaged for the central hours of the day (10:30 am to 02:30 pm), error bars represent standard deviation.

While soil and cuticles sink magnitudes were almost constant throughout the year (up to 40 % and 30 % respectively), the stomatal sink widely varied across the different seasons. The stomatal sink was the major one reaching up to 60 % of the total O_3 uptake during Spring. The high importance of stomatal uptake during the growing season makes the total O_3 uptake greatly dependent by water availability, so that drought occurring in Spring can highly decrease the ecosystem O_3 sink capacity. Other O_3 loss pathways, such as by chemical reactions with BVOCs and NO_x has been found to play a minor role at the forest site, as shown by a comparison of the three major O_3 sinks with total ozone fluxes (fig 6.1).

Proved that at the holm oak forest the major contribution to the O_3 uptake is provided by stomata, the intent in this work was to evaluate whether or not O_3 entering the leaves causes a reduction in carbon assimilation. The hypothesis of an O_3 detrimental effect was tested through two multivariate statistical methods: ANN (non-linear approach) and PLS (linear approach), which allowed to test the effects of O_3 stomatal uptake in parallel with other environmental and physiological parameters. Both methods found a carbon assimilation decrease during Spring and Summer, when photochemistry is activated by high radiation and temperature and [O_3] reaches high and phytotoxic levels. Comparing the two

approaches, ANN performed better than PLS, assigning the right importance to the predictor factors other than O_3. This is not surprising considering that the relationship between the predictor factors is often non-linear.

ANN results show that, although O_3 does not represent the main limiting factor to forest productivity as compared to drought, vapour pressure deficit and solar radiation, carbon sink potential is weakened by the exposure to O_3. The maximum rate of reduction in NEE for unit increase in stomatal O_3 uptake was 0.015, leading to a maximum NEE increase of 4% when [O_3] is 30 % lowered. Concerning the daily dynamic, the major damage was observed early in the afternoon, when the O_3 dose entering the stomata is highest. Indeed, although [O_3] is high during the central hour of day, O_3 entering the leaves is reduced by partial stomatal closure, a Mediterranean plant strategy to limit water loss through transpiration during the hottest hours.

Consistently with ANNs results, PLS analysis found a NEE reduction of 7 % attributable to the O_3 stomatal uptake during Spring / Summer period. However, this linear approach did not asses the right importance to all the environmental predictors, e.g. swc_{10}, highlighting that a non-linear approach is to be preferred in modelling NEE responses to the environmental and physiological parameters.

Conclusions

The results of this PhD work are important to demonstrate that this Mediterranean forest is an active carbon sink and contributes to ameliorate air quality removing O_3 from the atmosphere.

CO_2 absorption occurs all year long, while the magnitude and direction of CH_4 exchanges change towards the year. However, considering the whole year, CH_4 budget is close to neutrality and, at present, does not affect the global carbon balance at the site. O_3 uptake through stomata has been found to reduce carbon assimilation, although the magnitude of the carbon loss imputable to O_3 was low.

Among others, water availability was found to be the most important factor controlling CO_2, CH_4 and O_3 exchanges at the site. Draught stress has been found to reduce CO_2 assimilation, to enhance CH_4 emission and to reduce O_3 uptake. Considering that Mediterranean forests are among the most threatened ecosystems by climate changes and that this region is predicted to experience a pronounced decrease in precipitations and warming in the next years (Giorgi and Lionello, 2008), the benefits that the holm oak forest ecosystem currently provides may results severely reduced.

A list of the main results achieved in this PhD work:

* For the first time, a long term monitoring of CH_4 exchange above a Mediterranean forest was conducted, measuring that the ecosystem is a net CH_4 sink during the cold season and a net source during the dry season, thus making the net exchange close to the neutrality.
* Results provide evidences for a plant-mediated CH_4 transport through xylematic pathways and support the hypothesis that an UV-induced production of CH_4 from vegetation takes place.
* Among others, water availability highly impact the direction of CH_4 fluxes, influencing the balance between methanogenic / methanotrophic activity in the soil.

* The forest has been found to be a net sink of O_3 all year long, partitioning of the total O_3 fluxes between soil, cuticles and stomata highlights that the latter sink plays a major role at the forest site.
* Evidences that a portion of the nocturnal O_3 sink can be ascribed to reaction of O_3 with NO and BVOC were provided.
* The dependence of O_3 uptake from water availability has been proved.
* The influence of O_3 over NEE was tested using a novel approach, which combines non parametric time series decomposition (SSA) and the explanatory capacity of Artificial Neural Networks. Results suggest that O_3 has a detrimental effect over NEE during Spring and Summer seasons, although the magnitude of this reduction is low (rate of reduction of NEE for unit change of O_3 stomatal uptake = 0.015) in comparison to other stress factors, such as drought.
* A more conventional multivariate linear approach was applied (PLS regression), which confirmed the negative effect of O_3 over NEE, quantified as 7%.

Acknowledgements

The PhD research was made possible by a grant co-financed by the Department for Innovation in Biological, Agro-Food and Forest Systems (DIBAF) – Univesity of Tuscia, Viterbo, and the Council for Agricultural Research and Economics - Research Centre for the Soil-Plant System (CREA - RPS), Rome.

The research was also made possible thanks to the Scientific Commission of Castelporziano, the Multi-disciplinary Centre for the Study of Coastal Mediterranean Ecosystems and the Directorate of Castelporziano Estate.

There have been many people who supported me in the last three year, and in this few lines I want to thank all of them.

First of all, thanks to my supervisor, Silvano, for all the advices and corrections guiding the development of this work throughout the years. His enthusiasm has been inspiring and his support is invaluable.

Thanks to the micrometeorology lab colleagues: Tiziano, Valerio, Filippo, Roberto, Daniela, Alessandro and Adriano for their help in the field, for the laughers and encouragements.

Thanks to all the co-authors of the papers presented within this thesis, especially to Claudia for her willingness to help every time.

Thanks to Eiko Nemitz, for giving me the opportunity to work with him and his research group at the Centre for Ecology and Hydrology, Edinburgh. The stay was a great enriching experience. A special thanks goes to Federico, for sharing lunchtimes and so many coffees.

Thanks to Chiara and Enrica, for their support and friendship throughout these years.

Finally, thank to my family and to Marco, for the patience and support, for the happiness and optimism demonstrated for all these years.

Because of all of them, I've been able to complete this work. To each and every one of them, thanks.

References

Ainsworth, E. a, Yendrek, C.R., Sitch, S., Collins, W.J., Emberson, L.D., 2012. The effects of tropospheric ozone on net primary productivity and implications for climate change. Annu. Rev. Plant Biol. 63, 637–61. doi:10.1146/annurev-arplant-042110-103829

Aubinet, M., Vesala, T., Papale, D. (Eds.), 2012. Eddy Covariance. Springer Netherlands, Dordrecht. doi:10.1007/978-94-007-2351-1

Bauer, M., Hultman, N., 2000. Ozone deposition to a ponderosa pine plantation in the Sierra Nevada Mountains(CA)- A comparison of two different climatic years. J. Geophys. Res. 105, 22132–22136.

Berntsen, T., Fuglestvedt, J., Joshi, M., 2005. Response of climate to regional emissions of ozone precursors: sensitivities and warming potentials. Tellus B.

Bian, L., Gao, Z., Sun, Y., Ding, M., Tang, J., Schnell, R.C., 2016. CH_4 Monitoring and Background Concentration at Zhongshan Station, Antarctica. Atmos. Clim. Sci. 06, 135–144. doi:10.4236/acs.2016.61012

Biondi, F.A., Dowgiallo, G., Gisotti, G., Tinelli, A., Figliolia, A., Scarascia Mugnozza, G., 2001. Memorie illustrativa alla carta dei suoli della Tenuta di Castelporziano, in: Il Sistema Ambientale Della Tenuta Presidenziale Di Castelporziano. Accademia Nazionale delle scienze detta dei quaranta, Rome.

Brugnoli, E., Calfapietra, C., 2010. Carbonyl sulfide: a new tool for understanding the response of the land biosphere to climate change. New Phytol. 186, 783–785.

Bruhn, D., Mikkelsen, T.N., Øbro, J., Willats, W.G.T., Ambus, P., 2009. Effects of temperature, ultraviolet radiation and pectin methyl esterase on aerobic methane release from plant material. Plant Biol. 11, 43–48. doi:10.1111/j.1438-8677.2009.00202.x

Bruhn, D., Mikkelsen, T.N., Rolsted, M.M.M., Egsgaard, H., Ambus, P., 2014. Leaf surface wax is a source of plant methane formation under UV radiation and in the presence of oxygen. Plant Biol. 16, 512–516. doi:10.1111/plb.12137

Bruhn, D., Møller, I.M., Mikkelsen, T.N., Ambus, P., 2012. Terrestrial plant methane production and emission. Physiol. Plant. 144, 201–209. doi:10.1111/j.1399-3054.2011.01551.x

Bucci, M., 2006. The state of water resources, in: Ricerche Sulla Complessità Di Un Ecosistema Forestale Costiero Mediterraneo. Accademia Nazionale delle Scienze detta dei XL, Rome.

Burn, J., Henk, J., Bloemen, T., 1993. Chemistry and analysis of volatile organic compounds in the environment, Springer N. ed.

Cape, J.N., 2003. Effects of airborne volatile organic compounds on plants. Environ. Pollut. 122, 145–157. doi:10.1016/S0269-7491(02)00273-7

Castell, C., Terradas, J., Tenhunen, J., 1994. Water relations, gas exchange, and growth of resprouts and mature plant shoots of Arbutus unedo L. and Quercus ilex L. Oecologia 98, 201.211. doi:10.1007/BF00341473

Coyle, M., Nemitz, E., Storeton-West, R., Fowler, D., Cape, J.N., 2009. Measurements of ozone deposition to a potato canopy. Agric. For. Meteorol. 149, 655–666. doi:10.1016/j.agrformet.2008.10.020

Culf, A., Fisch, G., Malhi, Y., Nobre, C., 1997. The influence of the atmospheric boundary layer on carbon dioxide concentrations over a tropical forest. Agric. For. Meteorol. 85, 149–158. doi:10.1016/S0168-1923(96)02412-4

Davison, B., Taipale, R., Langford, B., Misztal, P., Fares, S., Matteucci, G., Loreto, F., Cape, J.N., Rinne, J., Hewitt, C.N., 2009. Concentrations and fluxes of biogenic volatile organic compounds above a Mediterranean macchia ecosystem in western Italy. Biogeosciences 6, 1655–1670.

Denman, K.L., Brasseur, G.P., Chidthaisong, A., Ciais, P., Cox, P.M., Dickinson, R.E., Hauglustaine, D.A., Heinze, C., Holland, E.A., Jacob, D.J., Lohmann, U., Ramachandran, S., Leite da Silva Dias, P., Wofsy, S.C., Zhang, X., Steffen, W., 2007. Couplings between changes in the climate system and biogeochemistry, in: Climate Change 2007: The Physical Science Basis. Contribution of Working Group I to the Fourth Assessment Report of the Intergovernmental Panel on Climate Change. Cambridge University Press, Cambridge, United Kingdom and New York, USA.

Denmead, O.T., 2008. Approaches to measuring fluxes of methane and nitrous oxide between landscapes and the atmosphere. Plant Soil 309, 5–24. doi:10.1007/s11104-008-9599-z

Dimopoulos, Y., Bourret, P., Lek, S., 1995. Use of some sensitivity criteria for choosing networks with good generalization ability. Neural Process. Lett. 2, 1–4. doi:10.1007/BF02309007

Erisman, J., Pul, A. Van, Wyers, P., 1994. Parametrization of surface resistance for the quantification of atmospheric deposition of acidifying pollutants and ozone. Atmos. Environ. 28, 2595–2607.

Etheridge, D., Pearman, G., Fraser, P., 1992. Changes in tropospheric methane between 1841 and 1978 from a high accumulation-rate Antarctic ice core. Tellus B 44, 282–294.

doi:10.1034/j.1600-0889.1992.t01-3-00006.x

Fares, S., McKay, M., Holzinger, R., Goldstein, A.H., 2010. Ozone fluxes in a Pinus ponderosa ecosystem are dominated by non-stomatal processes: Evidence from long-term continuous measurements. Agric. For. Meteorol. 150, 420–431. doi:10.1016/j.agrformet.2010.01.007

Fares, S., Mereu, S., Scarascia Mugnozza, G., Vitale, M., Manes, F., Frattoni, M., Ciccioli, P., Gerosa, G., Loreto, F., 2009. The ACCENT-VOCBAS field campaign on biosphere-atmosphere interactions in a Mediterranean ecosystem of Castelporziano (Rome): site characteristics, climatic and meteorological conditions, and eco-physiology of vegetation. Biogeosciences 6, 1043–1058. doi:10.5194/bg-6-1043-2009

Fares, S., Savi, F., Muller, J., Matteucci, G., Paoletti, E., 2014. Simultaneous measurements of above and below canopy ozone fluxes help partitioning ozone deposition between its various sinks in a Mediterranean Oak Forest. Agric. For. Meteorol. 198-199, 181–191. doi:10.1016/j.agrformet.2014.08.014

Fares, S., Vargas, R., Detto, M., Goldstein, A.H., Karlik, J., Paoletti, E., Vitale, M., 2013. Tropospheric ozone reduces carbon assimilation in trees: Estimates from analysis of continuous flux measurements. Glob. Chang. Biol. 19, 2427–2443. doi:10.1111/gcb.12222

Fares, S., Weber, R., Park, J.-H., Gentner, D., Karlik, J., Goldstein, A.H., 2012. Ozone deposition to an orange orchard: Partitioning between stomatal and non-stomatal sinks. Environ. Pollut. 169, 258–66. doi:10.1016/j.envpol.2012.01.030

Foken, T., 2008. Micrometeorology, Springer. ed. Berlin, Heidelberg.

Foken, T., Wichura, B., 1996. Tools for quality assessment of surface-based flux measurements. Agric. For. Meteorol. 78, 83–105. doi:10.1016/0168-1923(95)02248-1

Fowler, D., Pilegaard, K., Sutton, M.A., Ambus, P., Raivonen, M., Duyzer, J., Simpson, D., Fagerli, H., Fuzzi, S., Schjoerring, J.K., Granier, C., Neftel, A., Isaksen, I.S.A., Laj, P., Maione, M., Monks, P.S., Burkhardt, J., Daemmgen, U., Neirynck, J., Personne, E., Wichink-Kruit, R., Butterbach-Bahl, K., Flechard, C., Tuovinen, J.P., Coyle, M., Gerosa, G., Loubet, B., Altimir, N., Gruenhage, L., Ammann, C., Cieslik, S., Paoletti, E., Mikkelsen, T.N., Ro-Poulsen, H., Cellier, P., Cape, J.N., Horvath, L., Loreto, F., Niinemets, Ü., Palmer, P.I., Rinne, J., Misztal, P., Nemitz, E., Nilsson, D., Pryor, S., Gallagher, M.W., Vesala, T., Skiba, U., Bruggemann, N., Zechmeister-Boltenstern, S., Williams, J., O'Dowd, C., Facchini, M.C., de Leeuw, G., Flossman, A., Chaumerliac, N., Erisman, J.W., 2009. Atmospheric composition change: Ecosystems-Atmosphere interactions. Atmos. Environ. 43, 5193–5267. doi:10.1016/j.atmosenv.2009.07.068

Fusco, A.C., Logan, J.A., 2003. Analysis of 1970–1995 trends in tropospheric ozone at

Northern Hemisphere midlatitudes with the GEOS-CHEM model. J. Geophys. Res. 108, 4449. doi:10.1029/2002JD002742

Garland, J.A., 1977. The dry deposition of sulfure dioxide to land and water surfaces. Proc. R. Soc. Lond. A. 354, 245–268.

Garland, J.A., 1977. The Dry Deposition of Sulphur Dioxide to Land and Water Surfaces. Proc. R. Soc. A Math. Phys. Eng. Sci. 354, 245–268. doi:10.1098/rspa.1977.0066

Garratt, J., 1994. Review: the atmospheric boundary layer. Earth-Science Rev. 37, 89–134. doi:10.1016/0012-8252(94)90026-4

Gerosa, G., Derghi, F., Cieslik, S., 2007. Comparison of different algorithms for stomatal ozone flux determination from micrometeorological measurements. Water. Air. Soil Pollut. 179, 309–321. doi:10.1007/s11270-006-9234-7

Gerosa, G., Finco, A., Mereu, S., Vitale, M., Manes, F., Denti, A.B., 2009. Comparison of seasonal variations of ozone exposure and fluxes in a Mediterranean Holm oak forest between the exceptionally dry 2003 and the following year. Environ. Pollut. 157, 1737–44. doi:10.1016/j.envpol.2007.11.025

Gevrey, M., Dimopoulos, I., Lek, S., 2003. Review and comparison of methods to study the contribution of variables in artificial neural network models. Ecol. Modell. 160, 249–264. doi:10.1016/S0304-3800(02)00257-0

Gevrey, M., Dimopoulos, I., Lek, S., 2006. Two-way interaction of input variables in the sensitivity analysis of neural network models. Ecol. Modell. 195, 43–50. doi:10.1016/j.ecolmodel.2005.11.008

Giorgi, F., Lionello, P., 2008. Climate change projections for the Mediterranean region. Glob. Planet. Change 63, 90–104. doi:10.1016/j.gloplacha.2007.09.005

Godish, T., Davis, W.T., Fu, J.S., 2014. Air Quality, 5th Editio. ed. CRC Press Book, Boca Raton, FL.

Golyandina, N., Nekrutkin, V.V., Zhigljavsky, A.A., 2001. Analysis of Time Series Structure: SSA and Related Techniques 309. doi:10.1198/jasa.2002.s239

Granier, A., Reichstein, M., Bréda, N., Janssens, I.A., Falge, E., Ciais, P., Grünwald, T., Aubinet, M., Berbigier, P., Bernhofer, C., Buchmann, N., Facini, O., Grassi, G., Heinesch, B., Ilvesniemi, H., Keronen, P., Knohl, A., Köstner, B., Lagergren, F., Lindroth, A., Longdoz, B., Loustau, D., Mateus, J., Montagnani, L., Nys, C., Moors, E., Papale, D., Peiffer, M., Pilegaard, K., Pita, G., Pumpanen, J., Rambal, S., Rebmann, C., Rodrigues, A., Seufert, G., Tenhunen, J., Vesala, T., Wang, Q., 2007. Evidence for soil water control on carbon and water dynamics in European forests during the extremely dry year: 2003. Agric. For. Meteorol. 143, 123–145. doi:10.1016/j.agrformet.2006.12.004

Grünhage, L., Pleijel, H., Mills, G., Bender, J., Danielsson, H., Lehmann, Y., Castell, J.-F., Bethenod, O., 2012. Updated stomatal flux and flux-effect models for wheat for quantifying effects of ozone on grain yield, grain mass and protein yield. Environ. … 165, 147–157. doi:10.1016/j.envpol.2012.02.026

Guenther, A., Geron, C., Pierce, T., Lamb, B., Harley, P., Fall, R., 2000. Natural emissions of non-methane volatile organic compounds, carbon monoxide, and oxides of nitrogen from North America. Atmos. … 34, 2205–2230. doi:10.1016/S1352-2310(99)00465-3

Heath, R.L., 1980. Initial Events in Injury to Plants by Air Pollutants. Annu. Rev. Plant Physiol. 31, 395–431. doi:10.1146/annurev.pp.31.060180.002143

Hicks, B.B., Baldocchi, D.D., Meyers, T.P., Hosker, R.P., Matt, D.R., 1987. A preliminary multiple resistance routine for deriving dry deposition velocities from measured quantities. Water. Air. Soil Pollut. 36, 311–330. doi:10.1007/BF00229675

Hindawi, I.J., 1979. Air pollution injury to vegetation. National Air Pollution Control Administration,Washington, DC, Washington, DC.

Holzinger, R., Lee, A., Paw, K.T., Goldstein, U.A.H., 2005. Observations of oxidation products above a forest imply biogenic emissions of very reactive compounds. Atmos. Chem. Phys. 5, 67–75. doi:10.5194/acp-5-67-2005

Hsieh, C., Katul, G., Chi, T., 2000. An approximate analytical model for footprint estimation of scalar ¯ uxes in thermally strati ® ed atmospheric ¯ ows 23, 765–772.

IPCC, 2013. Contribution of Working Group I to the Fifth Assessment Report of the Intergovernmental Panel on Climate Change, in: Climate Change 2013: The Physical Science Basis. Cambridge University Press, Cambridge, United Kingdom and New York, USA.

Junge, C.E., 1963. Air chemistry and radioactivity, Academic P. ed. New York and London. Academic Press., New York and London.

Kampa, M., Castanas, E., 2008. Human health effects of air pollution. Environ. Pollut. 151, 362–7. doi:10.1016/j.envpol.2007.06.012

Karlsson, P.E., Pleijel, H., Pihl Karlsson, G., Medin, E.L., Skärby, L., 2000. Simulations of stomatal conductance and ozone uptake to Norway spruce saplings in open-top chambers. Environ. Pollut. 109, 443–451. doi:10.1016/S0269-7491(00)00047-6

Karlsson, P.E., Uddling, J., Braun, S., Broadmeadow, M., Elvira, S., Gimeno, B.S., Le Thiec, D., Oksanen, E., Vandermeiren, K., Wilkinson, M., Emberson, L., 2004. New critical levels for ozone effects on young trees based on AOT40 and simulated cumulative leaf uptake of ozone. Atmos. Environ. 38, 2283–2294. doi:10.1016/j.atmosenv.2004.01.027

Keppler, F., Hamilton, J.T.G., Braß, M., Röckmann, T., 2006. Methane emissions from terrestrial plants under aerobic conditions. Nature 439, 187–191. doi:10.1038/nature04420

Kesselmeier, J., Staudt, M., 1999. Biogenic Volatile Organic Compounds (VOC): An Overview on Emission, Physiology and Ecology. J. Atmos. Chem. 33, 23–88.

Kurpius, M.., McKay, M., Goldstein, A.., 2002. Annual ozone deposition to a Sierra Nevada ponderosa pine plantation. Atmos. Environ. 36, 4503–4515. doi:10.1016/S1352-2310(02)00423-5

Kurpius, M.R., Goldstein, A.H., 2003. Gas-phase chemistry dominates O 3 loss to a forest, implying a source of aerosols and hydroxyl radicals to the atmosphere. Geophys. Res. Lett. 30. doi:10.1029/2002GL016785

Lamaud, E., Carrara, A., Brunet, Y., Lopez, A., Druilhet, A., 2002. Ozone fluxes above and within a pine forest canopy in dry and wet conditions. Atmos. Environ. 36, 77–88. doi:10.1016/S1352-2310(01)00468-X

Langford, B., Acton, W., Ammann, C., Valach, A., Nemitz, E., 2015. Eddy-covariance data with low signal-to-noise ratio: Time-lag determination, uncertainties and limit of detection. Atmos. Meas. Tech. 8, 4197–4213. doi:10.5194/amt-8-4197-2015

Lathiere, J., Hauglustaine, D., 2006. Impact of climate variability and land use changes on global biogenic volatile organic compound emissions. Atmos. Chem. Phys. 6, 2129–2146.

Law, R.M., Mansfield, T.A., 1982. Effects of Gaseous Air Pollution in Agriculture and Horticulture, in: Unsworth, M.H., Ormrod, D.P. (Eds.), Effects of Gaseous Air Pollution in Agriculture and Horticulture. Butterworth Scientific, London, Boston, Sydney, Wellington, Durban, Toronto.

Lek, S., Guegan, J.-F., 2000. Artificial Neuronal Networks: Application to Ecology and Evolution. Springer-Verlag New York, Inc., Berlin.

Lelieveld, J., Crutzen, P., Dentener, F., 1998. Changing concentration, lifetime and climate forcing of atmospheric methane. Tellus B.

Llusia, J., Peñuelas, J., 2000. Seasonal patterns of terpene content and emission from seven Mediterranean woody species in field conditions. Am. J. Bot. 87, 133–140.

Loreto, F., Ciccioli, P., Brancaleoni, E., Valentini, R., De Lillis, M., Csiky, O., Seufert, G., 1998. A hypothesis on the evolution of isoprenoid emission by oaks based on the correlation between emission type and Quercus taxonomy. Oecologia 115, 302–305.

Loreto, F., Pinelli, P., Manes, F., Kollist, H., 2004. Impact of ozone on monoterpene emissions and evidence for an isoprene-like antioxidant action of monoterpenes emitted by

Quercus ilex leaves. Tree Physiol. 24, 361–367.

Manes, F., Vitale, M., Maria Fabi, A., De Santis, F., Zona, D., 2007. Estimates of potential ozone stomatal uptake in mature trees of Quercus ilex in a Mediterranean climate. Environ. Exp. Bot. 59, 235–241. doi:10.1016/j.envexpbot.2005.12.001

Manning, W.J., 2005. Establishing a cause and effect relationship for ambient ozone exposure and tree growth in the forest: progress and an experimental approach. Environ. Pollut. 137, 443–54. doi:10.1016/j.envpol.2005.01.031

Martins, C., Mesquita, S., Vaz, W., 1999. Cuticular waxes of the Holm (Quercus ilex L. subsp. ballota (desf.) samp.) and Cork (Q. suber L.) oaks. Phytochem. Anal. 10, 1–5.

Massman, W.J., 1998. A review of the molecular diffusivities of H2O, CO2, CH4, CO, O3, SO2, NH3, N2O, NO, and NO2 in air, O2 and N2 near STP. Atmos. Environ. 32, 1111–1127. doi:10.1016/S1352-2310(97)00391-9

McLeod, A.R., Fry, S.C., Loake, G.J., Messenger, D.J., Reay, D.S., Smith, K. a., Yun, B.W., 2008. Ultraviolet radiation drives methane emissions from terrestrial plant pectins. New Phytol. 180, 124–132. doi:10.1111/j.1469-8137.2008.02571.x

Melillo, J.M., McGuire, A.D., Kicklighter, D.W., Moore, B., Vorosmarty, C.J., Schloss, A.L., 1993. Global climate change and terrestrial net primary production. Nature 363, 234–240. doi:10.1038/363234a0

Mereu, S., Salvatori, E., Fusaro, L., Gerosa, G., Muys, B., Manes, F., 2009. An integrated approach shows different use of water resources from Mediterranean maquis species in a coastal dune ecosystem. Biogeosciences 6, 2599–2610. doi:10.5194/bg-6-2599-2009

Mészáros, R., Horváth, L., Weidinger, T., Neftel, A., Nemitz, E., Dämmgen, U., Cellier, P., Loubet, B., 2009. Measurement and modelling ozone fluxes over a cut and fertilized grassland. Biogeosciences 6, 1987–1999. doi:10.5194/bg-6-1987-2009

Monks, P.S., Archibald, A.T., Colette, A., Cooper, O., Coyle, M., Derwent, R., Fowler, D., Granier, C., Law, K.S., Mills, G.E., Stevenson, D.S., Tarasova, O., Thouret, V., Von Schneidemesser, E., Sommariva, R., Wild, O., Williams, M.L., 2015. Tropospheric ozone and its precursors from the urban to the global scale from air quality to short-lived climate forcer. Atmos. Chem. Phys. 15, 8889–8973. doi:10.5194/acp-15-8889-2015

Mukhin, V.A., Voronin, P.Y., 2011. Methane emission from living tree wood. Russ. J. Plant Physiol. 58, 344–350. doi:10.1134/S1021443711020117

Muller, J., Percival, C., Gallagher, M., Fowler, D., Coyle, M., Nemitz, E., 2009. Sources of uncertainty in eddy covariance ozone flux measurements made by dry chemiluminescence fast response analysers. Atmos. Meas. Tech. 3, 163–176.

Musselman, R., Llefohn, A., Masman, W., Heath, R., 2006. A critical review and analysis of the use of exposure- and flux-based ozone indices for predicting vegetation effects. Atmos. Environ. 40, 1869–1888. doi:10.1016/j.atmosenv.2005.10.064

Nakai, T., Shimoyama, K., 2012. Ultrasonic anemometer angle of attack errors under turbulent conditions. Agric. For. Meteorol. 162-163, 14–26. doi:10.1016/j.agrformet.2012.04.004

Nemitz, E., Sutton, M.A., Gut, A., San José, R., Husted, S., Schjoerring, J.K., 2000. Sources and sinks of ammonia within an oilseed rape canopy. Agric. For. Meteorol. 105, 385–404. doi:10.1016/S0168-1923(00)00205-7

Nicolini, G., Castaldi, S., Fratini, G., Valentini, R., 2013. A literature overview of micrometeorological CH4 and N2O flux measurements in terrestrial ecosystems. Atmos. Environ. doi:10.1016/j.atmosenv.2013.09.030

Noe, S., Copolovici, L., Niinemets, Ü., Vaino, E., 2008. Foliar limonene uptake scales positively with leaf lipid content:"Non-emitting" species absorb and release monoterpenes. Plant Biol. 10, 129–137. doi:10.1055/s-2007-965239

Olden, J.D., Jackson, D.A., 2002. Illuminating the "black box": a randomization approach for understanding variable contributions in artificial neural networks. Ecol. Modell. 154, 135–150. doi:10.1016/S0304-3800(02)00064-9

Olden, J.D., Joy, M.K., Death, R.G., 2004. An accurate comparison of methods for quantifying variable importance in artificial neural networks using simulated data. Ecol. Modell. 178, 389–397. doi:10.1016/j.ecolmodel.2004.03.013

Ollinger, S., Aber, J., Reich, P., 1997. Simulating ozone effects on forest productivity: interactions among leaf-, canopy-, and stand-level processes. Ecol. Appl. 7, 1237–1251. doi:10.1890/1051-0761(1997)007[1237:SOEOFP]2.0.CO;2

Owen, P., Thomson, W., 1963. Heat transfer across rough surfaces. J. Fluid Mech. 15, 321–334. doi:10.1017/S0022112063000288

Papale, D., Valentini, R., 2003. A new assessment of European forests carbon exchanges by eddy fluxes and artificial neural network spatialization. Glob. Chang. Biol. 9, 525–535. doi:10.1046/j.1365-2486.2003.00609.x

Parrish, D.D., Law, K.S., Staehelin, J., Derwent, R., Cooper, O.R., Tanimoto, H., Volz-Thomas, A., Gilge, S., Scheel, H.E., Steinbacher, M., Chan, E., 2012. Long-term changes in lower tropospheric baseline ozone concentrations at northern mid-latitudes. Atmos. Chem. Phys. 12, 11485–11504. doi:10.5194/acp-12-11485-2012

Paulson, C., 1970. The mathematical representation of wind speed and temperature profiles in the unstable atmospheric surface layer. J. Appl. Meteorol. 9, 857–861.

doi:10.1175/1520-0450(1970)009<0857:TMROWS>2.0.CO;2

Pearson, K., Lee, A., 1908. On the generalised probable error in multiple normal correlation. Biometrika 6, 59–68.

Pellegrini, E., Lorenzini, G., Nali, C., 2007. The 2003 European heat wave: which role for ozone? Some data from Tuscany, Central Italy. Water. Air. Soil Pollut. 181, 401–408.

Peltola, O., Mammarella, I., Haapanala, S., Burba, G., Vesala, T., 2013. Field intercomparison of four methane gas analyzers suitable for eddy covariance flux measurements. Biogeosciences 10, 3749–3765. doi:10.5194/bg-10-3749-2013

Peñuelas, J., Staudt, M., 2010. BVOCs and global change. Trends Plant Sci. 15, 133–144. doi:10.1016/j.tplants.2009.12.005

Pinzari, F., Trinchera, A., Benedetti, A., Sequi, P., 1999. Use of biochemical indices in the Mediterranean environment: comparison among soils under different forest vegetation. J. Microbiol. Methods 36, 21–28.

Pryor, W.A., Lightsey, J.W., 1981. Mechanisms of nitrogen dioxide reactions: initiation of lipid peroxidation and the production of nitrous Acid. Science 214, 435–7. doi:10.1126/science.214.4519.435

Raupach, 1989. Applying lagrangian fluid mechanics to infer scalar source distributions from concentration profiles in plant canopies 47, 85–108.

Rice, A.H., Pyle, E.H., Saleska, S.R., Hutyra, L., Palace, M., Keller, M., de Camargo, P.B., Portilho, K., Marques, D.F., Wofsy, S.C., 2004. Carbon balance and vegetation dynamic in an old-growth Amazonian forest. Ecol. Appl. 14, 55–71. doi:10.1890/02-6006

Rondón, A., Johansson, C., Granat, L., 1993. Dry deposition of nitrogen dioxide and ozone to coniferous forests. J. Geophys. Res. 98, 5159–5172. doi:10.1029/92JD02335

Rumelhart, D., 1986. Learning by error backpropagation, in: Parallel Distributed Processing. DE Rumelhart and JL McClelland, eds.

Schotanus, P., 1983. Temperature measurement with a sonic anemometer and its application to heat and moisture fluxes. Boundary-Layer Meteorol. 26, 81–93.

Seinfeld, J.H., Pandis, S.N., 2016. Atmospheric Chemistry and Physics: From Air Pollution to Climate Change, 2nd Edition -, 3nd ed. ed. John Wiley & Sons, Inc., Hoboken, NJ.

Sharpatyi, V., 2007. On the mechanism of methane emission by terrestrial plants. Oxid. Commun. 30, 48–50.

Shindell, D.T., Faluvegi, G., Koch, D.M., Schmidt, G.A., Unger, N., Bauer, S.E., 2009.

Improved Attribution of Climate Forcing to Emissions. Science (80-.). 326, 716–718. doi:10.1126/science.1174760

Srivastava, H., 1992. Nitrogenous pollutants in the atmosphere: Their assimilation and phytotoxicity. Curr. Sci. 63, 310–317.

Stams, A.J., Plugge, C.M., 2010. The Microbiology of Methanogenesis, in: Reay, D., Smith, P.A., Van Amstel, A. (Eds.), Methane and Climate Change. Earthscan, London and Washington, pp. 16–26.

Stewart, D.J., Almabrok, S.H., Lockhart, J.P., Mohamed, O.M., Nutt, D.R., Pfrang, C., Marston, G., 2013. The kinetics of the gas-phase reactions of selected monoterpenes and cyclo-alkenes with ozone and the NO3 radical. Atmos. Environ. 70, 227–235. doi:10.1016/j.atmosenv.2013.01.036

The Royal Society, 2008. Ground-level Ozone in the 21st Century: Future Trends, Impacts and Policy Implications. Sci. Policy, Rep. 15/08.

Thom, A., 1975. Momentum, mass and heat exchange of plant communities, in: Monteith, J.L. (Ed.), Vegetation and the Atmosphere. London, pp. 57–109.

Trotsenko, Y., Khmelenina, V., 2002. Biology of extremophilic and extremotolerant methanotrophs. Arch. Microbiol. 177, 123–131.

Tuzet, A., Perrier, A., Loubet, B., Cellier, P., 2011. Modelling ozone deposition fluxes: The relative roles of deposition and detoxification processes. Agric. For. Meteorol. 151, 480–492. doi:10.1016/j.agrformet.2010.12.004

Valentini, R., Matteucci, G., Dolman, A.J., Schulze, E.D., Rebmann, C., Moors, E.J., Granier, A., Gross, P., Jensen, N.O., Pilegaard, K., Lindroth, A., Grelle, A., Bernhofer, C., Grünwald, T., Aubinet, M., Ceulemans, R., Kowalski, A.S., Vesala, T., Rannik, U., Berbigier, P., Loustau, D., Gudmundsson, J., Thorgeirsson, H., Ibrom, A., Morgenstern, K., Clement, R., 2000. Respiration as the main determinant of carbon balance in European forests. Nature 404, 861–5. doi:10.1038/35009084

Van Grinsven, H.J.M., Holland, M., Jacobsen, B.H., Klimont, Z., Sutton, M.A., Jaap Willems, W., 2013. Costs and benefits of nitrogen for Europe and implications for mitigation. Environ. Sci. Technol. 47, 3571–9. doi:10.1021/es303804g

Vargas, R., Sonnentag, O., Abramowitz, G., Carrara, A., Chen, J.., Ciasis, P., Correira, A., Keenan, F., Kobayashi, H., et al., 2013. Drought influences the accuracy of simulated ecosystem fluxes: a model-data meta-analysis for Mediterranean oak woodlands. Ecosystems 16, 749–764.

Velchev, K., Cavalli, F., Hjorth, J., Marmer, E., Vignati, E., Dentener, F., Raes, F., 2011. Ozone over the Western Mediterranean Sea – results from two years of shipborne

measurements. Atmos. Chem. Phys. 11, 675–688. doi:10.5194/acp-11-675-2011

Vigano, I., Weelden, H. Van, Holzinger, R., Keppler, F., 2008. E ff ect of UV radiation and temperature on the emission of methane from plant biomass and structural components. Biogeosciences 5, 937–947.

Von Schneidermesser, E., Monks, P.S., Allam, J.D., Bruhwiler, L., Foster, P., Fowler, D., Lauer, A., Morgan, W.T., Paasonem, P., Righi, M., Sindelarova, K., Sutton, M., 2015. Chemistry and the linkages between air quality and climate change. Chem. Rev. 115, 3856–3897. doi:10.1021/acs.chemrev.5b00089

Wang, J.M., Murphy, J.G., Geddes, J. a., Winsborough, C.L., Basiliko, N., Thomas, S.C., 2013. Methane fluxes measured by eddy covariance and static chamber techniques at a temperate forest in central Ontario, Canada. Biogeosciences 10, 4371–4382. doi:10.5194/bg-10-4371-2013

Wang, Z.-P., Gulledge, J., Zheng, J.-Q., Liu, W., Li, L.-H., Han, X.-G., 2009. Physical injury stimulates aerobic methane emissions from terrestrial plants. Biogeosciences 6, 615–621.

Webb, E.K., Pearman, G.I.., Leuning, R., 1980. Correction of flux measurements for density effects due to heat and water vapour transfer. Quart. J. R. Met. Soc 106, 85–110.

Wesely, M.L., Hicks, B.B., 2000. A review of the current status of knowledge on dry deposition. Atmos. Environ. 34, 2261–2282.

Williams, C.A., Collatz, G.J., Masek, J., Huang, C., Goward, S.N., 2014. Impacts of disturbance history on forest carbon stocks and fluxes: Merging satellite disturbance mapping with forest inventory data in a carbon cycle model framework. Remote Sens. Environ. 151, 57–71. doi:10.1016/j.rse.2013.10.034

Wilson, K.B., Hanson, P.J., Mulholland, P.J., Baldocchi, D.D., Wullschleger, S.D., 2001. A comparison of methods for determining forest evapotranspiration and its components: sap-flow, soil water budget, eddy covariance and catchment water balance. Agric. For. Meteorol. 106, 153–168. doi:10.1016/S0168-1923(00)00199-4

Wilson, K.B., Meyers, T.P., 2001. The Spatial Variability of Energy and Carbon Dioxide Fluxes at the Floor of a Deciduous Forest. Boundary-Layer Meteorol. 98, 443–473. doi:10.1023/A:1018779506973

Zapletal, M., Cudlin, P., Chroust, P., Urban, O., Pokorny, R., Edwards-Jonsova, M., Czerny, R., Janous, D., Taufarova, K., Vecera, Z., Mikuska, P., Paoletti, E., 2011. Ozone flux over a Norway spruce forest and correlation with net ecosystem production. Environ. Pollut. 159, 1024–1034. doi:10.1016/j.envpol.2010.11.037

Zeikus, J.G., Ward, J.C., 1974. Methane formation in living trees: a microbial origin. Science

(80-.). 184, 1181–3. doi:10.1126/science.184.4142.1181

Zhang, L., Brook, J., Vet, R., 2002. On ozone dry deposition—with emphasis on non-stomatal uptake and wet canopies. Atmos. Environ. 36, 4787–4799.

Zona, D., Gioli, B., Fares, S., De Groote, T., Pilegaard, K., Ibrom, a., Ceulemans, R., 2014. Environmental controls on ozone fluxes in a poplar plantation in Western Europe. Environ. Pollut. 184, 201–210. doi:10.1016/j.envpol.2013.08.032